Long Term Thermal Performance and Application of Glass Fiber Core Vacuum Insulation Panels

By

Vivian Ting Ting Chan
Bachelor of Engineering, University of Victoria, 2017

A Thesis Submitted in Partial Fulfillment
of the Requirements for the Degree of

Master of Applied Science

In the Department of Civil Engineering

We acknowledge with respect the Lekwungen peoples on whose traditional territory the university stands and the Songhees, Esquimalt and W̱SÁNEĆ peoples whose historical relationships with the land continue to this day.

Long Term Thermal Performance and Application of Glass Fiber Core Vacuum Insulation Panels

By

Vivian Ting Ting Chan
Bachelor of Engineering, University of Victoria, 2017

SUPERVISORY COMMITTEE

Dr. Phalguni Mukhopadhyaya, Supervisor
Department of Civil Engineering

Dr. Min Sun, Department Member
Department of Civil Engineering

ABSTRACT

Glass fiber core Vacuum Insulation Panels (VIPs) have thermal performance per unit thickness of about 5-10 times higher than the traditionally used building insulation materials such as mineral wool, XPS, EPS, foam, etc. This advantage of VIP has made it very attractive new option for innovative building designs. Especially in Canada, where some of the areas have long and very cold winters.

Confidence in the service life of a building material is necessary before putting a product to market. Extensive research has been conducted on the product development, quality improvement, and field application of VIPs around the world. However, there is lack of consistent and simple prediction method for the long-term thermal performance of VIPs.

This paper discussed the process and performance of a field project using glass fiber VIPs to retrofit a commercial building in Yukon, Canada. The thermal performance of the VIPs used in this project was continuously monitored and critically analyzed since the start in 2011. The results have shown satisfactory thermal performance of VIPs for the past 8 years. The findings were also used to validate glass fiber core VIP accelerated aging tests conducted by the National Research Council Canada (Ottawa), and the aging rate of VIPs in a cold and dry climate was determined.

The second part of this study investigated the monitored performance results from two sets of simplified accelerated laboratory aging tests, the results were analyzed with the aim to separate the impact of air diffusion from water vapour on the long-term thermal performance of glass fiber VIPs.

In addition, this study also investigated the potential application of VIPs in balcony constructions to reduce heat transfer through thermal bridges. Computer modeling exercises, using a benchmarked (EN ISO 10211) three-dimensional transient and steady-state heat transfer simulation tool HEAT3, were carried out on the most optimal (thermal performance) balcony assemblies of wood framed buildings using VIP as insulation. This niche application of VIPs can significantly increase the energy efficiency of building envelopes/skins in extreme climates of Canada and elsewhere in the world.

TABLE OF CONTENTS

LIST OF FIGURES

LIST OF TABLES

NOMENCLATURE

This thesis references the Building Envelope Thermal Bridging Guide provided by B.C. Hydro. The table below is available in Section 2 – Glossary of Terms [1].

Term	Symbol	Unit	Definition
Conductivity	k or λ	W/m·K	The ability of a material to transmit heat in terms of energy per unit area per unit thickness for each degree of temperature difference.
Equivalent Conductivity	k_{eq}	W/m·K	The averaged or equivalent thermal conductivity of a component consisting of several building materials, effectively treating the component as a homogeneous material that provides the same thermal characteristics.
Heat Flow	Q	W	The amount of energy per unit time that passes through an assembly under a specific temperature drive of ΔT.
Thermal Transmission Coefficient	U	$W/m^2 \cdot K$	Heat flow per unit time through a unit area of an assembly per temperature degree difference. The convention is to include the impact of air films.
Thermal Resistance of a Material	R	$m^2 \cdot K/W$	A measure of a material's resistance to heat flow.
Effective Thermal Resistance	R_{eff}	$m^2 \cdot K/W$	A measure of an assembly's resistance to heat flow, including the effects of thermal bridging. The inverse of the assembly U-value.
Clear Filed Assembly Thermal Transmittance	U_0	$W/m^2 \cdot K$	Heat flow coefficient for an assembly with uniformly distributed thermal bridges, which are not practical to account for on an individual basis for U-value calculations.
Linear Heat Transmittance coefficient	ψ	W/m·K	Heat flow coefficient representing the added heat flow associated with linear thermal bridges that are not included in the clear field U_0. Linear thermal bridges typically occur at interface details.
Point Heat Transmittance Coefficient	χ	W/K	Heat flow coefficient representing the added heat flow associated with a point thermal bridge that is not included in the clear field U_0. Point thermal bridges are countable points and are considered feasible to account for on an individual basis for U-value
Length of a Linear Transmittance	L	m	The length of a linear thermal bridge, i.e. height of a corner or width of a slab.

The following terms are included to clarify discussions relating to the structural elements used when modeling various thermal bridges.

Term	Description
Beam	A structural element which carries joist loads to columns installed over an opening or clear span.
Built-up Beam	A beam created by laminating multiple layers of thinner beams together, typically side-by-side. Beams were nailed together to allow the beams to share load evenly.
Stud	An intermittent column spaced evenly through a wall to provide vertical and horizontal resistance for the structure.
Plates	A horizontal element which runs along the top and bottom of wall sections to provide bearing for joists, and beams. Also provides lateral stability to the structure.
Sheathing	A board product, typically plywood or Oriented Strain Board (OSB), applied the exterior face of walls to provide support for studs, provide surface for membranes, and provide lateral stability to the structure.
Insulation	A material with low thermal conductance intended to reduce the amount of thermal flux through an assembly. Materials include but are not limited to fiberglass, rock wool, and various chemical foams.
Ledger	Structural support fastened to the exterior face of walls to provide connection point for exterior elements such as balconies and awning.
Rim Joists	Element installed at joist ends to provide lateral support to the joists and to close ends of joists. Rim joist also assists with the transfer of lateral forces between storeys.
Dimensional Lumber	Kiln-dried natural wood products produced in standard sizes. Available in a variety of depths and thicknesses.
Engineered Wood Product	Manufactured products utilizing reorganized wood fibers. Typically used to increase consistency between various elements. Generally manufactured to the same sizes as dimensional lumber. Various types of products available (LVL, PSL, Glulam etc.)
Truss Joist I-Joist (TJI)	TJI are proprietary wood product that comprises of kiln-dried wood top and bottom chord with an OSB web separating the two chords.

AUTHOR CONTRIBUTIONS

This thesis was originally prepared and composed by Vivian Chan, who was responsible for the overall compilation of the information included in this work. The core of this thesis is made up of three chapters, the first of which, Chapter 2, has already been published as:

V. T. Chan, M. Ooms, J. Korn, D. MacLean, S. Mooney, S. Andre, P. Mukhopadhyaya, "Critical Analysis of In Situ Performance of Glass Fiber Core VIPs in Extreme Cold Climate," *Frontier in Energy Research,* vol 7, 2019.

> Vivian Chan was responsible for data analysis and composition of the first draft. Dr. Phalguni Mukhopadhyaya supervised this work. Matthew D. Ooms, Juergen Korn, Douglas MacLean, Stephen Mooney, and Shane Andre reviewed and provided valuable comments to the manuscript.

Chapter 3 and Chapter 4 will be submitted as peer-reviewed manuscripts. Below the preliminary author list, title and author contributions are clarified.

V. T. Chan, P. Mukhopadhyaya. Accelerated Laboratory Aging Test on Glass Fiber Core Vacuum Insulation Panels.

> In Chapter 3, Vivian Chan conducted the literature reviews, proposed the methodology, conducted the experiments and measurements, and performed the data analysis. Vivian also prepared the manuscript of this chapter. Dr. Phalguni Mukhopadhyaya reviewed and revised the methodology, suggested data analysis directions, and reviewed and revised this chapter.

V. T. Chan, J. Bourcet, P. Mukhopadhyaya. Optimization of Thermal Performance in Wood Frame Buildings.

> In Chapter 4, Vivian Chan was responsible for the creation and performance of all modeling work in HEAT3, the conduction of the literature reviews on linear and point transmittance along thermal brides and the published papers on thermal bridging modeling, the development of study methodology (along with John Bourcet), and data analysis (including calculation of the final results using the data obtained from HEAT3). Vivian also wrote the methodology, discussion and conclusions sections of the manuscript and prepared the figures that helped clarify the methodology.
>
> John Bourcet prepared the introduction, literature reviews on heat transfer background, assumptions used for modeling, study methodology (along with VC), reviewed the 3D models and results, and tabulated the results in Appendix B. Dr. Phalguni Mukhopadhyaya supervised Vivian and reviewed and provided feedback on the content of this chapter.

ACKNOWLEDGMENTS

I would first like to express my deep appreciation to my research supervisor Dr. Phalguni Mukhopadhyaya of the Civil Engineering Department at the University of Victoria. The door to Dr. Mukhopadhyaya's office was always open whenever I had a question about my research or writing. He consistently allowed this study to be my own work but steered me in the right direction whenever he thought I need it.

I would also like to thank the experts who were involved and supported this research project: Yukon Energy Mines and Resources – Matthew D. Ooms and Shane Andre; Yukon Housing Corporation – Juergen Korn; Retired, Yukon Energy Mines and Resources – Douglas MacLean; Yukon Research Centre – Stephen Mooney; Read Jones Christoffersen Engineers ltd – John Bourcet; Terry Bergen; Sameer Hasham; Cameron Marshall; University of Victoria Civil Engineering Lab support team – Dr. Armando Tura; Mitch Anderson; Geoff Burton and Matthew Walker.

I would also like to acknowledge Dr. Min Sun of the Civil Engineering Department at University of Victoria as the member in the supervisory committee, and Dr. Ajith Rao of the Corporate Innovation Centre at the USG Corporation as the external examiner. I am gratefully for their very valuable comments on this thesis.

Finally, I must express my very profound gratitude to my parents and my husband for providing me with unfailing support through my years of study and through the process of researching and writing this thesis. Thank you.

CHAPTER 1 INTRODUCTION

1.1 BACKGROUND

Most of the energy produced in the global energy system are originated from fossil fuels (coal, oil, gas). While the fossil energy played an important role in advancing the technological, social, economic and development progress globally. However, fossil fuels are the main source of local air pollution, combustion of fossil fuels is the largest human source of carbon dioxide emission, which leads to global warming and climatic change [2]. In 2008, carbon dioxide emission generated from the energy section accounts more than 50% of the total emission in the world [3]. If the global temperature increases over 2 degree Celsius, then the environment would go through irreversible changes, natural ecosystems would be severely damaged, and human health would be at great risk. Efforts in developing energy efficiency strategies have been made across various sectors of the economy targeting to limit the global temperature rise below 2 degrees Celsius that was set by United Nation member parties [3].

Heating and cooling in buildings require substantial amount of energy. Globally, the data of the final building energy consumption by end-use in 2010 shows that space heating is 32-33% of the total energy use in both residential and commercial buildings, it is the largest component of total energy use. Space cooling is 2-7% of the total energy use. Under a frozen scenario, it is predicted that the global energy consumption in building heating and cooling will increase by 80% in 2050 relative to 2010. Energy use in residential buildings is predicted to increase by 65%, it is mainly due to the increase in population and therefore the increase in the number of households, at the same time, there will be a decrease in the size of households due to urbanization, divorce rates, and mobility of young people. For commercial buildings, as the economy activity increases, the energy consumption is expected to be doubled [4].

In Canada, due to its extreme cold and long winters, data from 2013 shows that space heating was as high as 63% and 55% of total building energy consumption in residential and commercial buildings respectively [5], contributed to 14% and 9% and of the total greenhouse gases emitted.

Improved energy efficiency in buildings has been a primary goal for professionals in building sectors. In Canada, the minimum requirement of building energy performance is set by National Building Code [6], and its expectations have been increasing steadily in recent years. Provincial building code and various voluntary building standards such as Leadership in Energy and Environmental Design rating system, British Columbia Energy Step Code, and Passive House often set higher performance targets.

The application of thermal insulation has been the intuitive and efficient solution for a long time to improve buildings energy efficiency in building envelope. Thermal insulation in building is a material or composite material that has high thermal resistance and can reduce the heat flux between the interior of a space and its external environment. The thermal conductivities of some common building insulation materials are listed in Table 1 below:

Table 1. Thermal conductivities of common building insulation materials materials [7].

Material	Thermal Conductivity (W/m·K)
Fiberglass	0.033 – 0.04
Rockwool	0.037
Polyethylene	0.041
Expand Polystyrene (closed cell foam)	0.037 – 0.038
Extruded Polystyrene (closed cell foam)	0.030 – 0.032
Cellulose	0.046 – 0.054

If the traditional insulation materials from Table 1 above are used to satisfy the increasingly more stringent building energy requirements, the expected total thickness of the insulation can be up to 30 to 50 cm [8]. For renovation projects on existing buildings, sometimes there simply isn't enough space in the wall or floor cavity for so much insulation, and it could be aesthetically unappealing if the insulations were attached to the exterior of the walls.

State-of-the-art thermal insulation materials and solutions have been researched and developed in recent years, including closed cell foam, vacuum insulation panel (VIP), gas filled panel, aerogel and phase change material [9]. There are lots of interest in vacuum insulation panel or VIP because it has 5-10 times better thermal resistance per unit thickness than the traditional ones. A vacuum insulation panel consists of evacuated open porous core materials enclosed by a gas tight envelope. The core materials have high thermal resistance properties and they can bear the loads caused by atmospheric pressure, and the envelope is sealed to preserve the vacuum inside.

There are two commonly used VIP core materials on the market, namely, fumed silica and glass fiber. When the internal pore pressure of fumed silica core VIPs is lowered to 2,000 - 10,000 Pa at room temperature, the VIPs reaches its lowest possible thermal conductivity, which is around 0.004 W/m·K. The pore size of fumed silica is about 30- 100 nm and the thermal characteristics of fumed silica are stable below 5,000 Pa [8]. Fumed silica is least sensitive to increases in pressure among all core materials used in VIPs, and its internal pressure can be easily maintained with a moderately effective gas-tight envelope. Fumed silica VIPs with laminated aluminum foil envelopes are expected to function up to 50 years [8, 10]. Furthermore, even after total vacuum failure, fumed silica core VIPs can have thermal resistances twice as high (thermal conductivity = 0.020 W/m·K) as conventional insulation materials [8].

In comparison, glass fiber VIPs can achieve thermal conductivities as low as 0.002 W/m·K, however, the internal pressure they require to achieve this performance is about 10 Pa [11]. In addition, because its larger pore size (1-12 μm) the thermal conductivity of glass fiber VIPs will increase rapidly when the internal pressure rises above 100 Pa [10]. However, the cost to manufacture glass fiber VIPs is less when compared to fumed silica core VIPs and is about the same as foamed insulation per R-value. Therefore glass fiber core VIPs remain an attractive alternative as a building material [8].

Over time, air and water vapour permeating through the envelope will cause the thermal conductivity of VIP to rise. When the thermal conductivity increases to about 0.007 – 0.010 W/m·K, it is considered as at the end of the VIP's service life. This irreversible process is called the aging of VIPs.

VIPs has been widely used in areas such as insulating refrigerators, cold storages, etc. where the expected service life is around 5-10 years. There are hesitations from various stakeholder in applying VIPs in building envelopes due its cost, quality, possible construction challenges, and uncertain service life. In Canada, building materials are expected to have at least 25 to 50 years' service life, because to repair or change the insulation materials from wall cavities or floor or ceilings can be very difficult and costly proposition.

On the other hand, based on the extensive researches conducted on the whole building thermal performance, attention has been drawn to the importance in ensuring the continuity of insulation, meaning improving the thermal performance in assemblies that creates thermal bridges leading to the loss of thermal energy, such as floor slabs, intersecting walls, balconies, etc.

Thermal bridge is a physical phenomenon occurs in the building envelope when an assembly transfers heat through itself at a greater rate than the surrounding assemblies. It is caused by highly thermal conductive building members that penetrates the insulated building envelope members and often found to be at the intersection of different building envelope components, see Figure 1 below. Significant energy reduction is caused by the heat loss in the winter and the heat gain in the summer through building envelope. Moreover, simply adding more insulation materials will not solve this problem. Minimizing thermal bridges by careful investigation and optimized design can reduce whole building energy usage, increase the durability of building envelope by limiting freeze and thaw in its members, reduce the risk of condensation on cold surface and improve occupant comfort [1].

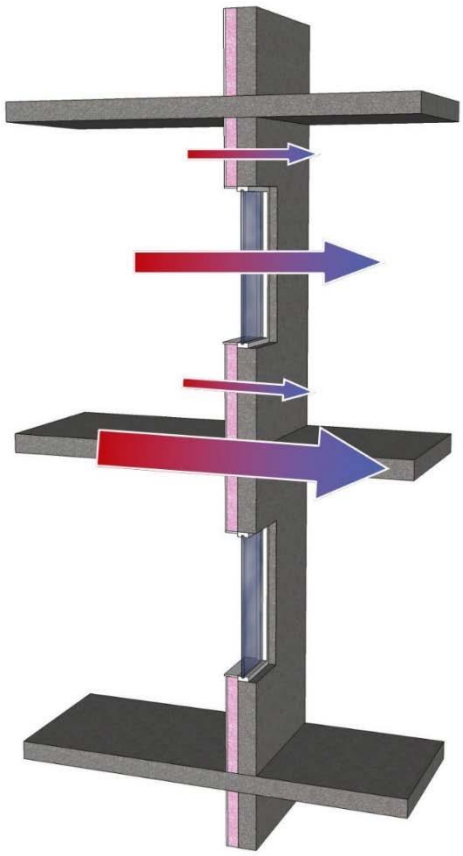

Figure 1. Heat flow paths across center of wall, floor slab and windows. Arrow size is relative to magnitude of heat flow [1].

1.2 Thesis Objectives

The primary objectives of this research are:

1. Critically analyze the long-term thermal performance of glass fiber core VIPs using field data from an 8-year (2011-2018) long retrofit project in Whitehorse, Yukon.
2. Conduct accelerated aging tests in the laboratory on glass fiber core VIPs to assess the long-term performance of VIPs.
3. Using computer simulation tool HEAT3 assess the heat loss through thermal bridges in wood-framed buildings, constructed with the optimized framing methods and state-of-art insulation material – VIPs.

The following sections present the summary of the work that have been done in three main areas, as mentioned above.

In 2011, glass fiber core VIPs were installed in a commercial building retrofit project in Yukon, Canada, and have been continuously monitored since. Chapter 2 summarizes the thermal performance of the glass fiber core VIPs over the period of 2011-2018 in extreme cold climate. Findings in this study provided valuable data to validate glass fiber core VIP accelerated aging test results conducted by the National Research Council Canada (Ottawa), and the aging rate of VIPs in a cold and dry climate was determined.

Chapter 3 summarizes the procedures and findings of the laboratory accelerated aging tests conducted on glass fiber core VIPs at the University of Victoria, Building Science Laboratory. Two sets of aging tests were conducted between winter 2018 – spring 2019. One set was kept at 70°C in the oven, and the other set was aged at 70°C and 95% RH in a custom-made climatic chamber. Results were analyzed with the aim to distinguish the effect of water vapour from dry air on the thermal performance degradation of VIPs.

Chapter 4 investigates the significance of thermal bridges in wood-framed building and evaluated the potential reduction of heat transfer through thermal bridge due to advanced framing system with optimized wood type, joist/slab spacing etc., construction details and use of VIP as thermal insulation. Specifically, thermal bridges at three types of balcony junctions – cantilever, ledger and rim joist were studied. 3-D thermal modeling software HEAT3 was used to simulate and calculate the linear and point thermal transmittance at each thermal bridge. Results are presented and analyzed. The best performing design parameter combinations were identified and recommended for each balcony type.

Each chapter contains its own introduction, literature reviews, methodology, results and discussion, and conclusions.

CHAPTER 2 CRITICAL ANALYSIS OF IN SITU PERFORMANCE OF GLASS FIBER CORE VIPS IN EXTREME COLD CLIMATE

2.1 ABSTRACT

Glass fiber core vacuum insulation panels (VIPs) are becoming an increasingly attractive option for building envelope construction due to lower cost and availability around the world. Although fumed silica core VIPs have shown superior long-term performance under accelerated aging tests compared to glass fiber core VIPS, these laboratory test results have yet to be verified with long-term field performance data. In 2011, glass fiber core VIPs were installed in a commercial building retrofit project in Yukon, Canada (one of Canada's most northern territories), and have been continuously monitored since. This paper summarizes the thermal performance of the glass fiber core VIPs over the period of 2011–2018 in an extreme cold climate. Findings from this study provided data to validate glass fiber core VIP accelerated aging test results and the aging rate of VIPs in a cold and dry climate was determined. These results will help developing a better understanding of the long-term performance of glass fiber core VIPs in a real-world context.

2.2 INTRODUCTION

Vacuum insulation panels (VIP) are one of the most promising advanced building insulation materials owing to their low thermal conductivity of about 0.004 W/m·K [8]. Traditional thermal insulation materials such as mineral wool, expanded polystyrene, extruded polystyrene, cellulose etc. are in the range of 0.025 – 0.040 W/m·K , have thermal conductivities 5 – 10 times higher than that of VIPs [9]. Integration of VIPs into building envelopes can help builders meet increasingly stringent code requirements, particularly when space is limited, and allow for greater aesthetic flexibility in architectural design. In spite of these benefits, VIPs have not been broadly adopted because of their high cost, concerns related to long-term effectiveness, thermal bridge effects at the panel edges, and the risk of condensation if appropriate moisture control is not considered in the design [12]. It is worth mentioning that integration and adoption of new materials and technologies in the building construction industry takes time and cannot be done prior to rigorous short- and long-term holistic performance evaluation. This is particularly true in Canada [13] for insulation because of the significant economic implications that can be expected should the insulation not perform as expected during Canada’s long and very cold winters. In the case of VIPs, there are also related concerns about the effects of damage to VIPs during construction and in service, as well as the unknown service life for VIPs.

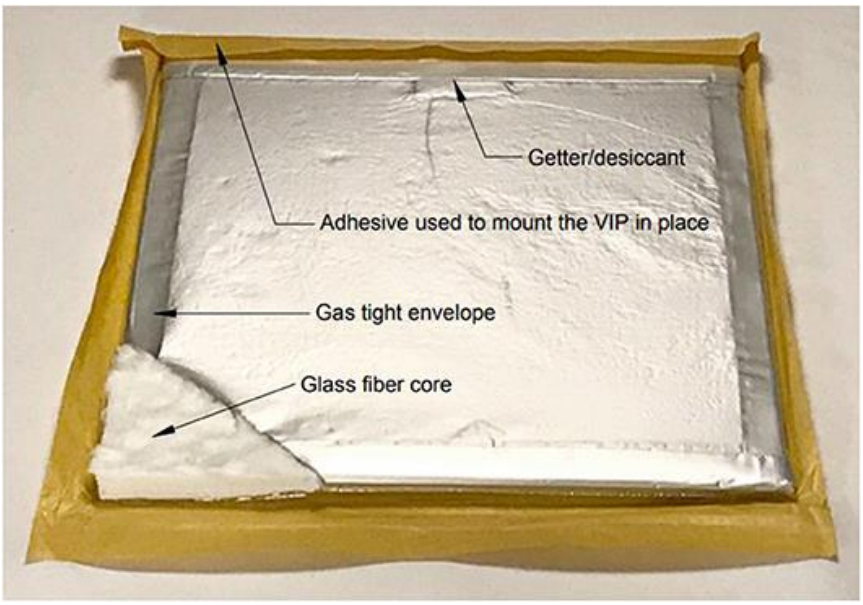

Figure 2. Schematic of a glass fiber core VIP. One corner of the gas-tight envelope has been removed to show the evacuated open-pore core. The getter/desiccant is in a sachet in the raised area at the top center. The brown wax paper backing covers the adhesive that is used to mount the VIP in place.

VIPs consist of an evacuated open-pore core enclosed within a gas-tight envelope, as shown in Figure 2. The core provides thermal resistance and adequate load bearing capacity to resist atmospheric pressure [14] while the single/multi-layer sealed envelope maintains the vacuum inside the panel. Opacifiers can be added to the core to reduce radiative heat transfer through the core, and getters/desiccants adsorb residual or permeating gas and moisture [8] and thus slow the aging rate. In these ways, heat transfer across the panel is minimized and the service life is extended.

To maintain high thermal performance, VIPs require their internal pressure to be kept very low, close to vacuum (zero). Permeation of dry air (e.g., oxygen and nitrogen) and water vapour through the envelope can compromise this vacuum and lead to an irreversible pressure increase and moisture accumulation inside the panel [15]. Temperature and relative humidity (RH) are the dominant factors impacting the rate of gas permeation through the envelope and consequently the VIP's expected service life.

The most commonly used VIP core materials are fumed silica and glass fiber. Fumed silica core VIPs can achieve thermal conductivities of 0.004 W/m·K when the pore pressure is reduced to 2,000 - 10,000 Pa at room temperature. Fumed silica has a pore size of about 30 - 100 nm and its thermal characteristics are stable up to about 5,000 Pa [8]. Among core materials, fumed silica is least sensitive to increases in pressure, and its internal pressure can be satisfactorily maintained with a moderately effective gas-tight envelope. Fumed silica VIPs with laminated aluminum foil envelopes are expected to have service lives of up to 50 years [8, 10]. Furthermore,

even after complete vacuum failure, fumed silica core VIPs can have thermal resistances twice as high (thermal conductivity = 0.020 W/m·K) as conventional insulation materials [8].

In comparison, glass fiber VIPs are able to achieve thermal conductivities as low as 0.002 W/m·K, the lowest of all core materials [11] although they require an internal presssure of about 10 Pa to achieve this performance. In addition, the larger pore size (1 - 12 μm) of glass fiber cores leads to a rapid increase in thermal conductivity when the internal pressure rises above 100 Pa [10]. Nevertheless, glass fiber core VIPs are less expensive to manufacture and therefore remain an attractive alternative as a building material [8]. Glass fiber VIPs have been used extensively in the aerospace and refrigerator industries where the expected service life is no more than 15 years [8]. While the expected service life of thermal insulation in building construction is 25 - 50 years, broad industry confidence in long-term thermal performance of glass fiber core VIPs still needs to be established.

Glass fiber core VIPs have been used as thermal insulation in retrofitting an existing wall of a commercial building in Whitehorse, Yukon, a subarctic city in Northern Canada. Buildings in Whitehorse typically have high space-heating demands due to the region's extremely cold winters, so interest in high performing building insulation systems is high. This paper is a continuation of a series of publications [11, 16-20] and presents the most up-to-date field performance data observed from continuous in situ monitoring of this installation (2011 - 2018), compares these results to accelerated aging test results presented in the literature, and discusses the lessons learned from VIP handling and installation.

2.3 Construction and Instrumentation

An 8.4 x 3.7 m^2 wall of an existing building was retrofitted with VIPs sandwiched between layers of extruded polystyrene foam (XPS) attaching to its concrete exterior. The VIP specimens used were 560 mm x 460 mm x 12 mm in size. The pre-installation thermal conductivity of the VIPs was measured using a 600 mm x 600 mm heat flow meter apparatus with 300 mm x 300 mm heat flow sensor and an accuracy of ± 2%, the thermal conductivity was found to be 0.0034 W/m·K at the center of the panel [18].

Figure 3. Existing wall selected for retrofit [11].

The existing exterior concrete block wall (Figure 3) was insulated with fiberglass batts. The thermal resistance of this existing wall was about 3.5 $m^2 \cdot K/W$, and the retrofitting goal was to increase the wall's thermal resistance to 8.8 – 10.6 $m^2 \cdot K/W$ [18]. The integrity of VIPs was verified by physical examination at the construction site before the assembly. Concerns regarding condensation in additional wall layers and mechanical rubbing on VIP surfaces caused by uneven proximate wall elements were addressed in the design described below [18]. In summary, additional layers of insulation were constructed on the exterior of the existing concrete block wall in the following order [18]:

- First, a 0.15 mm polyethylene air-vapour-moisture barrier was glued to the concrete block wall to minimize condensation in extra wall layers.
- Then, 25 mm extruded polystyrene (XPS) board was adhered to the polyethylene barrier, creating an even surface for subsequent mounting of the VIPs.
- 50 mm x 75 mm wood strapping was then attached over top of the XPS board and affixed to the concrete wall with anchors.
- Glass fiber core VIPs were adhered to the XPS board between the wood straps, using a "peel and stick" adhesive on one side.
- The VIPs were then covered with a layer of 6 mm flexible polyurethane foam that was held in place with sheathing tape.
- Lastly, a layer of 25 mm thick polystyrene board was installed over the polyurethane foam to avoid the potential risk of condensation and damage from mechanical rubbing.

Installations proceeded quickly and smoothly as documented in Figures 4 - 6.

Figure 4. Installation of VIPs over a layer of XPS and a 0.15 mm (6 mil) polyethylene air vapor barrier on the existing concrete block wall [11].

Figure 5. The second layer of XPS is shown in place over 6 mm polyurethane foam. The XPS layer ensured that the bottom surface of each VIP was attached to a smooth surface and protected from abrasion. A layer of 6 mm flexible polyurethane foam was placed over the exterior surface of the VIPs to help prevent mechanical rubbing of the outside surface of each VIP against the 25 mm polystyrene foam board placed on top of it.

Figure 6. Post-retrofit wall [11]. Because all holes for fasteners were drilled before the siding was put on the wall, it was possible to visually check that all fastening points were directly over the support members.

Four thermistors were installed to monitor the temperature at the interface between insulation layers, as shown schematically in Figure 7. These thermistors were set up approximately 2 m from the south edge of the wall and 1 m down from the top of the wall [18]. Three sensors were placed on the existing wall approximately 2 m from the north edge of the wall retrofitted area. These sensors were located approximately 1 m, 1.5 m and 3 m from the top of the wall, and they were used to monitor the thermal gradients from the top to the bottom of the wall [18].

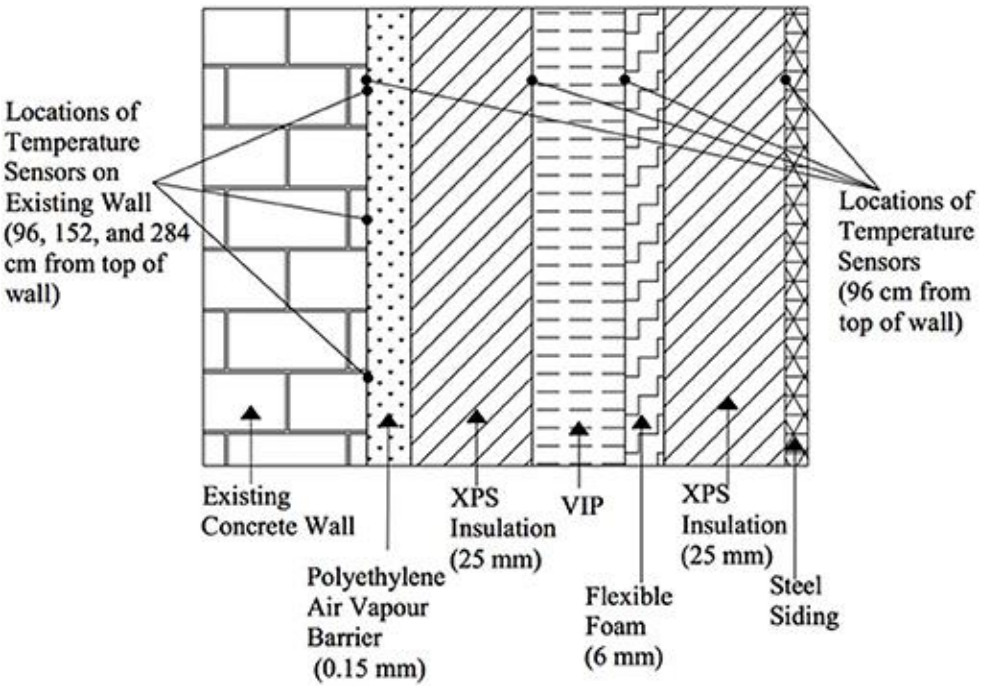

Figure 7. Schematic diagram of the retrofitted wall cross-section starting from cladding onwards and the locations of the temperature sensors (thermistors) [11]. This drawing is not to scale. Two sets of thermistors are installed at different locations along the length of the wall (one set is near the north edge and the other is near the south edge).

2.4 Results and Discussions

Infrared thermal images of the retrofitted wall were taken in 2011, 2014, 2016 and 2018 are shown in Figure 8. These images confirm that all VIPs installed in 2011 remain functional after eight years. Specifically, it is clear from the temperature of the wall over each VIP that none of the VIPs have lost their insulating value over eight years (failed VIPs will be indicated by abrupt change of colour in the infrared thermal images). This is a very significant finding for the long-term performance of glass fiber core VIPs in an extreme cold climate and demonstrates the effective integration of VIPs in an exterior building envelope retrofit. In order to gain greater insight into the thermal performance of the exterior wall and VIPs, the temperatures at the interfaces between insulation layers of the retrofitted wall were collected over the past eight years (2011-2018) since the project started, and selected data were analysed for the following colder winter time periods (summer data were not stable due to factors such as lack of thermal gradient, unstable indoor condition etc.):

December 13, 2011 – April 15, 2012
December 5, 2012 – May 23, 2013
November 1, 2013 – January 9, 2014
February 11, 2016 – March 31, 2016
November 1, 2016 – January 11, 2017
March 24, 2018 – June 8, 2018

The temperature drops across each layer of the composite exterior insulation (XPS-VIP-XPS) were calculated as a percentage of total temperature drop across the composite exterior insulation. A sample calculation can be found in Appendix A. Figure 9 shows the percentage of total temperature drop across each insulation layer averaged over the winter and/or spring months for six selected years. The average temperature drop for the VIP layer is about 66.49%, while that for the first (interior) and second (exterior) layers of XPS are 14.48% and 18.95% respectively. The exterior layer of XPS is a more effective thermal insulator than the identical interior XPS layer due to the cooler exterior temperature. This observation clearly validates a very basic physical principle of heat transfer and generates confidence in the recorded data and the analysis procedure. The graphical representation in Figure 9 shows that the effectiveness of the VIP layer is decreasing very slowly, from about 69% initially in winter 2011 to 63% in spring 2018, at an average rate of 0.9% per annum, and this rate of aging appears to be linear. However, it is to be noted that the aging rate of VIPs cannot be linear for ever and it is expected to increase rapidly as the internal pressure approaches atmospheric pressure. The transition from lower aging rate to higher aging rate depends on the functional relationship between thermal conductivity and internal pore pressure of the VIP core material.

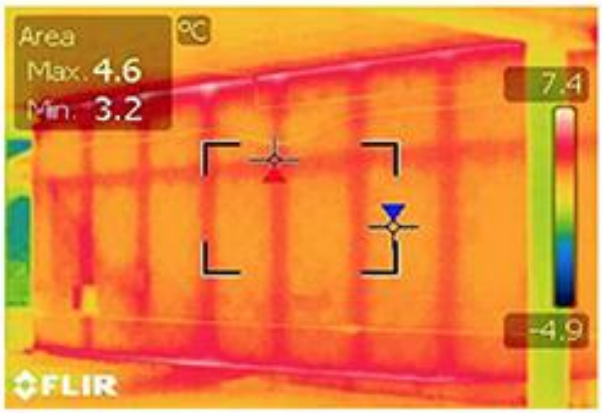

2011 Pre-retrofit

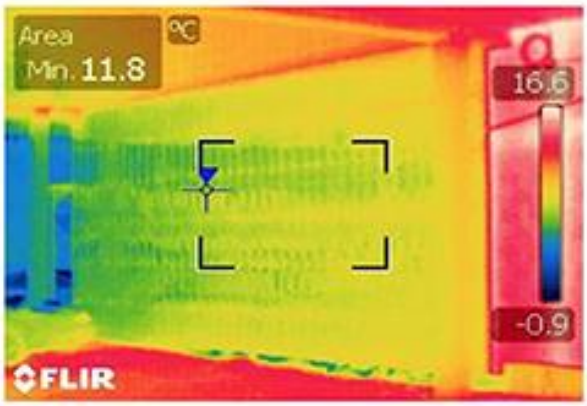

2011 Post-retrofit

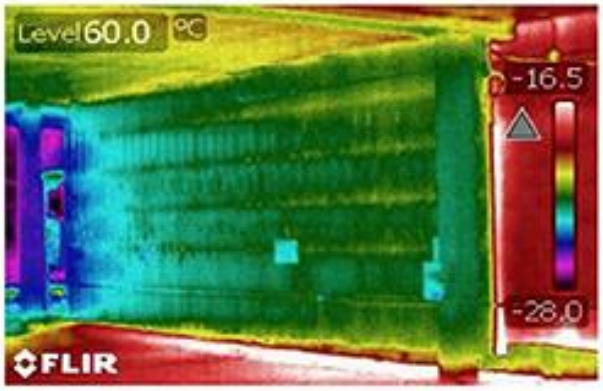

2014 Post-retrofit

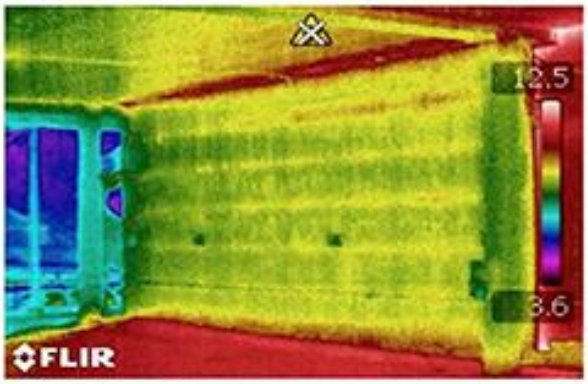

2016 Post-retrofit

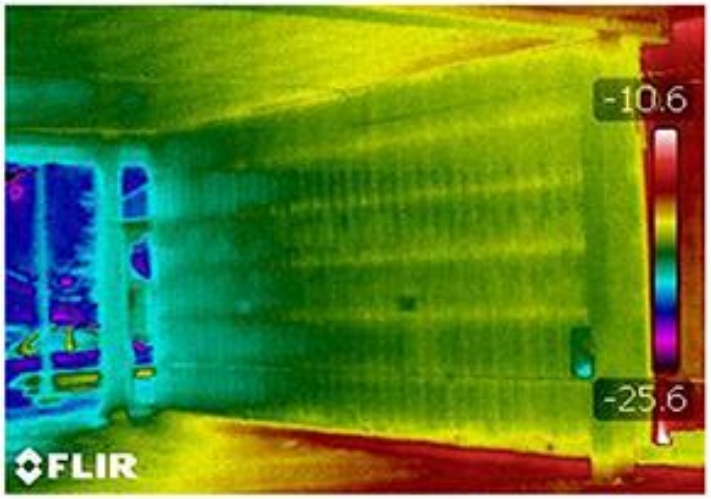

2018 Post-retrofit

Figure 8. Infrared images of the pre-retrofit wall. Images were taken in 2011, 2014, 2016, and 2018.

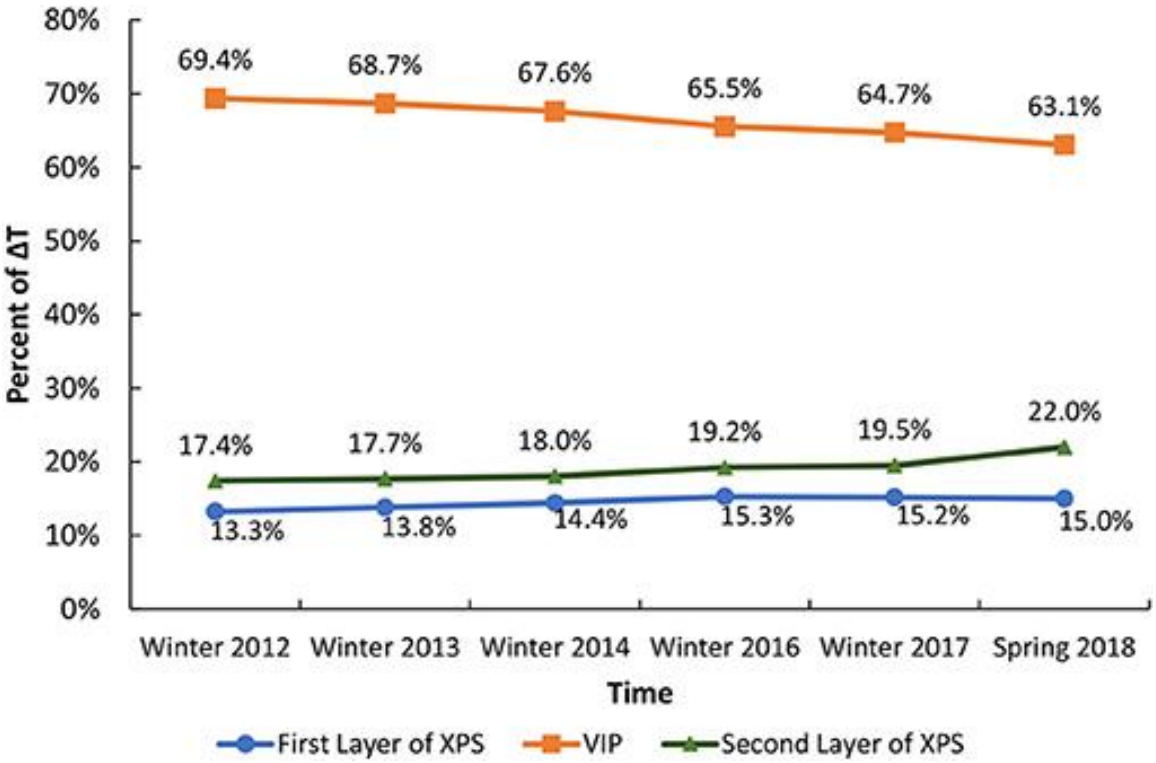

Figure 9. Percentage of temperature drop across wall components relative to the drop across the entire wall. Data averaged for the winter months 2011-2017 and spring months of 2018.

2.5 Accelerated Aging and In Situ Performance

Accelerated aging tests were conducted, at the National Research Council (NRC) Canada, in 2011 to establish long-term thermal performance of the glass fiber core VIPs used in this study [16]. Three VIP specimens (560 mm x 460 mm x 12 mm) were tested under cyclic exposure conditions. In one cycle, VIPs were kept at 23°C, 95% RH for one week and then changed to 70°C, 5% RH for the next week. The specimens went through 14 weeks of total exposure (i.e. a total of seven cycles). The thermal resistance of the panels was measured at the end of each week using a 600 mm x 600 mm heat flow meter. One specimen failed after eight weeks, and the average linear aging rate of the other two was found to be about 3.29% per cycle [21] as shown in Figure 10. The normalized in situ VIP aging rate (expressed as the percentage of its initial thermal resistance) was also plotted with the average of accelerated aging test results in Figure 10. It can be observed from the plot, that the two-year in situ aging rate is nearly equal to one cycle (two weeks) of the accelerated aging rate for the time period where field data are available. Based on this correlation, the linear extrapolation of the in-situ data predicts that the total reduction of thermal resistance in 2026 (14 years since construction) will be about 21% (thermal conductivity increased from 0.0034 W/m·K to 0.00429 W/m·K).

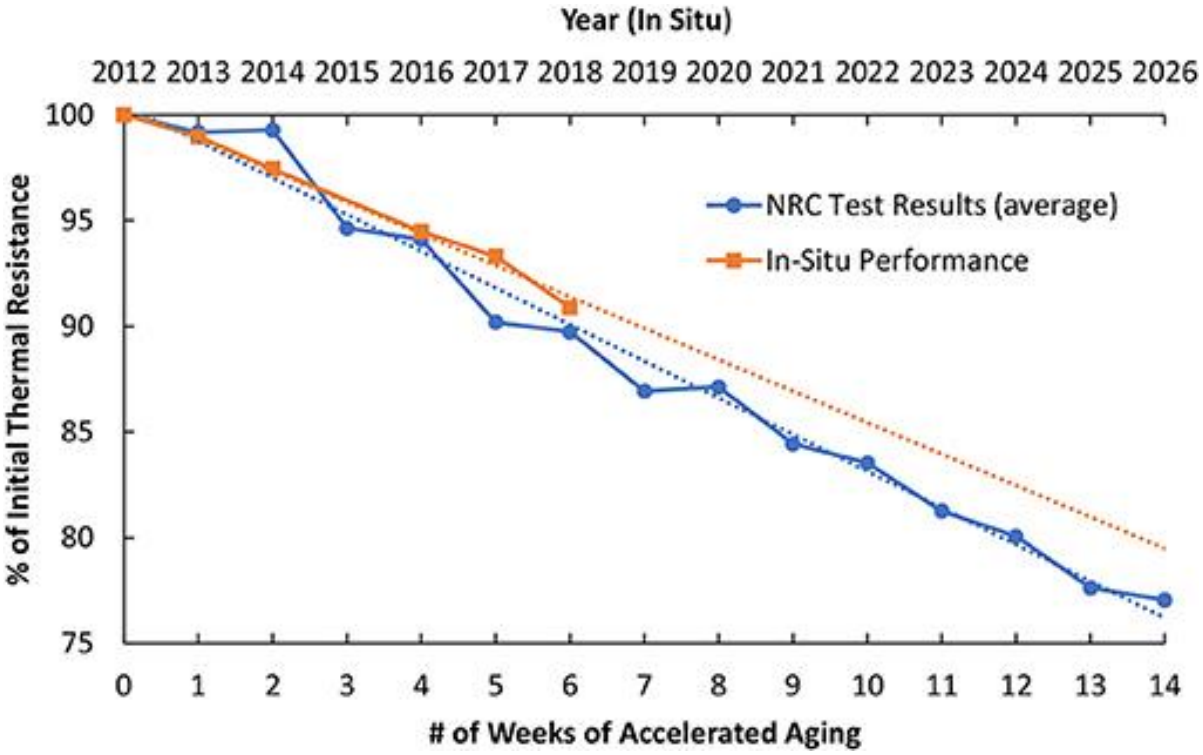

Figure 10. Aging rate of glass fiber core VIP in terms of pristine thermal resistance as a function of time determined from in situ performance and laboratory accelerated aging test results.

The small divergence between the accelerated aging test and the actual field performance of VIPs could be attributed to the different environmental (boundary) conditions that the VIPs were exposed to. Accelerated aging tests were conducted with the exposure in cyclic conditions of extreme high temperature and relative humidity (23°C, 95% and 70°C, 5%), while the in situ performance study was carried out in the subarctic climate of Whitehorse, Yukon with lower temperatures and high RH (an average of -13°C and 75% RH over winter months and an average of 11.5°C and 62% RH over summer months [22]). Since the permeability of gas through the VIPs envelope increases with temperature, the VIP aging rate is slower when subjected to lower temperatures. It is also to be noted that the XPS foam on both sides of the VIPs resisted water vapour movement and absorbed some amount of water vapour, thus buffering the VIP's exposure to moisture. Overall, the linear aging trends from in situ measurements and laboratory accelerated aging test results are quite similar. Additional field and accelerated aging test observations are required to elaborate on the relationship between VIP type, environment and comparison to laboratory tests and to establish more general rules or protocols for the prediction of long-term performance of glass fiber core VIPs.

2.6 Prediction of Service Life

The typical relationships between the thermal conductivity and internal pore pressure for glass fiber and fumed silica core VIPs are shown in Figure 11 [10]. These relationships clearly indicate that the rate of increasing thermal conductivity with pore pressure (i.e. the aging rate) of VIPs is

not linear during their service life. Derived from Figure 11, Figure 12 shows the aging of glass fiber and fumed silica core VIPs in terms of their initial thermal resistance as a function of internal gas pressure.

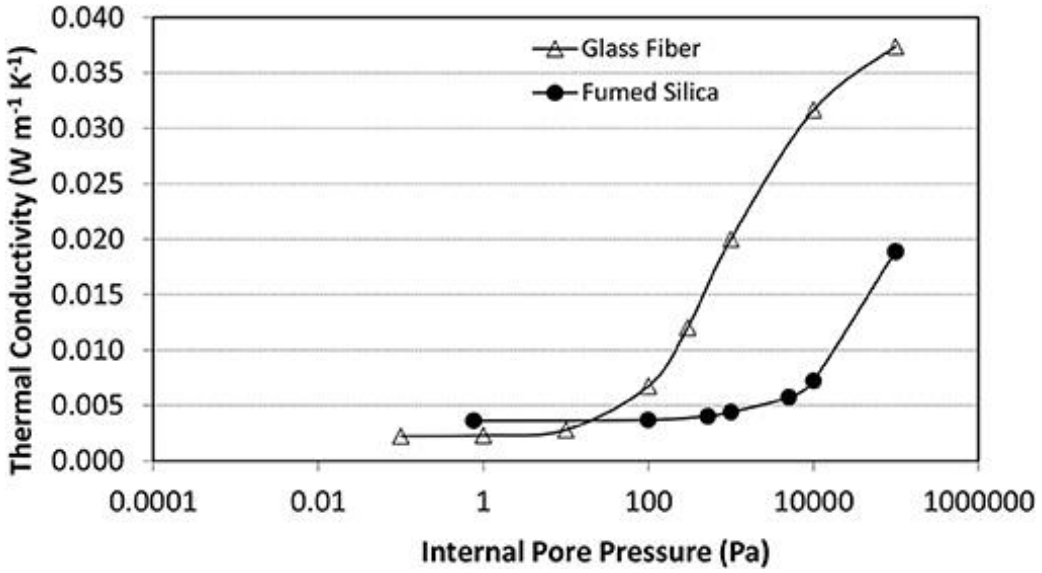

Figure 11. Typical thermal conductivity of glass fiber and fumed silica VIPs as a function of internal pore gas (air) pressure [14].

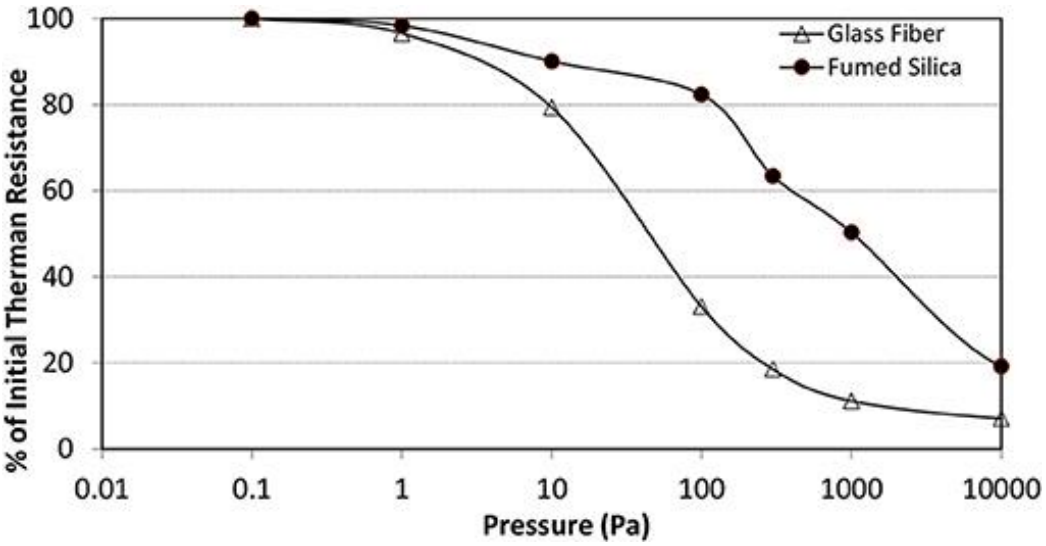

Figure 12. Aging of glass fiber and fumed silica core VIPs in terms of their initial thermal resistance as a function of gas (air) pressure (derived from Figure 11).

Figure 12 indicates that glass fiber core VIPs lose about 20% of their initial thermal resistance when the internal pore pressure reaches about 10 Pa and that this change of thermal resistance is almost a linear function of time. However, Figure 11 also shows that the thermal conductivity of glass fiber core VIPs will rise at a much faster rate between an internal pressure of 10 Pa and

100 Pa, but still thermal conductivity stays below 0.007 W/m·K at 100 Pa internal pore pressure. These observations further reinforce the relationship between accelerated aging and in situ performance of glass fiber core VIP presented in the previous section. Though in situ decrease in the thermal resistance is found to be slow and vary linearly with time until now. It is expected that the thermal resistance of glass fiber core VIPs will eventually decrease at a much faster rate. Hence, the in-situ performance observations in the coming years will be of particular interest and will help us to establish the true relationship between accelerated aging test results and the long-term in situ performance of glass fiber core VIPs.

2.7 Conclusions and Outlook

The results from the energy retrofit project in the Canadian subarctic climate in Whitehorse, Yukon, using a foam-VIP-foam sandwich (i.e., XPS-VIP-XPS) insulation have demonstrated the promising and satisfactory performance of glass fiber core VIPs over a period of eight years. Analysis of the temperature data from monitoring each insulation layer over a period of eight years (2011-2018) has shown a less than 0.9% per year change in the field thermal performance of the VIPs, which indicates that aging of glass fiber core VIPs in cold climate proceeds at a very slow rate. Moreover, this project has shown that many perceived challenges (i.e. handling, installation, etc.) relating to the application of VIPs in the construction industry could be addressed through careful planning and detailing. Ongoing in situ temperature monitoring of this project provides valuable field data that can be used for validating theoretical VIP aging predictions and laboratory accelerated aging results.

2.8 Funding

Funded by Energy Mines and Resources (Yukon Government).

2.9 Conflict of Interest Statement

The authors declare that the research was conducted in the absence of any commercial or financial relationships that could be construed as a potential conflict of interest.

2.10 Acknowledgements

The authors appreciate the support of Panasonic Canada Inc. and Panasonic Corporation for supplying the vacuum insulation panels used for this project. The authors gratefully acknowledge the National Research Council Canada (NRCC) for providing technical expertise and support. The authors would like to thank Yukon Housing Corporation for providing a wall on one of their buildings for this project, and for providing monitoring equipment and for assistance with data collection and handling. Cold Climate Innovation, Yukon Research Centre, Yukon College, and the Energy Solutions Centre must also be credited for providing financial and technical supports for this collaborative project.

CHAPTER 3 LABORATORY AGING TEST

3.1 ABSTRACT

Vacuum Insulation Panels (VIPs) present 5-10 times better thermal resistance per unit thickness comparing to other traditional insulation materials. However, the degree of degradation in thermal performance of VIPs over longer periods (25-50 years) is uncertain, and this uncertainty is one of the major obstacles preventing VIPs from being adopted as building insulation materials in Canada. This study investigated the impact of high temperature and high humidity on the thermal conductivity of glass fiber core VIPs. Two sets of tests were conducted in laboratory, one under 70°C, and the other under 70°C and 95% RH. Experimental results of the thermal conductivity for these VIPs are reported and analyzed. The aim is to use simple accelerate aging test methods to separate the impact of dry air diffusion from water vapour transmission on the thermal conductivity of VIPs.

3.2 INTRODUCTION

Vacuum insulation panels (VIP) can achieve high thermal performance mainly because the vacuum inside the panels has reduced heat transfer via gas conduction. Air and water vapor permeating through the envelope with time will cause irreversible rise of internal pressure inside the panel and moisture accumulation in the core material. Consequently, the thermal conductivity of VIP will increase, and the long-term thermal performance and the service life of VIP are affected. In this section, the thermal performance of a commercially available glass fiber core VIP was investigated in controlled accelerated laboratory conditions. The aim of this study is to distinguish the effect of water vapour from the dry air on the thermal performance degradation of VIPs.

3.3 LITERATURE REVIEWS

3.3.1 Heat Transfer Mechanisms of VIP

A VIP consists of evacuated porous core materials enclosed in multi-layered heat-sealed envelope. The core is open porous so that the air can be evacuated to create a vacuum. The air and vapour tight envelop maintains the vacuum inside the panel [12]. Since the panel is completely vacuumed and there is no heat transfer due to gas, the initial thermal conductivity of VIPs is due to solid conduction within material skeleton and radiation between internal pore surface only.

Opacifiers, desiccants, and getters are usually added to glass fiber VIPs. Opacifiers minimize heat transfer via radiation. Desiccants entrap moisture due to their highly hydroscopic molecular structure. In order to maintain low pressure inside the panel, the highly porous structures with large surfaces of getters are used to attract and bond with gas molecules. Core materials like fumed silica have properties like getters and desiccants, while glass fiber core does not. Therefore, getters and desiccants are essential for glass fiber core VIPs [12].

The thermal conductivity in VIPs can be described as [8]:

$$\lambda_{tot} = \lambda_{cd} + \lambda_g + \lambda_r + \lambda_{cv} + \lambda_{coup} \qquad \text{Equation 1}$$

Where λ_{cd} is the solid conduction within material skeleton, W/(m·K);
λ_g is the conduction of gas molecules within the material pores, W/(m·K);
λ_r is the radiation heat transfer between internal pore surfaces, W/(m·K);
λ_{cv} is the air and moisture convection within pores, W/(m·K);
λ_{coup} is the thermal conductivity accounting for second order effects between the above-mentioned terms.

In theory, the coupling term λ_{coup} in the Equation 1 is to account for the interaction between the first four terms in Equation 1, this term is described more in detail by Heinemann [23]. However, this term is very complex, so it is neglected in most theoretical approaches to VIP thermal performance. Another view is that this term accounts for the gas molecules and the solid material interaction in the pore walls, and this effect is included in a factor when the gas conductivity is calculated using Knudsen effect, which will be briefly described below.

VIP has low thermal conductivity because its gas conduction term is being reduced to almost zero as the pressure decreased to zero in the core material. This is because of the Knudsen effect that relates the gas conductivity to the pore size of a material and the number of gas molecules [8]. As the pressure decreases, the distance that a molecule travels between collisions decreases. When the pore diameter of the material becomes less than the average free length of the path of gas molecules, the molecules will only collide with the pore surfaces without transferring energy. Therefore the gas conduction could be eliminated at very small pressure [8].

The gas conduction in a porous material can be described as [8]:

$$\lambda_g = \frac{\lambda_{g0}}{1+2\beta K_n} \qquad \text{Equation 2}$$

Where $K_n = \frac{l_m}{\delta}$ is the Knudsen number;
β is a constant characterizing the energy transfer efficiency between the gas molecules and the solid-state pore walls, close to 1.5;
λ_{g0} is the free air conductivity, W/(m·K);
l_m is the mean free path of air, m;
and [8]:

$$l_m = \frac{k_B T}{\sqrt{2}\pi d_g^2 P_g} \qquad \text{Equation 3}$$

δ is the characteristic size of pores, m;
k_B is the Boltzmann's constant, J/K;
T is the temperature, K;
d_g is the diameter of the gas molecule, m; and

P_g is the gas pressure, Pa.

Equations 2 and 3 above were used to obtain the Equation 4 for the thermal conductivity of air in porous media [8]:

$$\lambda_g = \frac{\lambda_{g0}(T)}{1+C\frac{T}{\delta P_g}} = \frac{\lambda_{g0}(T)}{1+\frac{P_{1/2}}{P_g}} \qquad \text{Equation 4}$$

Where $P_{1/2}$ is the pressure at which thermal conductivity reaches one half the value of λ_{g0} and C is constant defined as $2\beta k_B/(\sqrt{2}\,\pi d_g^2)$.

Equation 4 shows the three important factors in determining the thermal conduction of gas are gas pressure, characteristic pore size and temperature [24].

3.3.2 VIP Aging Theories

The thermal performance of VIPs depends on how close the inside of the panel is close to vacuum and the dry state of the core. Therefore, any gain of gas through permeation across the envelope will decrease VIP's thermal resistance. Other than when VIPs envelope get damaged by external forces or due to low quality in the production process (material defects, design blunders, assembly errors etc.), the most important factors that are studied in evaluating VIP aging are the gas and moisture transport into the panels. For dry air gas such as oxygen and nitrogen, the transport is through macroscopic (order of 0.1 – 1.0 μm^2) defects in the envelope. On the other hand, the transport of water vapour is through the dissolution of water molecules in the polymers and the condensation in capillaries [8].

As evidenced in Equation 4 above, temperature, moisture and pressure are the primary factors affecting VIP aging. Other factors influencing VIP aging including gas and vapour permeation properties of barrier, off gassing of core materials, capacity of getter and desiccant, and pore structure of core materials.

Service life of VIPs is the time from the product production to the failure, which is indicated by when the product reached a specific thermal performance. For VIP application in building industry, a minimum service life of 25 to 50 years is expected, because to repair or change the failed VIP insulation between walls or ceilings would be a challenge. The industry has not yet established an end-of-life value for aged VIPs. One indicator is when the internal pressure of the dry core reaches 50 - 100 mbar, which translates to the dry gas pressure increases 2 mbar annually, and the total service life would be 25 - 50 years. If we ignore the effect caused by water vapour increase in the core, the thermal conductivity of the dry core (fumed silica) would increase from 0.004 W/m·K to 0.006 W/m·K after 25 years and to 0.008 W/m·K after 50 years. Alternatively, researchers sometimes use 0.007 – 0.010 W/m·K as the end of life value at the center of panel thermal conductivity [8].

International Energy Agency (IEA) Annex 39 researched and found the approximate relation for the fumed silica core VIPs that can be used to estimate VIP thermal characteristics as a function

of moisture content and gas pressure [8]. For instance, a linear relation for the hygroscopic isotherm behaviour is [8]:

$$s = \frac{dX_w}{d\varphi} \approx 0.08\%\ mass\ per\ \%RH \qquad \text{Equation 5}$$

Where s is the slope of the sorption isotherm;
X_w is the moisture content, % -mass;
φ is relative humidity, %.

Equation 5 is valid up to about 80% RH. For example, the moisture content at 50% RH is about 4% - mass [8].

The following approximations can be used to determine the influence of moisture content and dry gas pressure on the thermal conductivity of fumed silica core VIPs [8]:

$$\frac{\partial \lambda}{\partial X_w} \approx 0.5\ \frac{mW}{mK\%-mass} \qquad \text{Equation 6}$$

$$\frac{\partial \lambda}{\partial p} \approx 0.035\ \frac{mW}{mK\ mbar}\ in\ the\ range\ up\ to\ 100\ mbar \qquad \text{Equation 7}$$

Where λ is the thermal conductivity, W/(m·K);
p is the dry gas pressure in the pores, mbar.

Assuming gas pressure and water content act independently to the overall thermal conductivity of the VIP, and by simply adding the two factors up we have [8]:

$$\lambda\left(p_{gas}, X_w\right) = \lambda_{evac} + \lambda_{gas}\left(p_{gas}\right) + \lambda_w(X_w) \qquad \text{Equation 8}$$

Where λ_{evac} is the thermal conductivity in the evacuated and dry state;
$\lambda_{gas}(p_{gas})$ is the gaseous thermal conductivity at pressure p_{gas} inside of the VIP;
$\lambda_w(X_w)$ is the thermal conductivity caused by the water content X_w.

3.3.3 Accelerated Aging Tests of VIPs

Accelerated aging tests speed up gas/water vapor penetration into a VIP envelope by exposing the panels to higher than typical temperature and/or humidity in building applications and have been used for this purpose in previous studies of VIPs [8].

Wegger et al. [25] initiated several experiments to evaluate changes in thermal performance of silica core VIP under accelerated conditions including severe temperature, moisture and pressure. The dimensions of the VIP specimen were 100 cm x 60 cm x 2.0 cm and one VIP sample were used for each testing procedure described below:

- Cycling in alternating climate for 8 cycles, each cycle consists of 8 hours at 80 ± 3°C and 16 hours at -15 ± 3°C, then thermal aging at 80 ± 3°C for 180 days.

- Two VIP specimens were exposed to cyclic climate conditions in a vertical climate simulator, one sample is fully exposed in the simulator and one is placed in a wooden frame structure. They were exposed at UV-radiation and IR-radiation giving a black panel temperature of 63 ± 5°C for one hour, then wetting with water, freezing at -20 ± 5°C for one hour and thawing at laboratory climate.

- Exposure to high vapour pressure at 70°C and 90 - 100% RH for 90 days.

The changes in thermal conductivity during aging were quite small comparing to the initial thermal conductivity of the VIPs. The VIPs exposed to high temperature and high humidity had highest thermal conductivity jump. Some physical changes were observed on the VIPs aged under high temperature and the exposed VIP tested in the climate simulator, such as swelling, curing and delamination of the outer layer.

Di et al. [26] investigated the thermal property of VIPs made of glass fiber as core material and three-fold metalized polymer laminate barrier envelopes, and a service life prediction model was proposed based on the Arrhenius law. The size of VIP samples was 40 cm x 40 cm x 2.0 cm, getters were added to core material in some of the samples for comparison purpose. Three samples were kept at 25°C and 50% RH, and the samples went through accelerated aging tests at four different temperatures (20°C, 50°C, 70°C and 80°C), samples were also exposed to unregulated partial water vapour pressure. The gas permeation rate across the envelope barrier was measured using a helium leak detector by differential pressure method in accordance with ASTM D1434 and the thermal conductivity of the VIP samples was measured by a heat flow meter.

This study used Arrhenius equation as theoretical support. Arrhenius law is often used to describe the temperature dependence of the permeability K for polymeric materials [25]:

$$K = K_0 \, exp(\frac{-E_a}{RT}) \qquad \text{Equation 9}$$

Where R is the gas constant, 8.314 x 10^{-3} kJ/(mol·K);
T is the temperature in K;
E_a is the activation energy with the reference range of 20 - 45 kJ/mol.

From the results of the accelerated aging tests, the annual internal pressure increase rates at different testing temperatures were determined from the plots of the pressure versus time graphs. Di et al. then plotted the annually pressure increase rates as a function of temperature in a log versus inverse temperature 1/T graph according to the Arrhenius law [25]:

$$ln\, P = ln\, P_0 - \frac{E_a}{R}\frac{1}{T} \qquad \text{Equation 10}$$

Where ln(P) is the annual pressure increase rate, in Pa/year.

P_0 indicates the Y-intercept, and $-E_a/R$ indicates the slope of fit line.
The linear shape of the plot indicated an Arrhenius-like temperature dependence of the yearly pressure increase rate. The activation energy found from the plot is approximately 24 kJ/mol, which is within the reference range for polymers. The annually pressure increases rate at given temperature can be derived from the plot and corresponding service life for VIPs can be calculated according to a theoretical formula [25]:

$$\lambda_{tot} = \lambda_{evac} + \frac{\lambda_{g0}}{1+(CT/\delta P_g)} \qquad \text{Equation 11}$$

Where λ_{g0} is the thermal conductivity of free air, 0.0242 W/(m·K);
C is a factor defined as $C = 2\beta K_B/\sqrt{2}\pi {d_g}^2$;
β is the parameter that considers the energy transfer efficiency when gas molecules collide the solid structure of the material, for air β = 2.0;
K_B is the Boltzman's constant, 1.38 x 10^{-23} J/K;
d_g is diameter of the air molecules, 3.72 x 10^{-10} m;
δ is the characteristic size of pores;
P_g is gas pressure, Pa.

From the theoretical and experimental results, the authors found that the VIPs with glass fiber as core material and a three-fold aluminum-coated polymer laminate as barrier envelope at 25°C and 50% RH can only last 5 years. However, with the addition of appropriate adsorbent, the study concluded that VIPs can achieve a service life of 20 years.

Di et al. [27] studied two types of glass fiber VIPs whose cores were manufactured using different processes, namely marble melt and flame attenuation. The impact of gas pressure on thermal conductivity of VIPs was estimated using the theoretical formula (Equation 11) based on the Kunsden effect and measured in the lab. The theoretical results agree with the lab measurements at low gas pressure (below 60 Pa), however at high pressure, because the theoretical formula neglected the convection and coupling effect, and coupling effect do exist at high pressure, as a result, the theoretical result is smaller than the measured one. Some samples were kept at constant temperature and humidity (25°C and 50% RH) for a year, and others were stored in high temperature and high humidity (70°C and 90% RH). The results showed that the increase in thermal conductivity for one month in accelerated aging test is approximately equal to that of three years at constant ambient conditions. The thermal conductivity of the samples with getter was about 0.003 W/m·K at three months into accelerated aging (its initial thermal conductivity was 0.0014 W/m·K, had an increase of 0.0016 W/m·K), therefore, it is predicted that the thermal conductivity under everyday conditions will be about 0.005 W/m·K after 15 years.

Kunič [28] evaluated the aging rate of VIP panels as a function of the thermal loads. Specially processed glass fibers core VIPs without any absorbents and silica powder core VIPs were used in accelerated aging test, these VIPs were sealed by multilayer films. The thermal conductivity values of the core materials were 0.0032 and 0.0022 W/m·K, respectively, and the service life was considered ended when the thermal conductivity of VIP panel doubles its initial value.

Accelerated aging test was performed on total 112 VIP sample panels with dimensions of 25 cm x 25 cm in an oven at 100°C, 90°C, 80°C, 70°C and 60°C. The time exposures were from half a day to 3 months and longer. This study used Arrhenius equation as theoretical foundation, which describes the kinetic energy of molecules at absolute temperature according to Maxwell-Boltzmann's distribution of statistical mechanics [27]:

$$k = A \times e^{-\frac{E_a}{R \times T}} \qquad \text{Equation 12}$$

Where E_a is activation energy, J/mol;
R is ideal gas constant;
T is temperature, K;
k is specific rate of reaction, reaction constant factor or reaction speed, 1/s;
A is pre-exponent factor or frequency factor of a certain reaction, 1/s.

After applying the natural logarithm to both sides of the equation, the Arrhenius equation can be expressed as [27]:

$$ln\, k = -\frac{E_a}{R} \times \frac{1}{T} + ln\, A \qquad \text{Equation 13}$$

Given the specific rates of reactions: k_1 and k_2 at two different temperatures, T_1 and T_2, the activation energy can be determined using the following equation [27]:

$$ln\frac{k_2}{k_1} = ln\, a_T = \frac{E_a}{R} \times \frac{T_2 - T_1}{T_1 \times T_2} \qquad \text{Equation 14}$$

Where a_T is coefficient of acceleration of aging due to degradation at elevated temperatures. Arrhenius equation was used to describe temperature dependence of VIP panels' aging process here, and to calculate the activation energy of VIPs. Using the experimentally accelerated aging test results, activation energy obtained from the Arrhenius law, and the basis of the calculated times and temperatures of aging, the study found the relationship between the expected aging period and the degree of aging in terms of aging temperature. The results show that the thermal conductivity of a VIP panel under constant ambient temperature doubles after 26.2 years and its thermal conductivity value reaches 0.012 W/m·K after 48.1 years [27].

Simmler and Brunner [29] estimated the service life of VIPs in a terrace in Switzerland that is primarily insulated with VIPs to save energy. The end of life of silica core VIPs was defined as when the inner pressure of VIP reaches to 100 mbar. The maximum acceptable increase is 2 mbar per year if 50 years of service life is expected. Simmler and Brunner conducted accelerated aging tests on VIP specimens with dimensions of 250 mm x 250 mm x 20 mm under four conditions. 1) constant climate of 80°C and 80% RH for 150 days; 2) cyclic climate of 80°C and 80% RH for 8 hours and then 25°C and 50% RH for 4 hours for 50 days; 3) constant climate of 30°C and 90% RH for 50 days; 4) constant climate of 80°C and dry for 150 days.

Cyclic conditions caused the most air and water vapour permeance on VIPs due to the mismatch of thermal expansion properties between polymer and metal layers in the envelope. Results also found a clear correlation between internal pressure and moisture content, which shows that water vapour the is the main cause for pressure increase. At the fourth condition, where the relative humidity is near zero, the pressure increase is much lower comparing to aging at other conditions and the moisture content inside the envelope is close to zero. The pressure increase rate at the third condition is like that at the fourth condition.

In the service life prediction section, Simmler and Brunner determined the annual inner pressure increase and moisture accumulation at constant 80% RH for various temperatures, by applying the Arrhenius Law and graphing ln(P) vs 1/T, the annual inner pressure increase at any temperature with 80% RH can be estimated. Authors used building simulation tool HELIOS to calculate the surface temperature and heat fluxes on both sides of VIPs for a terrace building in Switzerland that is insulated by VIP. The annual pressure increase was determined to be 2.1 mbar per year and the equilibrium moisture content is about 6.4 mass% at 80% RH, based on these two numbers and integration of Equation 15, authors concluded that the service life is 31.6 years after the initial thermal conductivity has increased by 4 mW/m·K [28].

$$\dot{\lambda} = \frac{\partial \lambda}{\partial p}\dot{p}(T,\varphi) + \frac{\partial \lambda}{\partial u}\dot{u}(T,\varphi) \qquad \text{Equation 15}$$

Where p is the inner pressure, mbar;
T is the temperature, K;
φ is relative humidity;
u is moisture accumulation, mass%.

Kim et al. [30] evaluated the thermal performance and internal pressure of VIP products on the Korean market and analyzed their long-term performance after accelerated aging. Two VIP samples A and B with fumed silica core and a metalized film envelope from two different manufactures were studied under accelerated aging tests. The size of the samples was 300 mm x 300 mm x 20 mm. The samples were placed in a temperature and humidity chamber with recurring temperature changes at 12-h intervals from 80°C to -15°C. Thermal conductivity of the samples were tested prior to, 8 days and 16 days after the aging test using a heat flow meter. Internal pressure was tested prior to and 8 days after the aging test using pressure compensation method in a vacuum chamber. Results showed that there is 1.8% and 0.5% increase in thermal conductivity in sample A and B after 8 days, and 7.5% increase for sample B after 16 days comparing to the initial thermal conductivity. The internal pressure determined using pressure compensation method before aging for sample A and B were 240 Pa and 170 Pa respectively, and the pressure increased slightly to 300 Pa and 180 Pa after aging. Kim et al. used the long-term thermal performance prediction equation (Equation 16) of VIPs to calculate the expected thermal conductivity after 25 years. The calculated results are 7.9 mW/m·K and 8.1 mW/m·K respectively, which are slightly higher than anticipated values.

$$\lambda_a(t) = \lambda_{90/90} + \lambda_p \times P_a \times t + \lambda_{XW} \times X_{w,eq} \times (1 - e^{\left(-\frac{t}{\tau}\right)}) \qquad \text{Equation 16}$$

Where $\lambda_{90/90}$ is the 90% fractile with a confidence level of 90% for the thermal conductivity, W/(m·K); λ_p is the pressure increase of the thermal conductivity, (W/m)KPA/year; P_a is the annual increase of internal pressure of the VIP (Pa/yr), t is a time constant, year; λ_{XW} is the humidity dependent increase of the thermal conductivity (W/m K)/mass-%, $X_{W,eq}$ is the water content at 23 °C, 50% RH (mass-%); and τ is the time constant humidity compensation mass-%/(mass-%/yr).

Mukhopadhyaya et al. [16] conducted laboratory accelerated aging tests at National Research Center of Canada. Three glass fiber core VIPs went through cyclic aging conditions, one week under 22°C and 95% RH, next week under 70°C and less than 5% RH for total 14 weeks of exposure. The dimensions of the specimens were 560 mm x 460 mm x 12 mm, and the average aging rate was found to be 3.29% per cycle.

Mukhopadhyaya et al. [31] presented the results and observations from laboratory, accelerated aging and field aging tests performed on VIPs with various sizes and geographical origins collected over 10 years. The paper also proposes laboratory accelerated aging test conditions, supported by available field performance test data, to predict the long-term thermal performance of VIPs to be used in building envelope applications.

Four testing conditions together representing the extremes of building envelope exposure conditions were considered in accelerated aging tests, 90°C and ambient RH; 23°C and 95% RH; -30°C and ambient RH; and 70°C and 95% RH. The testing duration of these conditions was 90 days. Five different types of VIPs were used in this study, they were from different manufactures and made with different core and envelope materials. The dimensions of the VIPs were between 300 mm x 600 mm (length) to 300 mm and 600 mm (width) x 8 mm to 40 mm (thickness). The average aging values after 30 and 90 days were found to be 5% and 8%, respectively. The results have shown that 1) high temperature and high humidity aging condition causes the maximum thermal resistance degradation of VIPs, 2) very cold temperature have least or no impact on the degradation of VIPs' thermal resistance, and 3) the degradation performances in 30 and 90 days are consistent. Based on the published research findings, Canadian field performance data, and the results from accelerated aging tests in this study, the authors predicted that the thermal degradation response of VIPs exposed to Canadian cold climate is about 1.5% per year. Furthermore, for VIPs satisfying thermal performance requirements proposed by authors are expected to age 2% per year and the thermal resistance would be about 70% of their initial value after 15 years.

3.4 Methodology

3.4.1 Test samples

This study evaluated the thermal performance of six glass fiber core VIP specimens in accelerated laboratory conditions. The VIP specimens used in this study were manufactured by Panasonic. Glass fiber VIP consists of glass fiber (glass wool) core, getter, desiccant and multi-layer metalized film barrier (Aluminum foil film on one side and aluminum metalized film on the other side). The size of the samples was 300 mm x 300 mm x 25 mm, as shown in Figures 13 and Figure 14.

Figure 13. Layers of glass fiber sheet inside the VIP specimen.

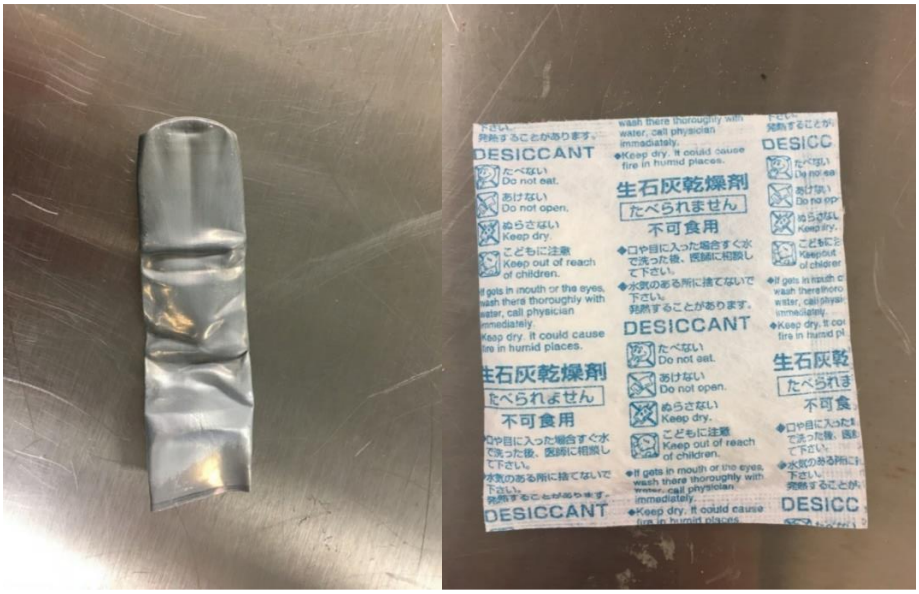

Figure 14. Getter (left) and desiccant (right) were placed between the glass fibre sheet in the VIP specimen. Getter is used to absorbing the gas from core material outgassing and permeated through the envelope from outside. Desiccant is used to absorb the moisture permeated through the envelope from outside.

3.4.2 Test Conditions

Laboratory accelerated aging tests were carried out in the following three conditions:

Condition 1: Three specimens were placed at (70 ± 1)°C and (0 ± 5)% in a gravity convection oven from November 7, 2018 to April 1, 2019, total about 22 weeks.

Condition 2: Three specimens were placed under (70 ± 1)°C and (95 ± 5)% RH in an in-house customize built climate chamber, from January 14, 2019 to May 13, 2019, total about 17 weeks.

Condition 3: Three specimens were kept under laboratory room conditions, which is about (23 ± 2)°C and (50 ± 5)% RH, from November 7, 2018 to May 13, 2019, and they were used as the control of this experiment.

Thermal conductivities of the specimens were taken approximated every 5-10 days for the period before February 28, 2019 and once a month in March, April and May 2020. Before each thermal conductivity measurement, the specimens were taken out of the oven and the climatic chamber and conditioned in laboratory room for 24 hours.

3.4.3 Test apparatus

The thermal conductivities of the specimen were measured using a heat flow meter (HFM 436 Lambda, shown in Figure 15) in laboratory, following the procedures outlined in *ASTM C1667-15 Standard Test Method for Using Heat Flow Meter Apparatus to Measure the Center-of-Panel Thermal Transmission Properties of Vacuum Insulation Panels*. The initial thermal conductivity and weight of the samples was measured and recorded.

Figure 15. Heat flow meter, model number: HFM 436 Lambda. It was used to measure the thermal conductivity at centre-of-the panel of the VIP specimens in the lab.

The heat flow meter consists of a hot plate and a cold plate, heat flux sensor and a thickness measurement sensor. Specimens were tested between two heat flux sensors in fixed temperature gradients. As the test progresses toward equilibrium, temperature and heat flux readings were taken once each minute from sensors embedded in the two plates. After the system reached equilibrium, the external computer determines the thermal conductivity of the sample under steady-state conditions. The heat flow meter method complies with *ISO 8301 – Standard test technique for measurements of insulating materials using the heat flow meter method* and ASTM C518 American standard for measurements of insulating materials using the heat flow meter method. Expanded polystyrene (EPS) foam was used as calibration test panel according to Test Method C518.

The measurements were collected at mean temperature of 24°C, temperature gradient between the cold and hot plates in the heat flow meter was 20°C. Specifically, the cold side temperature was set to 14°C and the hot side was set to 34°C.

Update rate is every 1-minute, rough block size is 15 points, maximum rough error is 1.0 %, fine block size is 10 points and maximum fine error is 0.3%. Meaning that the equilibrium was reached when the last ten successive readings of thermal conductivity fall within 0.3% of the mean value of these 10 readings, and these 10 readings must not show a monotonic variation.

However, since the thermal conductivity of the specimens is extremely low, the measurements required a very long settling time comparing to more conductive insulation materials. In addition, because the VIP sample used in this study consists of a getter and a desiccant, in addition to layers of glass fiber sheets. Therefore, the samples are not only non-homogeneous, but one side of the panel also had noticeable irregularities after the gas inside the envelope was vacuumed due to the existence of the getter, see Figure 16 below. Each measurement was running more than 8 hours, and the equilibrium was never reached for samples with thermal conductivities lower than 0.04 W/m·K. Thermal conductivity value for such scenarios was the mean value calculated from the data obtained in the eighth hour of measurement.

Figure 16. Back side of the VIP sample, showing obvious indentation caused by getter after vacuum.

The thermal conductivity value recorded in this study reflects the heat flow through the evacuated region and through the envelope material.

VWR gravity oven (Figure 17) was used to heat up the air in it to 70°C. Three VIP samples were placed in it; the arrangement was to maximize the air convection around the samples, see Figure 18. A temperature and humidity sensor was placed in the oven to monitor the climatic conditions during the aging tests (Figure 19).

Figure 17. VWR gravity convection oven, a laboratory device designed for heating samples at operating temperatures between 50°C and 250°C. This oven is equipped with precise temperature control, and it is adjustable in steps of one degree.

Figure 18.Three glass fibre core VIP specimens were placed in the oven, arranged in a way that none of the envelope edges were touching the inside wall of the oven, for the purpose of allowing maximum possible air convection to occur around the specimens and as evenly distributed as possible.

Figure 19. Omega-62 temperature and humidity data logger was placed next to the samples in the oven to monitor the actual temperature and humidity.

The in-house custom-built climatic chamber (Figure 20 – 24) consists of a heating pad at the bottom of a water tank. The water tank is covered by insulating foam and is placed in a large plastic box. To achieve high humidity in this climatic chamber, we put some water in the water tank and water vapour filled up the tank after turning on the heat pad. A temperature sensor is placed in the water to monitor the temperature inside the water tank.

Figure 20. Picture showing the oven and climatic chamber (blue) that were used for aging tests.

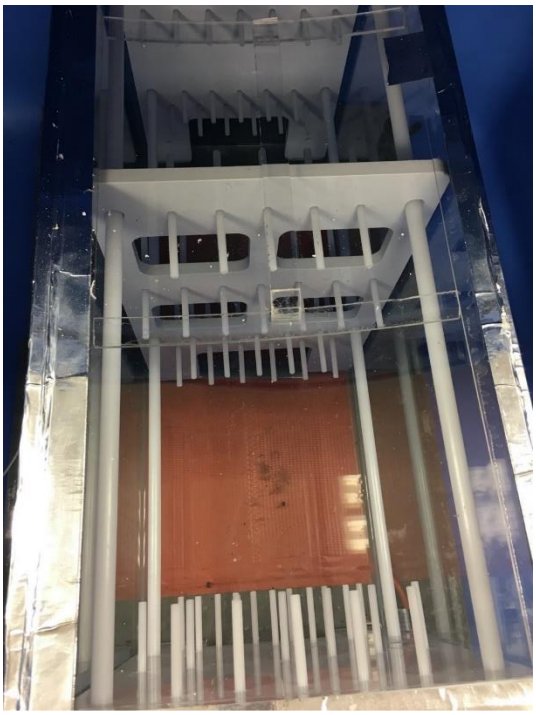

Figure 21. Picture of inside of the in-house custom-made climatic chamber, showing a container sitting on a heating pad, there are some water at the bottom of the container and the racks for holding the VIP specimens.

Figure 22. Picture of the in-house custom-made climatic chamber, right after its lid was lifted, it was full of water vapour after the water being heat up to 70°C.

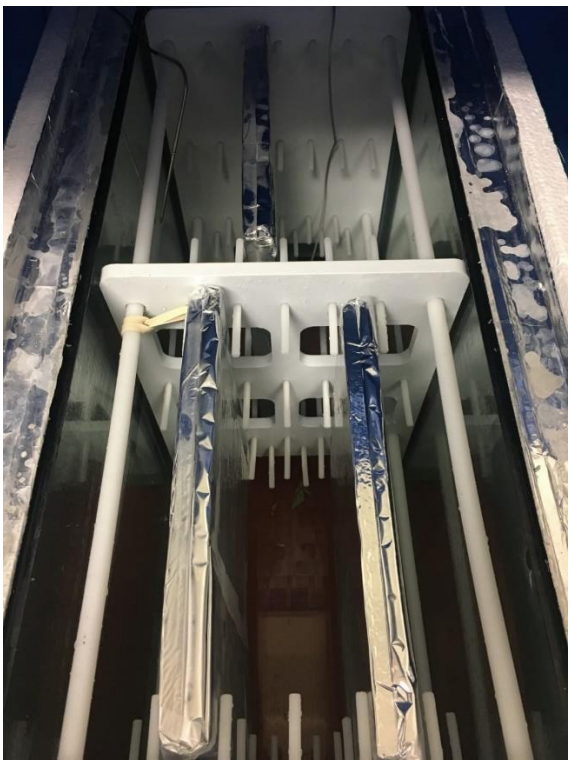

Figure 23. Picture of the in-house custom-made climatic chamber and the glass fibre VIP specimens.

Figure 24. Condensation occurred at the surface of the glass fibre VIP specimen, and the photo was taken right after the sample was removed from the climatic chamber.

A thermal conductivity of glass fiber core VIPs with respect to its internal pressure generated in Germany was found in literature [32] and presented in Figure 25.

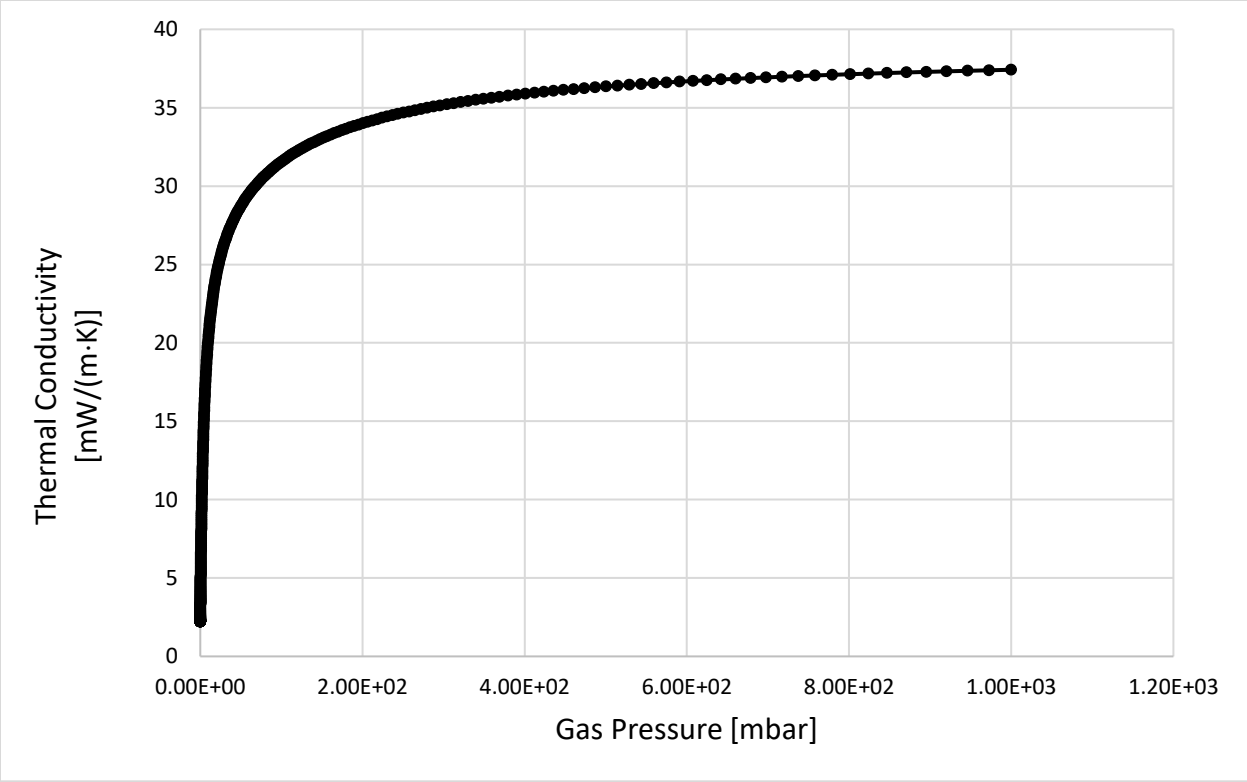

Figure 25. Relationship between the thermal conductivity and internal gas pressure inside glass core VIPs, generated in Germany [32].

3.5 Results and Discussion

The weight and thermal conductivity of three VIP samples aged at 70°C are summarized in Table 2 below, and for the three VIP samples aged at 70°C and 95% RH are summarized in Table 3. For the three control samples placed in room conditions, the weight and thermal conductivity stayed the same over the course of the experiments.

Table 2. Measured weight and thermal conductivity of three VIP samples H1, H2 and H3 aged at 70°C, and the internal gas pressure corresponding to the averaged thermal conductivity of three samples. The internal gas pressures are interpolated from the thermal conductivity-pressure curve for glass fiber VIP generated in Germany (See Figure 25 above).

#	Date	Sample H1		Sample H2		Sample H3		Average	
		Weight (g)	λ (mW/m·K)	Weight (g)	λ (mW/m·K)	Weight (g)	λ (mW/m·K)	λ (mW/m·K)	Internal Pressure (mbar)
1	**Nov 09, 2018**	597.62	2.954	629.41	2.402	610.08	2.374	2.577	0.065734
2	**Nov 19, 2018**	597.20	2.662	629.29	2.402	608.04	2.520	2.528	0.055740
3	**Nov 27, 2018**	597.73	2.764	631.63	2.568	608.24	2.715	2.682	0.085969
4	**Dec 05, 2018**	597.24	2.794	630.16	2.637	607.93	2.747	2.726	0.094498
5	**Dec 13, 2018**	597.33	2.719	629.35	2.652	607.08	2.719	2.697	0.085389
6	**Jan 14, 2019**	597.13	3.250	629.35	3.628	608.00	3.959	3.612	0.272622
7	**Jan 23, 2019**	597.23	3.335	629.18	3.709	608.01	4.129	3.724	0.296040
8	**Jan 30, 2019**	597.15	3.813	629.33	4.632	607.98	5.126	4.524	0.469620

9	**Feb 06, 2019**	597.22	4.230	629.31	4.940	607.86	5.370	4.847	0.543005
10	**Feb 14, 2019**	597.20	4.210	629.34	5.275	608.04	5.780	5.088	0.599050
11	**Feb 21, 2019**	597.23	4.350	629.31	5.780	607.98	6.240	5.457	0.687128
12	**Feb 26, 2019**	597.25	4.840	629.32	6.170	607.96	6.700	5.903	0.797388
13	**Mar 14, 2019**	595.99	5.770	629.47	7.120	606.81	7.480	6.790	1.029922
14	**Apr 01, 2019**	597.36	6.760	629.54	8.470	608.29	8.710	7.980	1.372852

Table 3. Measured weight and thermal conductivity of three VIP samples CC1, CC2 and CC3 aged at 70°C and 95% RH, and the internal gas pressure corresponds to the averaged thermal conductivity of three samples. The internal gas pressures are interpolated from the lambda-pressure curve for glass fiber VIP generated in Germany.

#	Date	Sample CC1		Sample CC2		Sample CC3		Average	
		Weight (g)	λ (mW/m·K)	Weight (g)	λ (mW/m·K)	Weight (g)	λ (mW/m·K)	λ (mW/m·K)	Internal Pressure (mbar)
1	**Jan 14, 2019**	616.74	2.708	628.10	2.304	631.48	2.302	2.438	0.039192
2	**Jan 22, 2019**	619.09	2.706	630.06	2.381	639.33	2.316	2.468	0.044896
3	**Jan 28, 2019**	624.25	2.478	635.15	2.478	638.74	2.405	2.454	0.042233
4	**Feb 02, 2019**	626.18	2.819	637.66	2.512	638.86	2.436	2.589	0.068037
5	**Feb 12, 2019**	626.72	2.890	636.85	2.506	638.89	2.550	2.649	0.079591
6	**Feb 19, 2019**	626.22	2.939	637.98	2.546	639.77	2.528	2.671	0.083841
7	**Feb 25, 2019**	626.48	3.290	638.02	3.011	640.58	2.895	3.065	0.161194
8	**Mar 12, 2019**	627.35	3.760	636.70	3.250	642.77	3.430	3.480	0.245289
9	**Apr 01, 2019**	628.22	7.900	639.37	22.350	643.89	24.020	18.090	7.201680
10	**May 13, 2019**	N/A*	34.140	N/A*	33.890	N/A*	35.140	34.390	227.236900

∗ The weight of samples CC1, CC2 and CC3 were not measured on May 13, 2019.

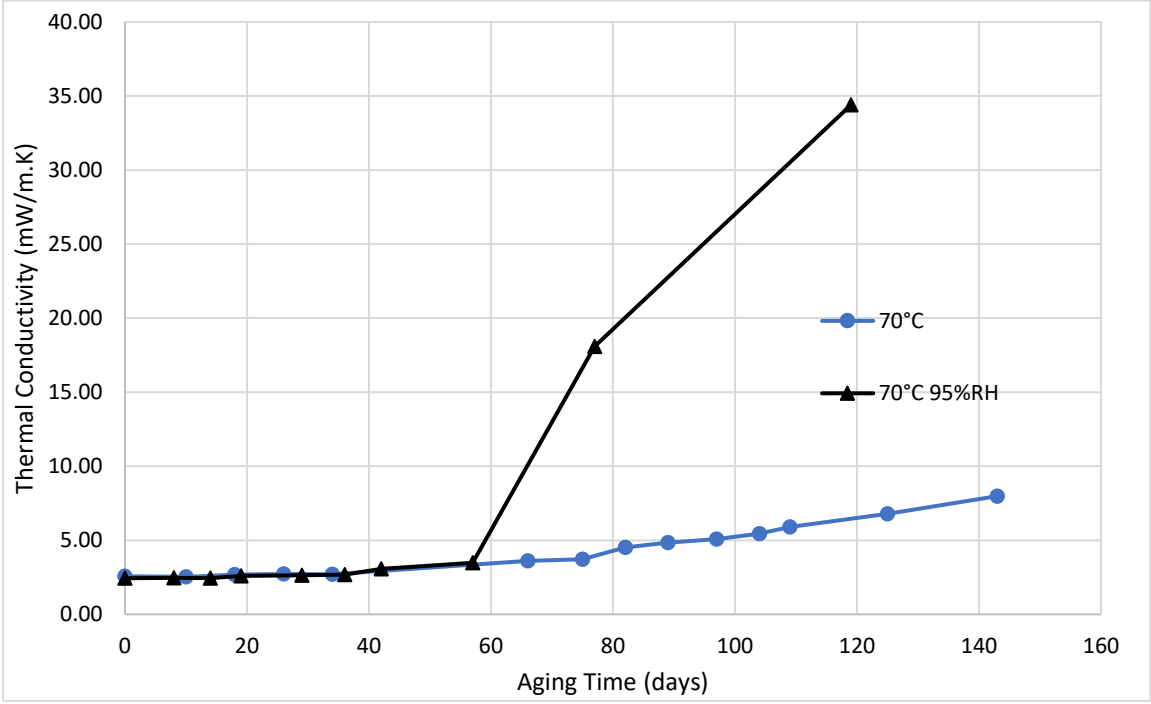

Figure 26. Thermal conductivity of VIPs aged in laboratory (70°C, 70°C and 95% RH) over time.

In Figure 26, thermal conductivity of VIPs increases over time and the trends are similar for test conditions at 70°C and the first part (prior to 58 days) of 70°C, 95% RH. However, an abrupt jump in thermal conductivity for the VIPs aged at 70°C and 95% RH occurred 58 days into the aging test.

This change is due to the water vapour transmitted into the envelope being absorbed by the desiccant (Figure 14) until the desiccant reaches its capacity around day 58. In the first stage (up to 58 days into testing), the rate of thermal conductivity increases at 70°C and 95% RH is similar to the results from VIPs aging at 70°C. The change in thermal conductivity can be explained using the Arrhenius Law (Equation 12), the rate of air transmission across the VIP envelope was accelerated as the VIPs were subjected to high temperature. More air molecules got into the envelope and the internal pressure rises, leading to an increase in thermal conductivity due to gas conduction according to the Knudsen effect. Around day 58, the desiccant reaches its capacity and the water vapour increases the thermal conductivity through heat transfer mechanisms such as water vapour conduction, air-water convection, and additional internal pressure.

Data from 70°C, 95% RH were separated into two stages (aging due to air and aging due to water vapour and air). Data from the first stage were plotted with the results from aging at 70°C (Figure 27), and data from the second stage were plotted in Figure 28.

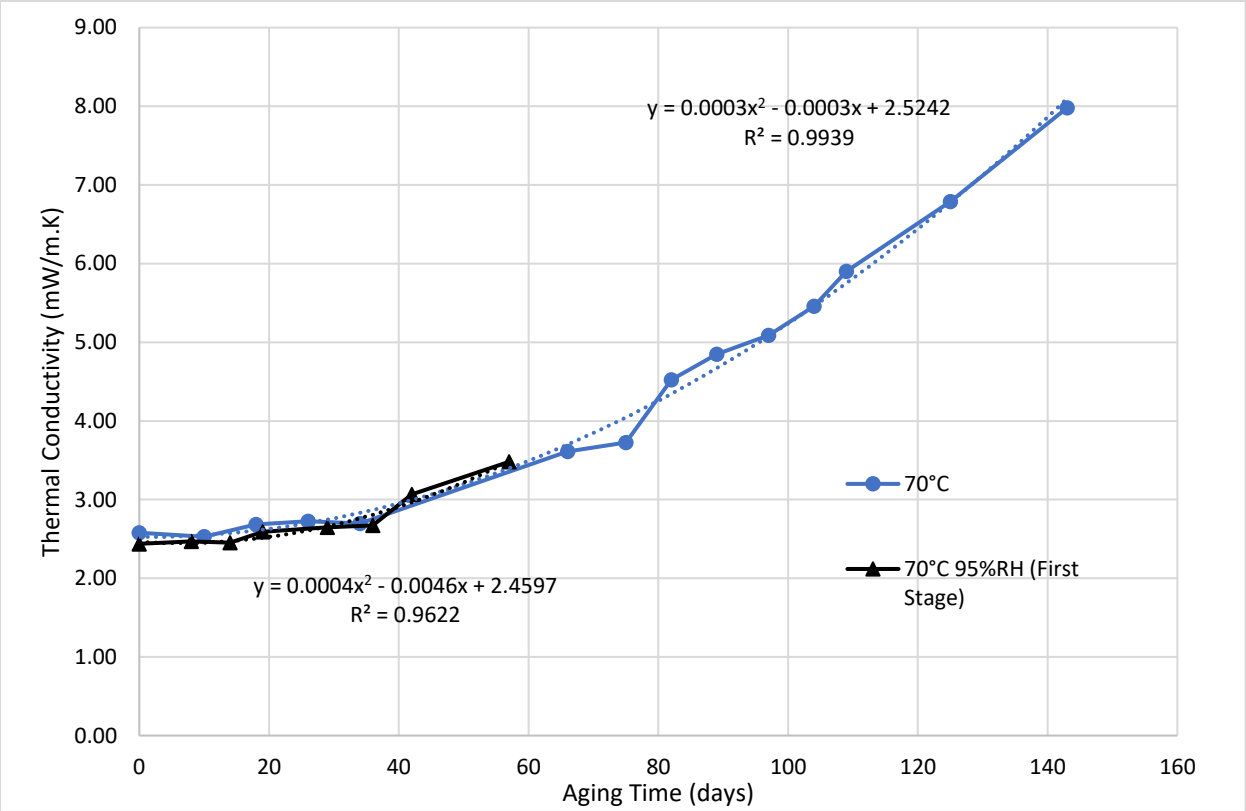

Figure 27. Thermal conductivity of VIPs aged in laboratory (70°C and first stage at 70°C and 95% RH) over time.

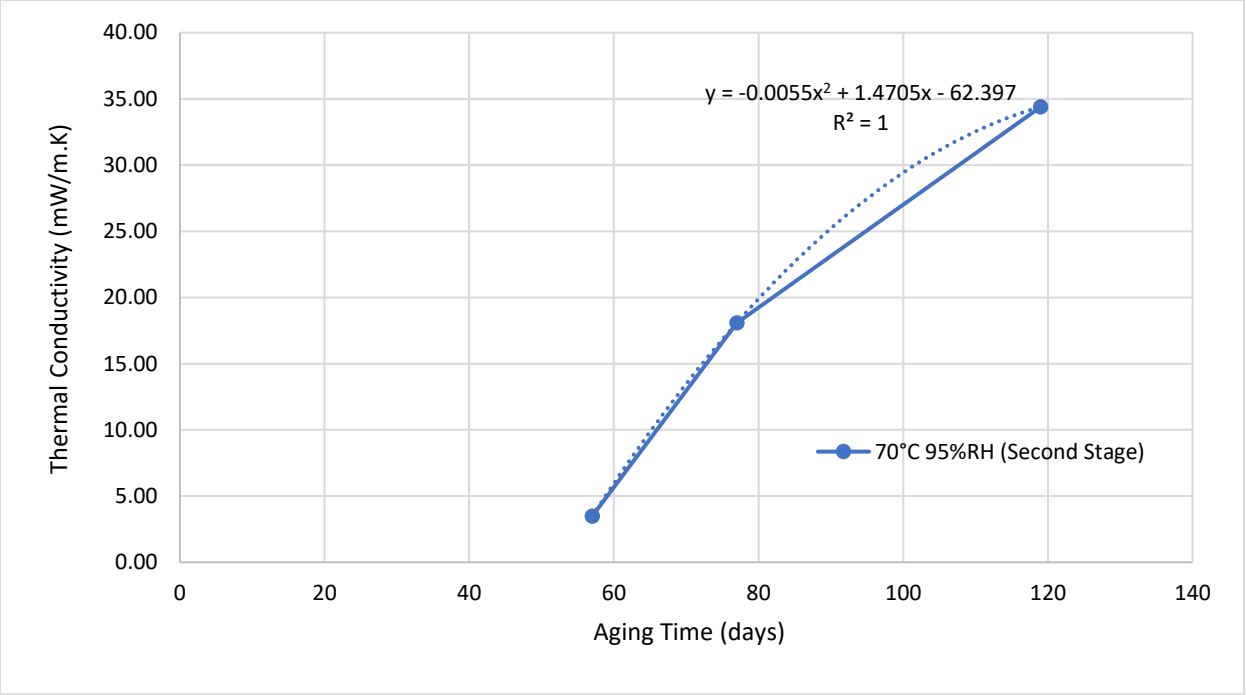

Figure 28. Thermal conductivity of VIPs aged in laboratory (second stage at 70°C and 95% RH) over time.

The mean rate of change in thermal conductivity with respect to aging time due to dry air diffusion was calculated from the rate of change in thermal conductivity observed at 70°C and the first stage at 70°C 95% RH (Figure 27). It can be described as:

$$\lambda_{air}(t) = 0.00035 \times t^2 - 0.00245 \times t + 2.49195 \qquad \text{Equation 17}$$

Where t is in days.

The rate of change in thermal conductivity with respect to aging time due to both dry air diffusion and water vapour is determined from the results obtained at the second stage at 70°C 95% RH (Figure 28):

$$\lambda_{air+vapour}(t) = -0.0055 \times t^2 + 1.4705 \times t - 62.397 \qquad \text{Equation 18}$$

By subtracting Equation 18 from Equation 17, the rate of change in thermal conductivity with respect to aging time due to water vapour diffusion can be determined as:

$$\lambda_{vapour}(\mathrm{t}) = 0.00585 \times t^2 + 1.46805 \times t - 59.9051 \qquad \text{Equation 19}$$

Similarly, thermal conductivity of VIPs with respect to internal pressure was graphed in Figure 29 below. The data were separated into two stages and presented in Figure 30 and 31.

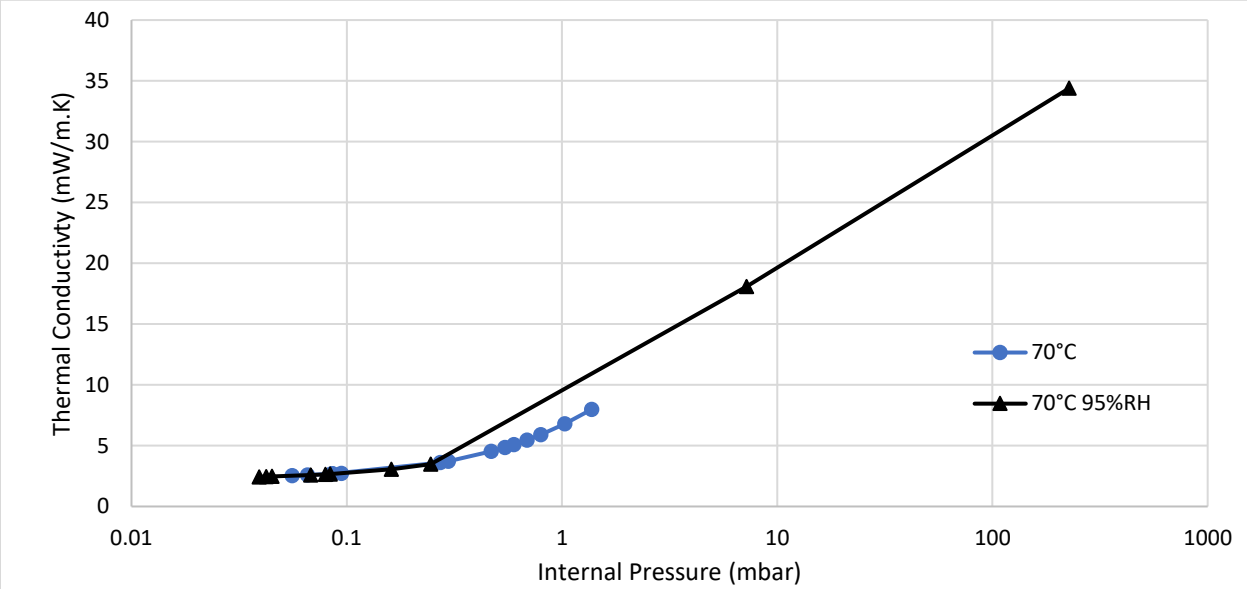

Figure 29. Thermal conductivity of VIPs aged in laboratory (70°C and 70°C 95% RH) with respect to internal pressure, graph in log scale.

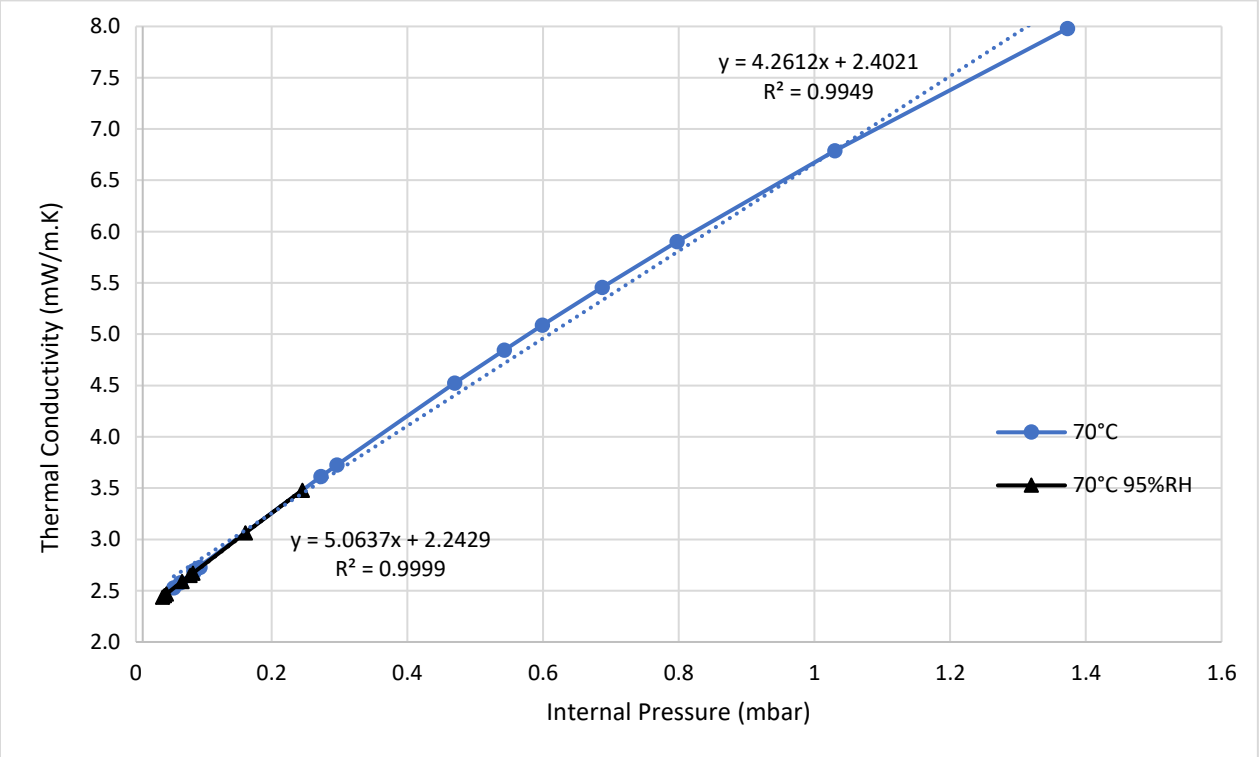

Figure 30. Thermal conductivity of VIPs aged in laboratory (70°C and first stage at 70°C and 95% RH) with respect to internal pressure.

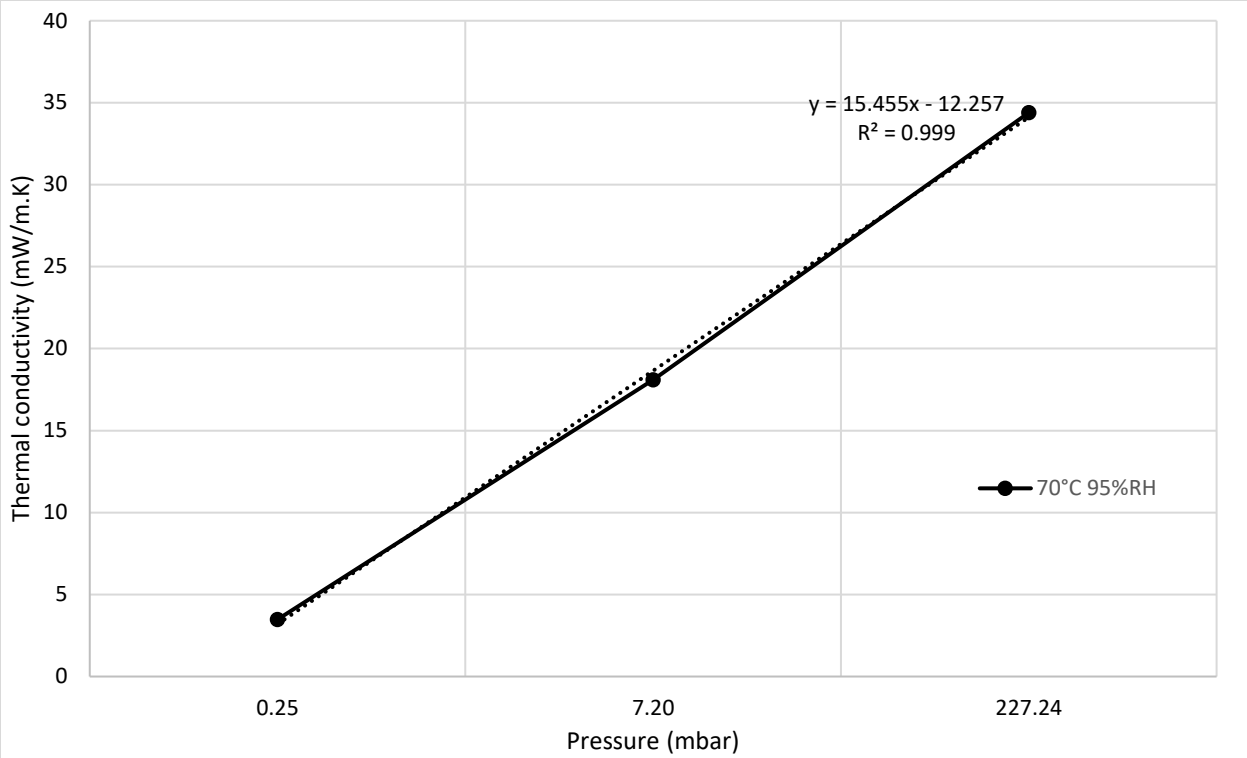

Figure 31. Thermal conductivity of VIPs aged in laboratory (second stage at 70°C and 95% RH) with respect to internal pressure.

The mean rate of change in thermal conductivity with respect to internal pressure due to dry air diffusion was calculated from the rate of change in thermal conductivity observed at 70°C and the first stage at 70°C 95% RH (Figure 30). It can be written as:

$$\lambda_{air} = 4.66245 \times P + 2.3225 \qquad \text{Equation 20}$$

Where λ in mW/(m·K) and P in mbar.

The rate of change in thermal conductivity with respect to internal pressure due to both dry air diffusion and water vapour is approximated from the results obtained at the second stage at 70°C 95% RH (Figure 31):

$$\lambda_{(air+water\ vapour)} = 15.455 \times P - 12.257 \qquad \text{Equation 21}$$

By subtracting Equation 21 from Equation 20, the rate of change in thermal conductivity with respect to internal pressure due to water vapour diffusion can be quantified as:

$$\lambda_{vapour} = 10.79255 \times P - 14.5795 \qquad \text{Equation 22}$$

3.6 Conclusion

Thermal conductivity of glass fiber core VIPs subjecting to high temperature increased in almost linear fashion. While significant changes in the rate of thermal conductivity change was observed in VIPs aging under high temperature and high humidity. This is due to combined effect of dry air and water vapour diffusion, specifically, increased heat transfer inside the panel through gas conduction, water vapour conduction and air-water convection. Based on the results obtained from the aging experiments, equations of thermal conductivity change due to dry air was obtained. Subsequently, equations of thermal conductivity degradation due to water vapour of glass fiber VIPs with respect to aging time, and with respect to the increase of internal pressure were produced.

3.7 Limitations

The inner pressure of the glass fiber core VIPs in this study were not directly measured due to lack of relevant equipment. The most used method to measure internal pressure of the panel is called “lift-off” method, which is to place a VIP specimen in a vacuum chamber and reduce the pressure around the specimen continuously. The envelope laminate will lift off the core surface when the pressure in the chamber reduces below the VIP internal pressure. The distance of the envelope surface is continuously measure with laser distance meters. The “equilibrium pressure” is then determined by analysis of the distance curve [8]. The internal pressure in this study is obtained from interpolating an internal pressure vs. thermal conductivity curve generated by a Germany study on glass fiber core VIPs. However, internal pressure of VIPs can be very sensitive to small environmental changes, and the type of barrier it has. Moreover, internal pressure of VIPs are very small numbers, they are less than 100 mbar, any small discrepancy can lead to inaccurate conclusions.

The thermal conductivity measurements were not taken in smaller time increments due to the scheduling conflicts of the heat flow meter with other researchers. Only three data points were available to construct the curve of changes in thermal conductivity due to diffusion of dry and water vapour, so there was insufficient data to be certain that our curve accurately reflects the relationship between the thermal conductivity increase due to dry air and water vapour with respect to aging time.

We were not able to conduct aging experiments in more than a single combination of temperature and relative humidity in the climatic chamber at a time. The physical properties of the components of VIPs sample were not provided by the manufacture and were not able to determine them in the University laboratory. Therefore, we weren’t be able to cross check our results using the combinations of existing theoretical prediction formulas and relevant laws of physics (parameterized Arrhenius).

3.8 Future directions

Additional accelerated aging experiments of glass fiber core VIPs at different temperature and relative humidity combinations would help to generate results to determine a long-term thermal performance prediction model.

CHAPTER 4 OPTIMIZATION OF THERMAL PERFORMANCE IN WOOD FRAME BUILDINGS

4.1 ABSTRACT

The objectives of this chapter are to investigate the significance of thermal bridges in wood-frame building and evaluate the potential improvement on reducing thermal bridges. Computer modeling software Heat3 was used to create and simulate simplified models of cantilever, ledger, and rim joist balcony/wall junctions. By creating scenarios with different combinations of wood types, joist/slab spacing, wall sizes, and adopting the state-of-art innovative insulating materials – Vacuum Insulation Panels for the junction cavity, the thermal loss due to thermal bridging were calculated and compared. The best performing design parameter combinations were identified and recommended for each balcony type.

4.2 INTRODUCTION

With the recent inclusion of energy step codes in the British Columbia Building Code, as well as the federal government's mandate for all new construction to be Net-Zero by 2030 (2032 in B.C. besides the City of Vancouver), steps are now being taken to reduce our heating and cooling loads in our occupied spaces. These changes are also in updated versions of ASHRAE 90.1 [33] and the National Energy Code of Canada for Buildings [34] with their efforts towards achieving lower thermal transmittance through exterior building envelopes.

The dominance of wood-frame construction in B.C. is plainly visible if one drives through most metropolitan areas, where mid-rise residential construction is dominated by wood-frame construction. The government of British Columbia implemented the Wood First Act in 2009 to promote the use of wood products in provincial projects. As per the Wood First Act, its purpose is:

> *… to facilitate a culture of wood by*
> *requiring the use of wood as the primary building material in all new provincially funded buildings, in a manner consistent with the building regulations within the meaning of the Building Act.*

Even more, the Federal Government of Canada is promoting the use of wood in mid-to-high rise structures with recent modifications to the building code to allow for tall wood structures. These modifications are an attempt to disrupt the dominance of reinforced concrete structures in this domain of construction. The federal government has even gone so far as to create the Green Construction through Wood Program which will cover up to 100% of the incremental costs of going to tall wood structures over conventional systems. The benefits of this program include providing opportunities for economic growth and reducing greenhouse gas emissions [35].

Examples of these tall wood structures include the Wood Innovation Centre in Prince George and the Brock Commons Building at the University of British Columbia [35].

The aim of this study is to promote wood-frame constructions in B.C. by providing a catalogue of the thermal performance of common wood-frame exterior building envelope assemblies and interface details used in B.C. The objectives of this study are to investigate the significance of thermal bridges in wood-frame building and evaluate the potential improvement on reducing thermal bridges. Heat3 3D computer modeling was used to create and simulate simplified models of cantilever, ledger, and rim joist balcony/wall junctions. By creating scenarios with different wood types, joist/slab spacing, wall sizes, and adopting the state-of-art innovative insulating materials – Vacuum Insulation Panels for the junction cavity, the thermal loss due to thermal bridging were calculated and compared. We used these results to create a catalog, and designers can use this catalogue to find the heat flow caused by thermal bridges in their design detail and simply add up the number of occurrences of these thermal bridging to find the overall heat flow caused by thermal bridges in the building envelope.

4.3 Background

4.3.1 Brief Thermal Transmittance Overview

This section briefly discusses the basic principles of thermal transmittance. More in depth information regarding the principles behind thermal conductance through building assemblies can be found in The Building Envelope Thermal Bridging Guide provide by B.C. Hydro [1].

Energy can be transferred through three different phenomena: conduction, convection, and radiation. The thermal analysis completed in this study relies solely on conduction and does not take into account convection nor radiation. Although convection and radiation can play a role in thermal performance and thermal comfort, they rely primarily on the specifics of the built environment (fluid dynamics surrounding the building, orientation of the building with respect to the sun, ect.) and not simply on the physical contact between solid materials.

Conduction relies on the transfer of energy through materials that are in intimate contact, specifically when there is a thermal gradient present through the materials. The thermal resistance of a material is derived from its depth parallel to the direction of the thermal flux, divided by its conductivitiy:

$$R_{material} = {}^{d_{material}}/_{k_{material}} \qquad \text{Equation 23}$$

Where R is thermal resistance ($m^2 \cdot K/W$), d is thickness (m) and k is thermal conductivity ($W/m \cdot K$) of a material.

In simple assemblies where their construction is homogenous across its cross-section, the total thermal resistance can be idealized by the sum of the materials running in parallel to the thermal flux, including the thermal resistance of the interior and exterior air films:

$$R_{total} = R_{si} + \sum_{i=1}^{\infty} {}^{d_i}/_{k_i} + R_{se}$$ Equation 24

Where Rsi and Rse are thermal resistance of the interior and exterior air films respectively.

The overall thermal transmission coefficient is the reciprocal of the overal material resistance:

$$U = {}^{1}/_{R} = \frac{1}{R_{si} + \sum_{i=1}^{\infty} {}^{d_i}/_{\lambda_i} + R_{se}}$$ Equation 25

Where U is the thermal transmission coefficient ($W/m^2 \cdot K$).

The heat load through the specific element is then calculated by multiplying the area of the element by its thermal transmission coefficient and the thermal gradient:

$$P_T = A \times U \times \Delta T$$ Equation 16

Where P is heat load (W), A is area (m^2), and ΔT is temperature gradient (K).

For example, there would be no conduction through a wall that is at 20°C inside and 20°C outside; however, the wall assembly would still have an overall thermal transmission coefficient (U) which defines the wall's ability to resist conduction given a thermal gradient. To put it simply, a highly insulated wall system in a temperate climate would provide less of an advantage compared to one in a cold climate as the thermal gradient through the wall would be considerably less. For instance, a building in Vancouver would have an overall U-value almost twice as high as a building in Prince George but have the same peak load demand based on the winter design temperature normally used when designing home heating systems.

4.3.2 Thermal Bridges

Thermal bridging is the effect of having materials with dissimilar conductivity values running through an assembly. Heat flows from high potential to low potential through the path of least resistance. This increased heat flux through the highly conductive material reduces the assembly's overall ability to resist heat loss as it "short circuits" the insulation.

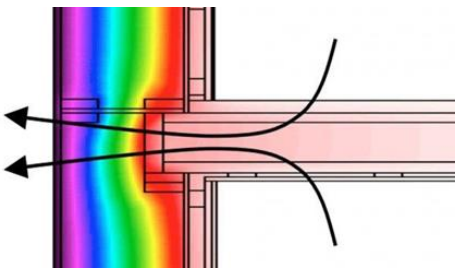

Figure 32. Illustration of a thermal bridge where heat transfers along the least resistance path from the warmer side to the colder side of the assembly [1].

A tangible typical example of how this can affect building performance is what occurs in Toronto, Ontario. Concrete towers with cantilevered concrete balconies create a considerable thermal bridge, causing the floor to become a condensation plate. This condensation eventually leads to frost forming on the floors adjacent to the balcony. The commonly used solution to this problem is to provide base-board-heaters along the curb of the balcony to force more thermal flow out of the building. Although the thermal conductivity of wood is approximately three times less than that of concrete, there is still a potential for moderate heat flow through wood-frame thermal bridges.

4.3.3 Methodology for Determining Thermal Performance of Building Envelope Assemblies

There are two types of opaque building components that are important in assessing the thermal performance of a building envelope that contains a thermal bridge: clear field assemblies and interface details. Simply put, clear field assemblies are wall, roof or floor assemblies that include all the components that form a wall. The effects of thermal bridges included in the clear field transmittance are only those uniformly distributed, and therefore not practical to account for on an individual basis. Examples of components included in clear field assemblies are brick ties. Interface details are alterations in construction or geometry that cause thermal bridging in a clear field. Examples of interface details include slab edges, opaque to glazing or wall transitions, parapets, corners and through wall penetrations. Finding out the thermal performance of both the clear field and the interface details are essential for calculating the impact of heat flows through the thermal bridge on building envelope.

4.3.3.1 Determining Thermal Performance of Clear Field Assemblies

There are three methods that are commonly used to find out the thermal performance of clear field assemblies, namely, hand calculation, heat flow modeling and physical testing. Thermal performance of clear field assemblies is usually expressed in thermal transmittance coefficient (U-value) or effective thermal resistance (R-value).

Hand calculations can be used for simple assemblies with heat flow through thermal bridges occurring in one or two dimensions. For calculating heat flow in one dimensional assemblies, such as a wall or a roof, the R-value of the system is simply the combination of the R-value of each individual layer. For two dimensional steady-state heat transfer analysis through wall assemblies, the approximate overall rate of heat transfer can be calculated by hand using parallel-path method, isothermal-planes method, and the zone method and the modified zone method. The parallel-path method is used when the conductivity of the dissimilar materials in the plane are quite alike (e.g. wood-frame walls). The isothermal-planes method is suitable for materials with conductivities moderately different from those of neighboring materials (e.g. masonry). The zone method and the modified zone method are suitable for materials with a very high difference in conductivity (two orders of magnitude or more), such as with constructions containing metal. Examples of above-mentioned hand calculation methods can be found in the 2017 ASHRAE Handbook Fundamentals [36]. Note these methods do not factor in heat storage in the materials, nor the varying material properties such as temperature or moisture content dependent thermal conductivities.

For some constructions with one dimensional heat flow path, simple hand solution is not suitable. In attics, where the temperature of the assembly is very different from the outside temperature, or in basement walls and floors, where there exists great thermal inertia of soil causing ground temperature varies with depth, and there is significant time lag between changes in outdoor air temperature and corresponding changes in ground temperatures. For complex building envelope geometries where two- and three-dimensional heat flow paths can influence each other, such as corners and junctures of different materials, these assemblies are not appropriate for hand calculations [36]. Computer based finite element software can be used to model and estimate the energy efficiency of these complex assemblies, both 2D (such as THERM) and 3D (such as HEAT3, WUFI PLUS) software are available to perform steady state or transient state simulations.

Thermal performance values of a wide range of typical clear field construction have been determined and made available to public [1].

4.3.3.2 Determining Thermal Transmittance Due to Thermal Bridge

The combined effect of thermal bridges on the thermal transmittance of clear field assemblies and interface details is usually calculated using area-weighted method [37]. This method involves finding the area being affected by thermal bridging and average with the heat transmittance of the unaffected area of the assembly. It is straightforward for assemblies with clear geometry and U-values, such as walls with windows, and when the thermal anomaly is that with low thermal conductivities, such as some wood-frame structures. However, the disadvantages of this method is that finding the affected area can be cumbersome, especially when the heat flow paths are in three dimensions and influences each other, such as at the corner of a roof and exterior wall, where the insulation level of the roof and the exterior wall are different [37], as well as when the thermal bridge anomy is made of moderate to highly conductive materials [1]. In addition, the effects of thermal bridges were averaged over the entire area, making it nearly impossible to know the contribution of each thermal anomaly.

Comparing to the area-weighted method, the linear transmittance method is much simpler for thermal anomalies in opaque building envelope assemblies. In this approach, the total heat flow of the interface detail assembly with thermal bridges minus that of without the thermal bridges is the extra heat flow caused by the thermal anomaly. This value is then expressed as heat flow per linear length or as a point heat flow depending on the type of thermal anomaly.

There are three types of building components involved in this method, clear field, linear anomaly, and point anomaly. A building component example of a linear anomaly would be a slab shelf attached to a wall, and an example of a point anomaly would be a structural beam penetrating a wall [37]. The heat flow through these building assemblies are computed by 2D or 3D modeling software, 3D is used for greater accuracy since most of time the heat flow path is 3 dimensional and they influence each other.

Linear transmittance (Ψ) is the extra heat flow caused by thermal bridges that are linear, such as slab edges. It is a heat flow per unit length. The linear transmittance is calculated by subtracting the clear field transmittance (Q_0) from the overall transmittance of the model including linear

thermal bridge (Q), then dividing the length of the linear transmittance (L), as illustrated below using an example of an exterior insulated steel stud wall penetrated by a cantilevered balcony slab [37]:

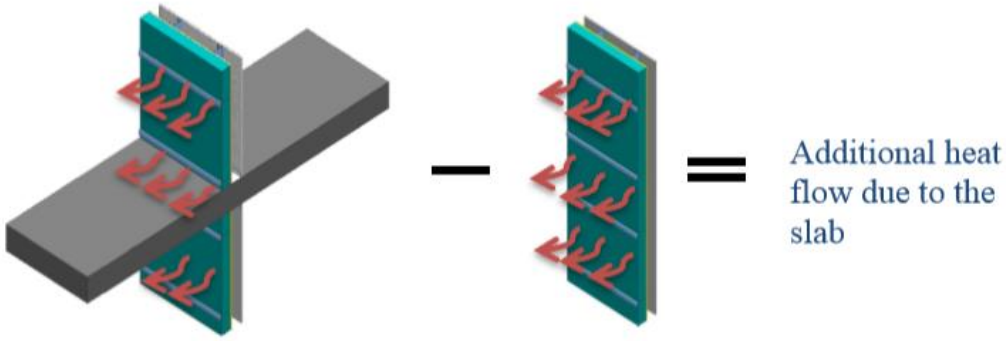

Figure 33. Graphic illusion of the calculation of additional heat flow due to a slab penetrating a wall [1].

Or mathematically

$$\psi = \frac{Q - Q_0}{L} \qquad \text{Equation 27}$$

Where Ψ is the linear transmittance of the balcony slab, W/(m·K);
Q is the heat flow per unit temperature through the assembly with the balcony slab (W/K);
Q_0 is the heat flow per unit temperature through the exterior wall without the balcony slab W/K;
L is the width of the penetrating balcony slab, m.

Point transmittance (χ) is the additional heat flow caused by thermal bridges that only take place at a single location. It is simply the difference between the total heat flow of the interface assembly and that of the clear field assembly. It can be expressed mathematically in Equation 28 below:

$$\chi = Q - Q_0 \qquad \text{Equation 28}$$

Where χ is the point transmittance of the anomaly, W/K.

Overall thermal transmittance of a wall with multiple thermal anomalies is simply the sum of the clear field thermal transmittance, linear transmittance and point transmittance, as shown in Equation 29 below:

$$Q = \sum Q_{anomalies} + Q_0 = \sum \psi \times L + \sum \chi + Q_0 \qquad \text{Equation 29}$$

Where $Q_{anomalies}$ is the heat flow from the anomalies, W/K.

This study used the linear thermal transmittance method in the determination of thermal transmittance of building assemblies.

4.3.3.3 Thermal Modeling Methods

In the literature, software modeling methods that were commonly used for determining overall thermal transmittance of assemblies with thermal bridges and evaluating the impact of thermal bridges on the whole building energy performance are equivalent U-value method, equivalent wall method and direct 3D dynamic modeling.

The equivalent U-value method is to adjust the insulation level of the one-dimensional multi-layered envelope component such that its thermal transmittance is equal to the effective overall U-value of the envelope detail with thermal bridges, while the material properties of the multi-layered component are kept unchanged [1]. This can be done by hand calculation or by 2D thermal modeling using computer software such as THERM [1]. However, the presence of thermal bridging not only changes the overall thermal transmittance of building envelope, it also changes the dynamic thermal characteristics of the envelope (the thermal mass distribution in a structure, the temperature distribution in the steady-state heat flow due to the unit boundary temperature difference, and total resistance and capacity). By using the equivalent U-value method, the effect of thermal bridges on the overall thermal resistance is considered, while the thermal inertia effect of the thermal bridges is ignored, therefore, the accuracy of using this method in energy modeling to evaluate energy performance is not high.

The equivalent wall method uses a one-dimensional multi-layered structure with the same dynamic thermal characteristics as the complex wall system with thermal bridges [1]. Therefore, the thermal inertia effect can be accounted for.

In 2012, Ge et al. [38] investigated the impact of thermal bridges caused by concrete balcony slabs on the energy performance of a typical high rise residential building in Toronto, Canada. Two-dimensional heat transfer simulation of the balcony/wall junction was carried out using THERM under steady-state and eQuest was used for calculating the space heating and cooling energy consumption for seven scenarios with and without a balcony thermal break under typical winter design conditions in Toronto. The results from THERM have shown that using a thermal break in the balcony lowered the overall U-value of the balcony by 72-85% and increased the minimum floor surface temperature by 4.4 °C. Whole building energy simulations results from eQuest showed that by reducing the heat transfer through balcony slabs, the annual space heating energy consumption is reduced by 5-11% and annual space cooling energy consumption is reduced less than 1%. The balcony cross-section area in this study building is approximately 4% of the total exterior wall, however, may contribute up to 11% of the space heating energy consumption.

In 2015, Baba and Ge [39] studied the dynamic effect of balcony slabs as thermal bridges on the energy performance of a high-rise residential building. They compared the annual energy consumption used for space conditioning calculated using the equivalent U-value method to the result from direct 3D dynamic modeling of the balcony junctions implemented in WUFI Plus

program, a whole building Heat, Air and Moisture (HAM) modeling program, where the 3D dynamic modeling method took account of the thermal inertia effect. The simulations were carried out in three Canadian cities - Vancouver, Toronto and Edmonton, which are in climate zone 4, 5 and 7 respectively according to National Energy Code of Canada for buildings. This study finds that when the area ratio of balcony to façade is small, the dynamic effect of thermal bridge, in this case, the balcony slabs, on the annual space conditioning is small, and the equivalent U-value method underestimates the annual heating loads by 2.8-4.4%. As the increase of the amount of thermal bridges and higher level of insulations in the building envelope, the dynamic effect of balcony slab on the energy consumption increases to 8.6-15.2%. In a hypothetical scenario where walls are well-insulated and the balcony to façade area ratio is 100%, the difference in calculated spacing heating loads between the equivalent U-value method and 3D dynamic modeling is up to 15.2%. However, when the thermal breaks are applied, the difference in energy consumption results from the two modeling methods is reduced to 1.9-11.5% and the annual heating loads are reduced by 8.8-25.7%. As a result, this study showed the importance of removing thermal bridges in building envelop designs, especially in well-insulated building envelops.

Ge and Baba in 2015 [40] investigated the dynamic effect of thermal bridge represented by typical junctions and balcony slabs on the space heating and cooling load of a 2-storey residential building using three simulation methods – equivalent U-value method, equivalent wall method and direct 2D/3D modeling method - that are implemented in WUFI Plus. The simulations were carried out in two climate conditions - Quebec City and Phoenix, representing heating-dominated cold climate and cooling dominated hot climatic respectively. For the cold climate, the results from simulation show the annual heating load modeled using the 3D dynamic method is 8-13% higher than that modeled using the equivalent U-value method, and 4-9% higher than that modeled using the equivalent wall method. For the hot climate, simulation results show that the inclusion of thermal bridges increases the annual cooling load by 20%. The results from modeling using 3D dynamic method is 17% higher than that modeled using the equivalent U-value method, and 14% higher than that modeled using the equivalent wall method, demonstrating the importance of using 3D methods in simulation techniques. This study also shows that the percentage effect of thermal bridges on the heating load increases as the insulation level increases, while the differences among the three methods decreases.

It is especially important to use 3D methods to model conventional wood framing due to certain characteristics of wood construction. Although wood has many beneficial properties, one being a much lower thermal transmittance when compared to concrete or metal, the way we build with wood generates some complications when looking into thermal bridging effects. The primary issue is that it is not possible to model conventional wood framing accurately with 2D models as the structure is not homogeneous and is 3-Dimensional. Conventional wood-framing is multi-directional and discontinuous, creating multiple thermal bridges in various directions as one junction. For instance, the thermal flux through a wood joist oriented in the x-y plane can influence the thermal flux through the wall plates in the x-z plane. The interdependency of each plane's thermal flux makes the approximation of overall thermal transmittance difficult using 2D methods.

This study used direct 3D modeling method to simulate the heat transfer through the wood-frame assemblies. It considered important factors such as thermal inertia in heat transfer and the unique thermal characteristics in wood. The assemblies were drawn in HEAT3 [41] by inputting the exact dimensions along x, y, and z axes with the right materials and boundary conditions assigned.

4.4 Methodology

4.4.1 3D Modeling Using HEAT3

HEAT3 Version 8.02 [41] was used to calculate the total heat transfer across the assemblies. It is a PC-program for three-dimensional transient and steady-state heat transfer developed by Blocon. HEAT3 is validated against the standard ISO 10211:2017 – *Thermal bridges in building construction – Heat flows and surface temperatures – Detailed calculations* [42], a standard that provides the resulting thermal values for various scenarios to act as a benchmark for assessing 3D heat transfer software. HEAT3 is a common software used in building industry for determining the thermal transmittance of 3D thermal bridges in North America, an example (Figure 34) of its application is to model and calculate the surface temperature for a corner with wall/roof connection.

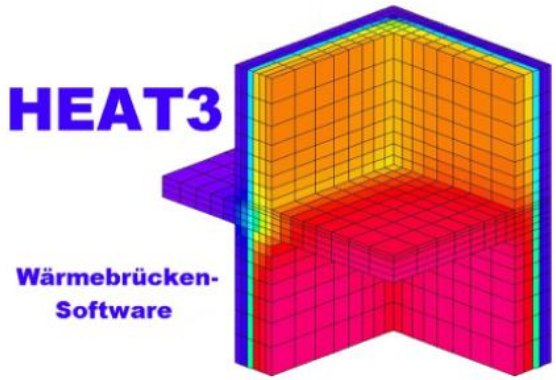

Figure 34. Illustration of surface temperature for a corner with wall/roof connection calculated in HEAT3 [41].

As specified in ISO 10211:2017 [42], the boundary conditions in HEAT3 models were set as an interior temperature of 20°C, with surface resistance of 0.13 $m^2 \cdot K/W$, the exterior temperature of 0°C, with surface resistance of 0.04 $m^2 \cdot K/W$. Material physical properties were assumed to be independent of temperature and dimensions (i.e. thermal conductivity of wood is assumed to be the same between parallel to grain and perpendicular to grain directions with consistent moisture content), and there were no heat sources modeled within the assemblies.

Mesh was set to a maximum of 370 to achieve the best accuracy in all simulations under steady state. Stopping criterion was set to when the absolute differences between two boundary flows reach under 1%, meaning the amount of heat flows out of the exterior surface is nearly equal to

the amount of heat flows into the interior surface, therefore indicating the equilibrium state had achieved.

The cut-off planes in all models were positioned to be exactly 1 meter from the center of the assembly junction. In other words, the length of the interior and exterior slabs, the height of the wall above and below the floor are all exactly 1 meter. This set up conforms to the requirements listed in subsection 7.2.2 of ISO 10211:2017 [42] and ensures all heat transfer caused by thermal bridges is included in the simulation.

Three types of balcony construction were modelled, namely cantilever (Figure 35), ledger (Figure 36), and rim joist (Figure 37). The reasons these types of connection were chosen for this study is that they are the most used ones in Canadian wood frame buildings.

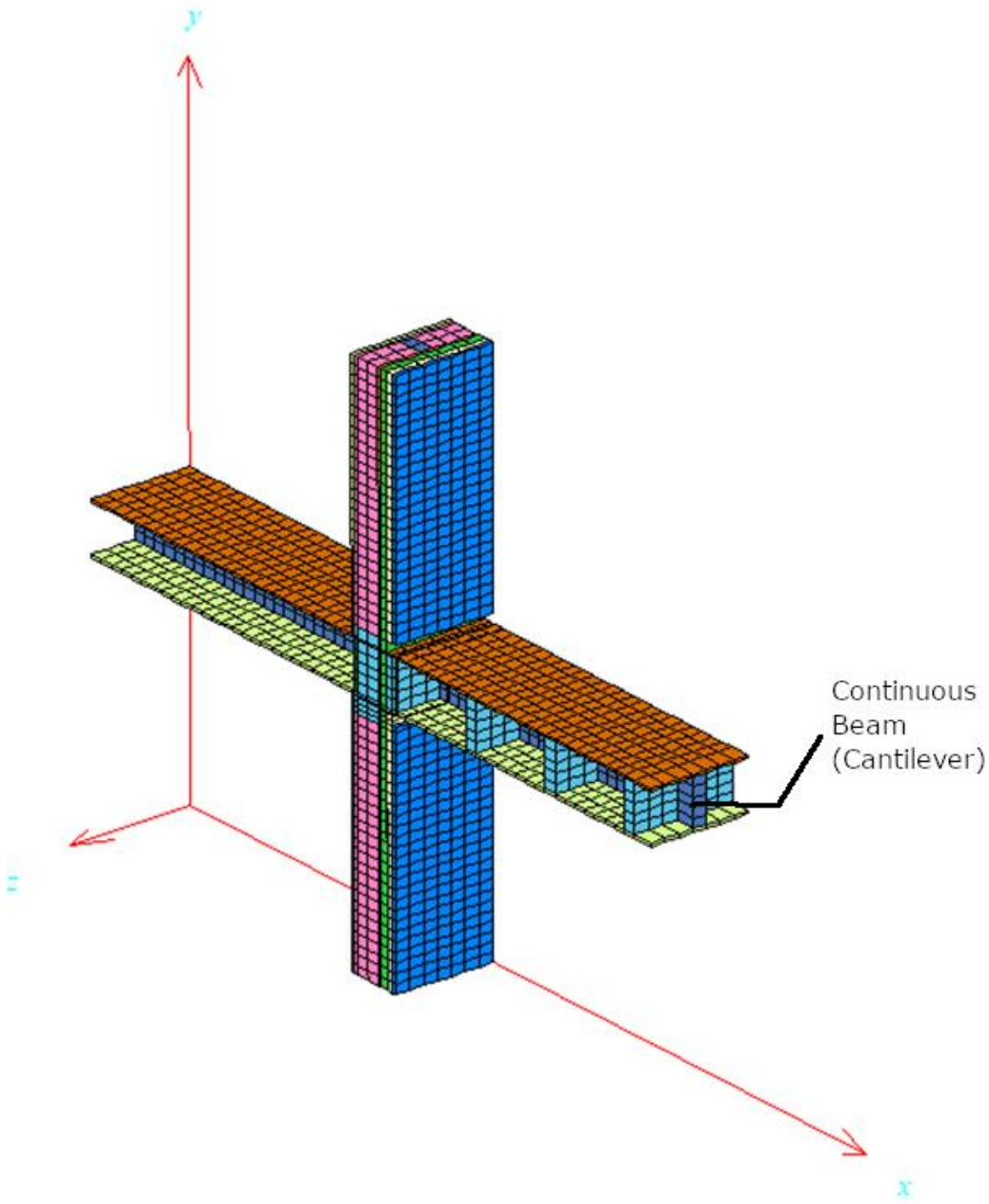

Figure 35. Cantilever balcony has a continuous beam running through the wall and support the floor slab above.

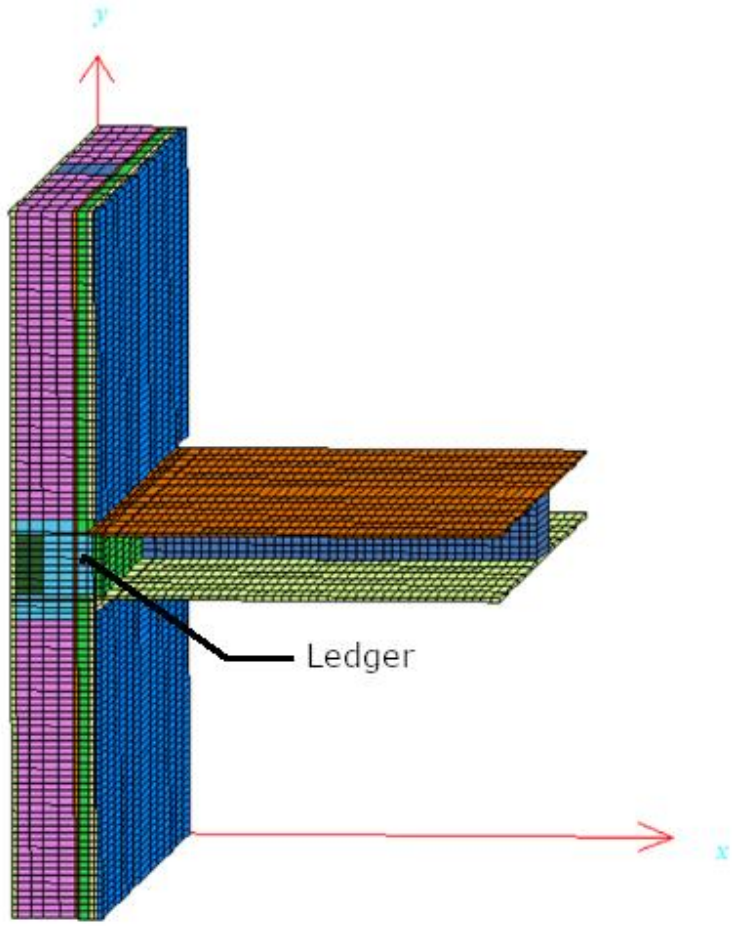

Figure 36. A ledger balcony, the deck joist is connected to a ledger that is attached to the exterior wall to support the floor slab.

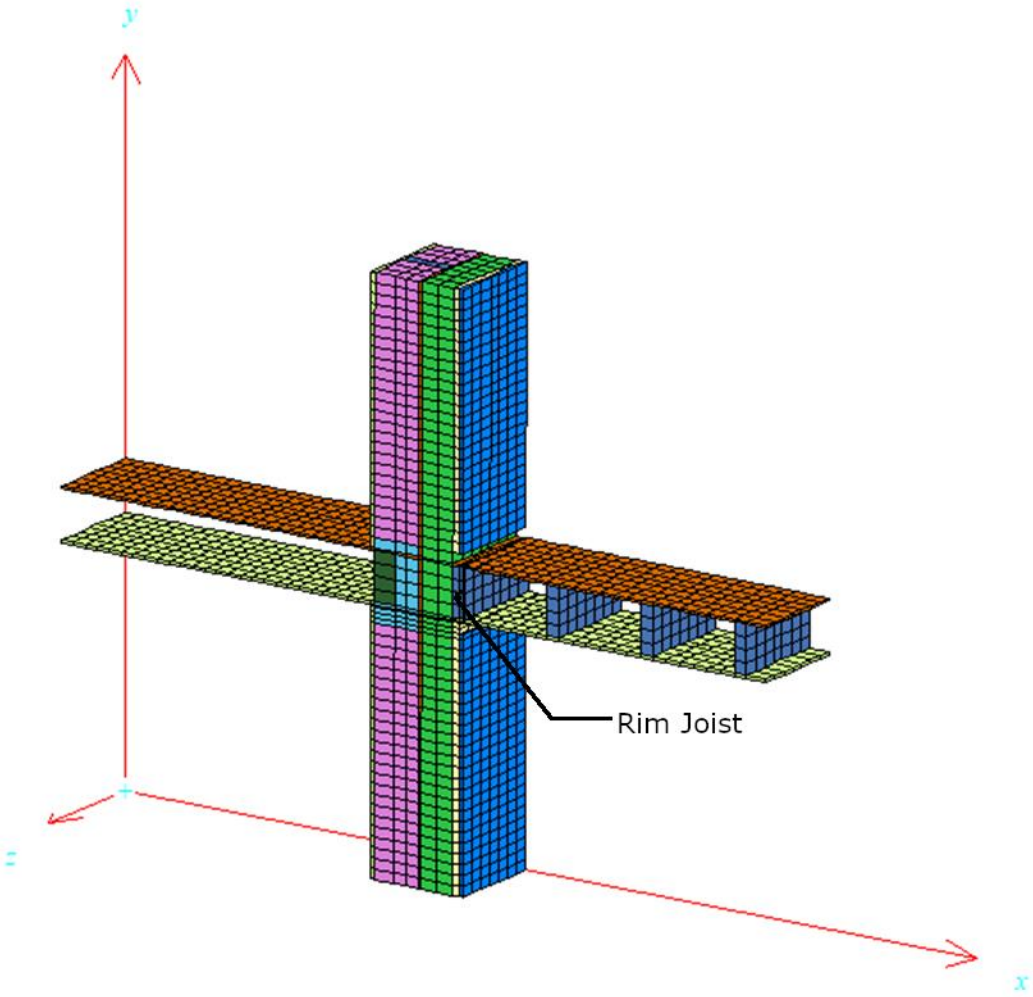

Figure 37. Rim joist provide lateral stability to the floor joists which land on the bearing wall.

4.4.2 Cantilever

Cantilevers (Figures 38-39, 41-43, and 45-47) are typically used in balcony constructions where exterior posts are not considered. To provide adequate support to the balcony, the floor joists are running from the interior of the building, through the exterior walls, extending to the desired balcony depth. Cantilevered floor joists provide the most obvious thermal bridges with wood members extending clear through the building enclosure.

For linear transmittance along the wall caused by a cantilever beam passing through the wall, the following variables listed in Table 4 were studied through HEAT3 modeling. The linear heat transmittance was then calculated using Equation 27, using the amount of total heat transfer in assemblies with thermal bridging (Figure 38-39, and 41-43) subtract the heat transfer in the corresponding clear field (Figure 40, and 44 respectively), and divide the depth of the assembly (300 mm in this case) and the temperature gradient (20 K).

Table 4. Scenarios studied in cantilever balconies.

Wall Size (inch)	Exterior Insulation Level (inch)	Plies Of Beam	Spacing between Beams (mm)	Wood Type and Beam Size (mm/inch)
2x4	0, 1, 2	1, 2, 3	300	Dimensional Lumber 38x184 (2x8), Dimensional Lumber 38x235 (2x10), Dimensional Lumber 38x286 (2x12), Engineered Wood Product 44x184 (2x8), Engineered Wood Product 44x235 (2x10), Engineered Wood Product 44x286 (2x12)
2x6	0, 1, 2 ,3, 4			

A cross section of the model is shown in Figure 38, this model is made of a 2x4 wall, 1 ply of 38x184 mm (2x8) dimensional lumber structural beam, and 1-inch exterior insulation (Roxul Comfortboard). The corresponding 3D diagram from HEAT3 is shown in Figure 39. A clear field of the assembly (wall without balcony and interior floor/ceiling) was modeled as shown in Figure 40.

The clear field assembly is composed of 12.5 mm gypsum board, cavity insulation (R-14 for 2x4 wall and R-22 for 2x6 wall), 9.5 mm plywood, exterior insulation (Roxul Comfortboard where applicable), 19 mm air space and finishes with 12 mm cementitious siding.

The interior floor is composed of 9.5 mm plywood, air space, and dimensional lumber or engineered wood product beam where applicable. The interior ceiling was modeled using a single layer of 12.5 mm gypsum board.

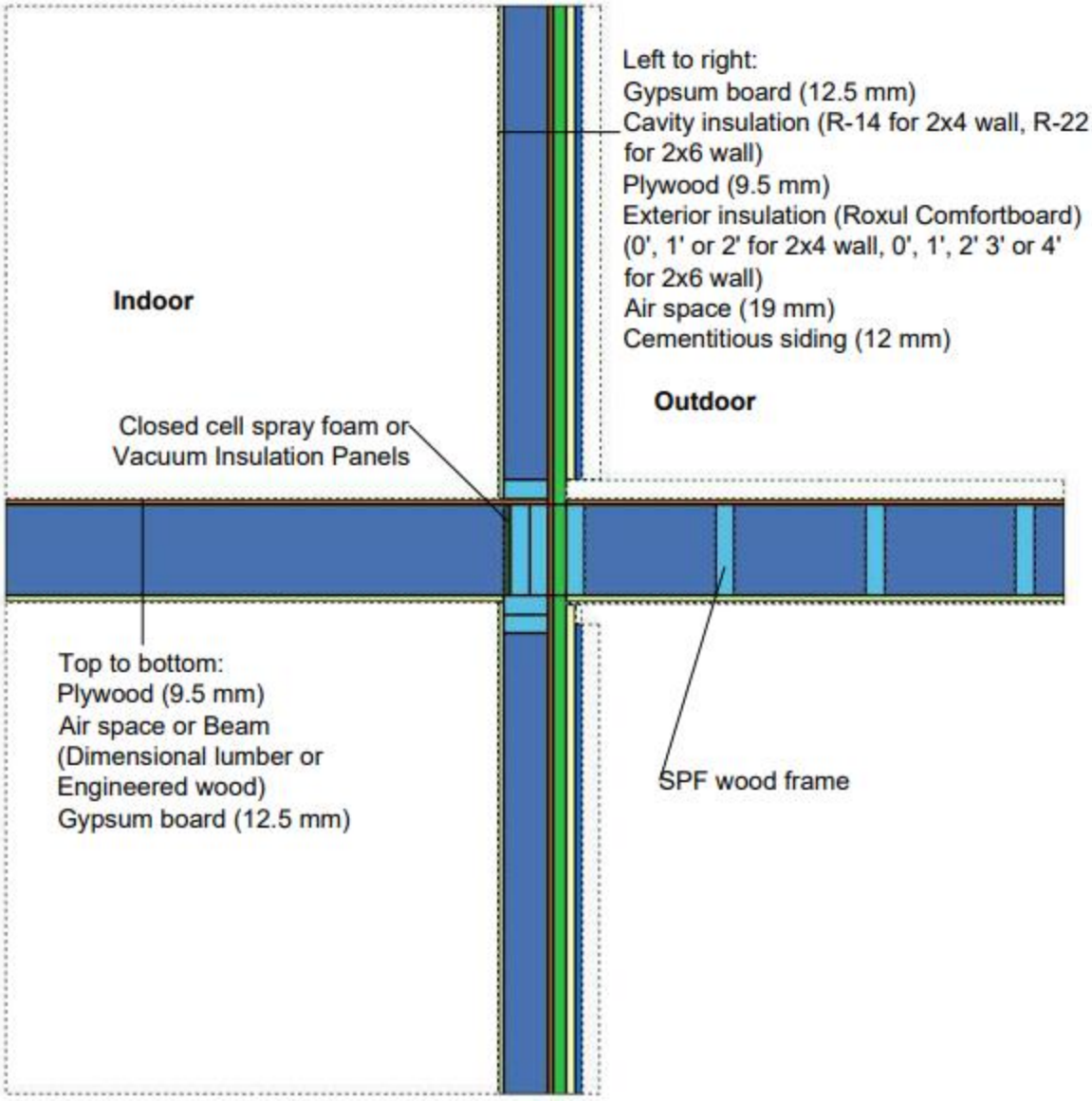

Figure 38. Cross section of a cantilever balcony.

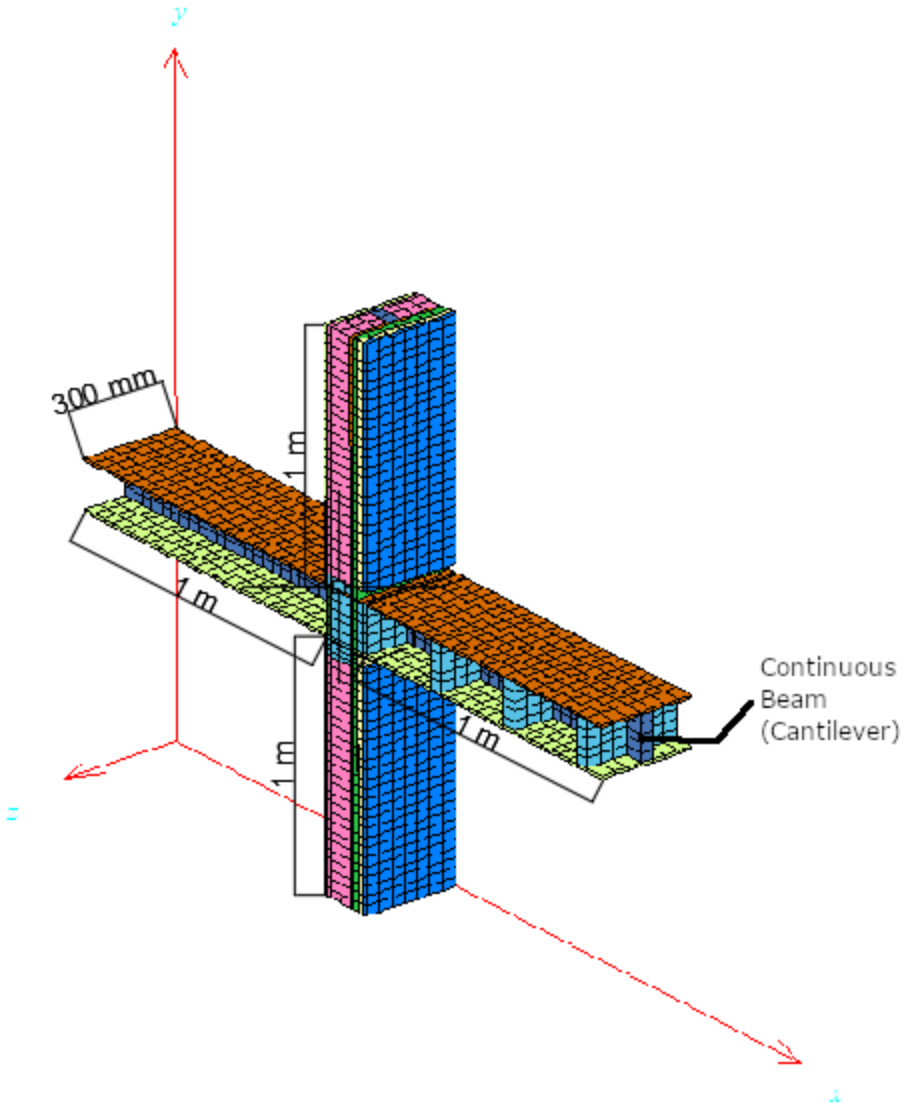

Figure 39. Cantilever balcony modeled in HEAT3, the height of the wall above and below the center junction are 1 m each, the length of the interior floor and exterior balcony slab are both 1 m as well. The depth of the assembly is the 300 m as the beams are spaced as 300 m apart center to center.

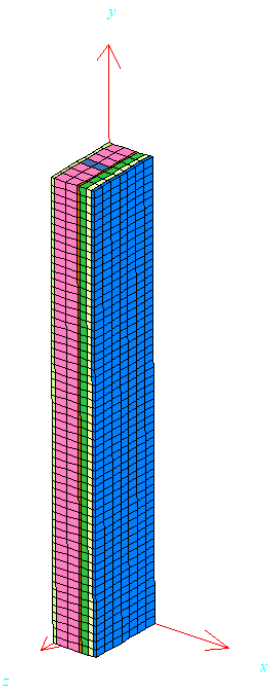

Figure 40. Clear field (wall) modeled in HEAT3.

For point transmittance at a corner caused by a cantilever beam sitting parallel to a wall, the following variables listed in Table 5 were studied through HEAT3 modeling. Figures 41-44 below show the 3D models of a corner with thermal bridge and the corresponding clear field without thermal bridge simulated in HEAT3. This corner shown was built with 2x4 wall, 1 ply of 2x8 engineered wood product beam and without any exterior insulation. Figures 45-47 show the 3D models of a corner made with 2x6 wall, 3 plies of 2x8 engineered wood product beam with 3-inch exterior insulation and the corresponding clear field. The point transmittance due to thermal bridging was calculated using Equation 28, for example, by subtracting the heat transmittance in Figure 44 from that in Figure 41 and divide by the temperature gradient (20 K).

Table 5. Scenarios studied for determining point transmittance at corners with wall/slab connection.

Wall Size (inch)	**Exterior Insulation Level (inch)**	**Plies of Beam**	**Wood Type and Beam Size (mm/inch)**
2x4	0, 1, 2	1, 2	Engineered Wood Product 44x184 (2x8), Engineered Wood Product 44x235 (2x10), Engineered Wood Product 44x286 (2x12)
2x6	0, 1, 2, 3, 4	1, 2, 3	

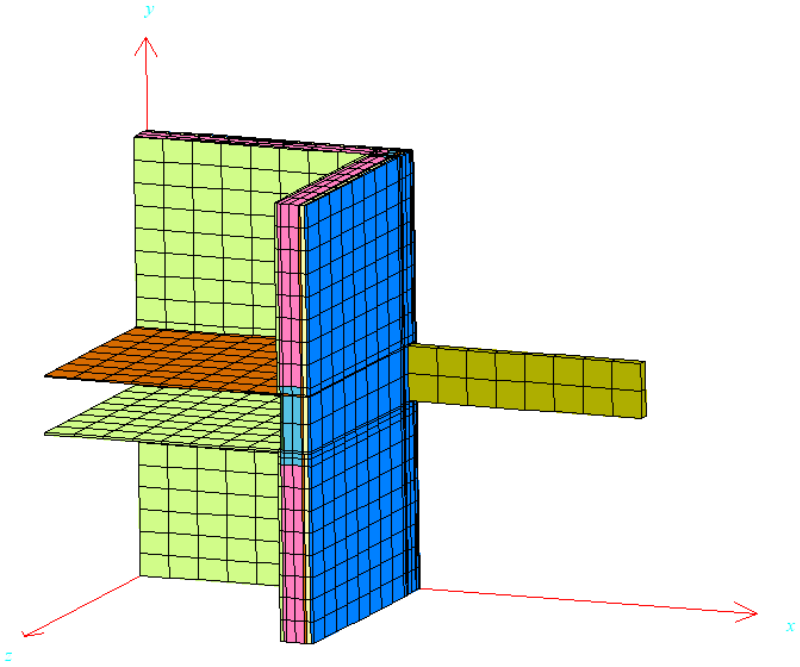

Figure 41. Corner junction (2x4wall, 1 ply of 2x8 engineered wood product beam, and no exterior insulation) modeled in HEAT3.

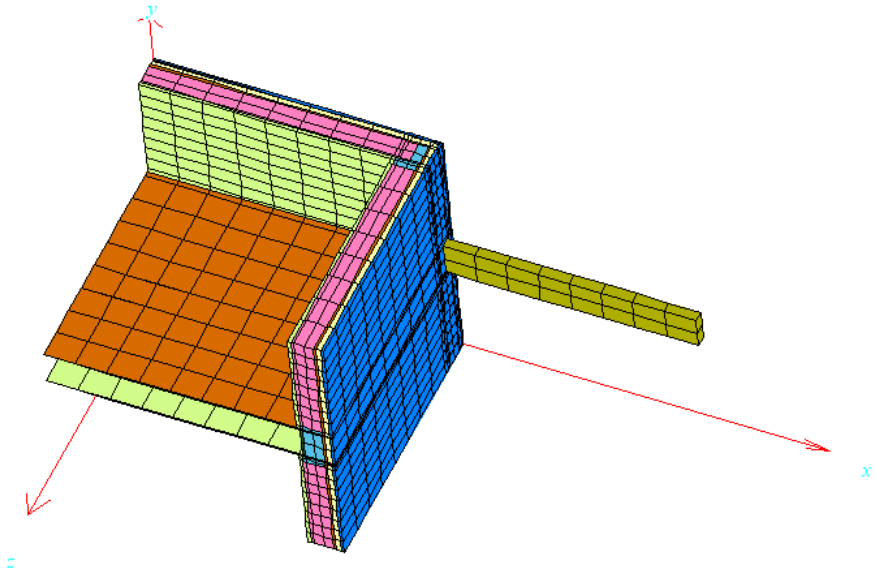

Figure 42. Corner junction (2x4wall, 1 ply of 2x8 engineered wood product beam, and no exterior insulation) modeled in HEAT3, top view.

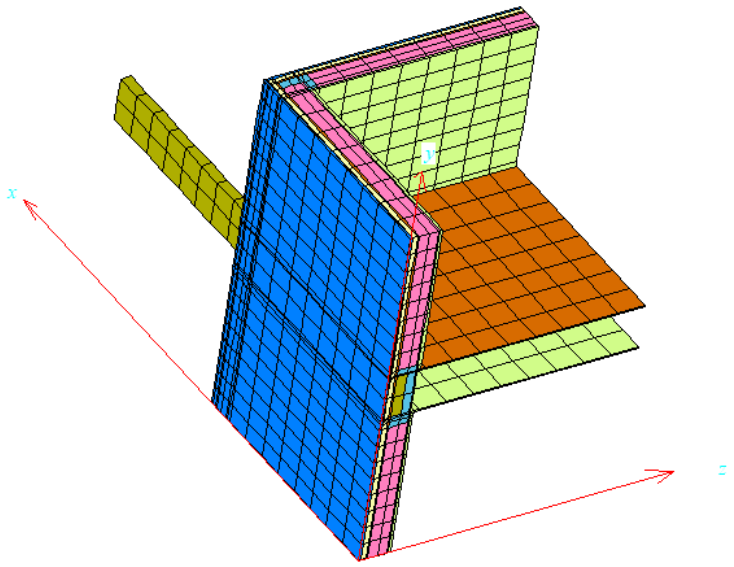

Figure 43. Corner junction (2x4wall, 1 ply of 2x8 engineered wood product beam, and no exterior insulation) modeled in HEAT3., side view.

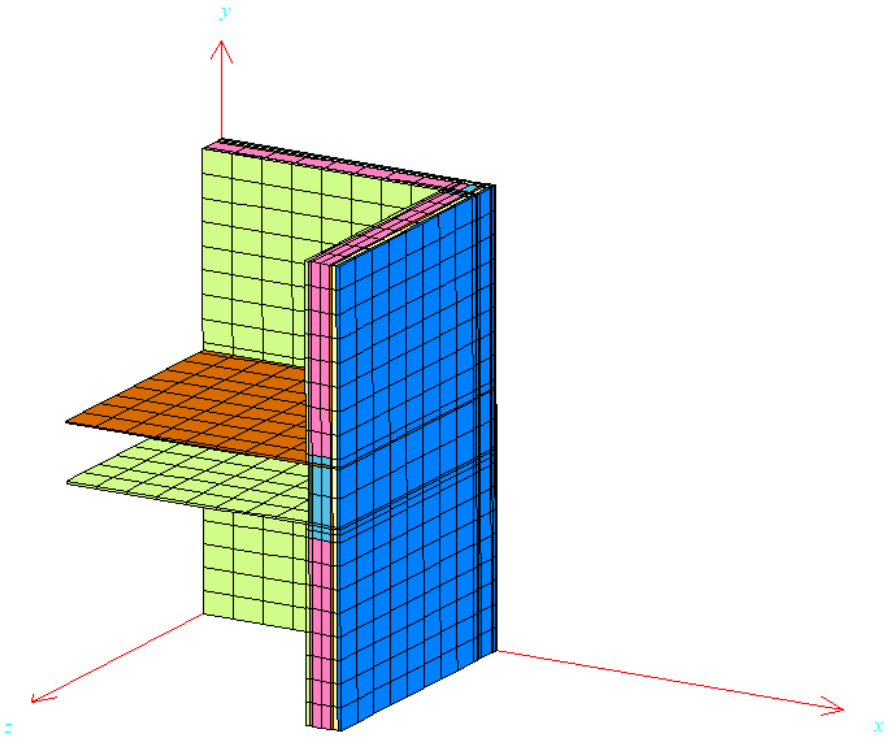

Figure 44. Clear field of a corner (2x4 wall, no exterior insulation) modeled in HEAT3.

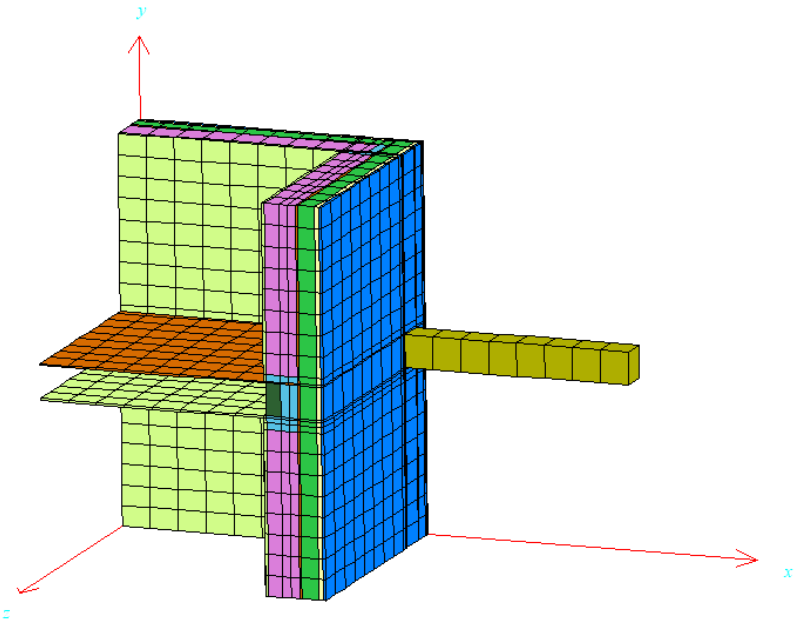

Figure 45. Corner junction (2x6 wall, 3 plies of 2x8 engineered wood product beam, and 3-inch exterior insulation) modeled in HEAT3.

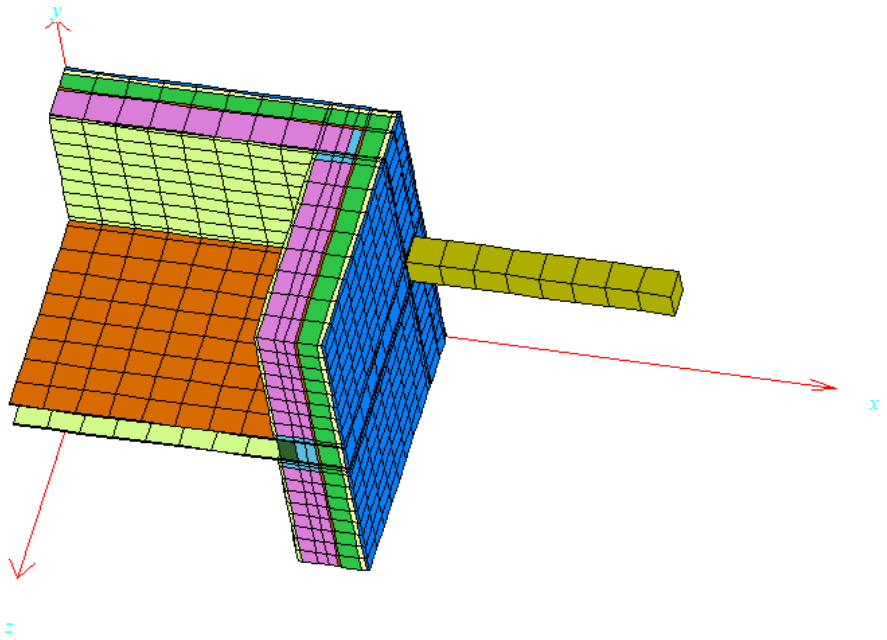

Figure 46. Corner junction (2x6 wall, 3 plies of 2x8 engineered wood product beam, and 3-inch exterior insulation) modeled in HEAT3, top view.

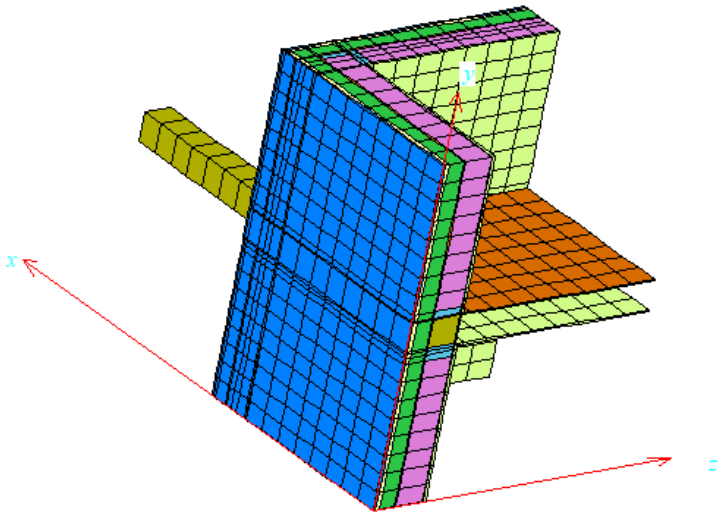

Figure 47. Corner junction (2x6 wall, 3 plies of 2x8 engineered wood product beam, and 3-inch exterior insulation) modeled in HEAT3, side view.

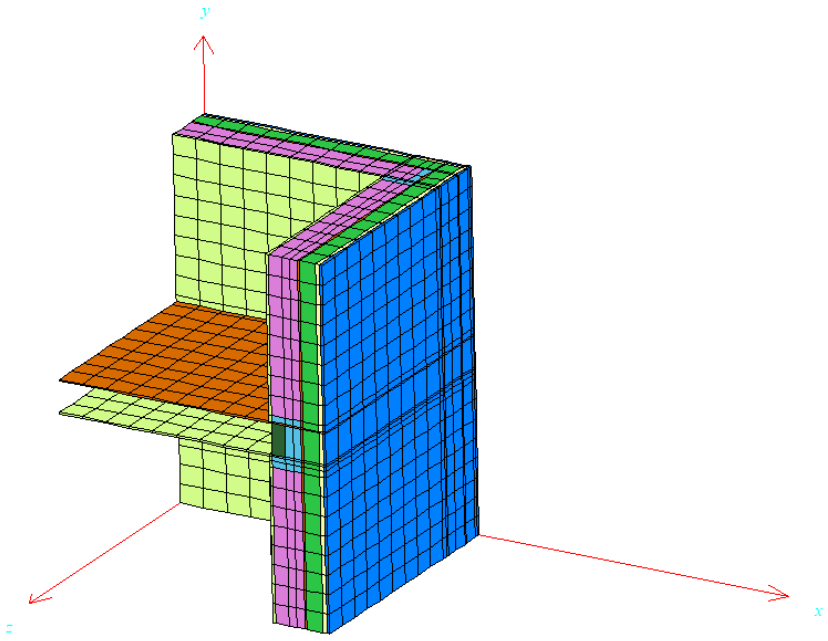

Figure 48. Clear field (2x6 wall, and 3-inch exterior insulation) modeled in HEAT3.

4.4.3 Ledger

Ledgers (Figures 49-52) are typically used in situations where balconies are being considered with exterior posts. In this case, it is not essential that the balcony joists be continuous to the inside of the building as they can be simply supported. Ledgers are installed against the rim joists with larger fasteners allowing for conventional wood frame hangers to be used to support the balcony joists. Ledgers generally have a limited effect on the overall thermal performance when compared to the results of the rim joists; however, we have included this information for consistency and completeness.

Two types of frames were modelled for ledger connection, one without interior floor/ceiling (Figures 49 and 50), and the other one included interior floor/ceiling (Figures 51 and 52). Variables studied in this section include wall sizes, exterior insulation levels, frame types, spacing between beams, and wood types and beam sizes, they are tabulated in Table 6 below.

Table 6. Scenarios studied to determine linear transmittance along a ledger connection.

Wall Size (inch)	Exterior Insulation Level (inch)	Frames	Spacing between Beams (mm)	Wood Type and Beam Size (mm/inch)
2x4	0, 1, 2	With interior floor/ceiling, Without interior floor/ceiling	300, 400, 600	Dimensional Lumber 38x184 (2x8), Dimensional Lumber 38x235 (2x10), Dimensional Lumber 38x286 (2x12), Engineered Wood Product 44x184 (2x8), Engineered Wood Product 44x235 (2x10), Engineered Wood Product 44x286 (2x12)
2x6	0, 1, 2, 3, 4			

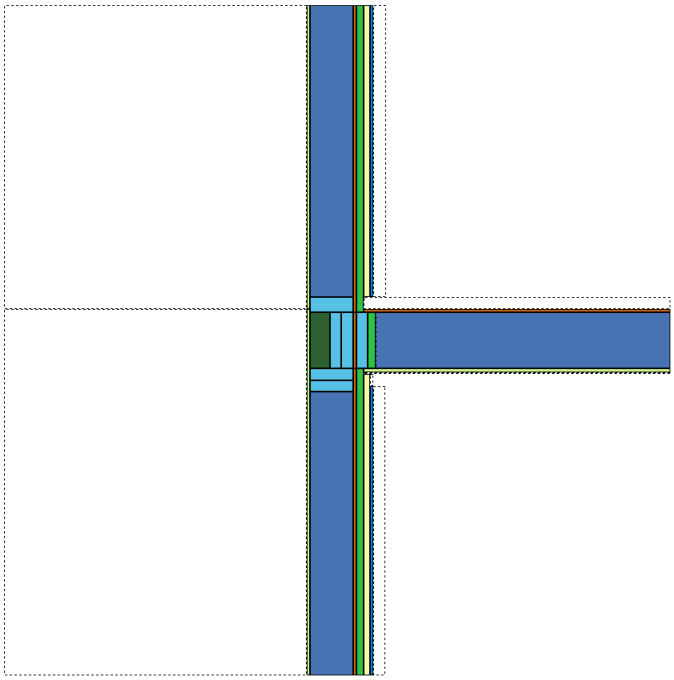

Figure 49. Crossed section of a ledger balcony connection without modeling the interior floor/ceiling.

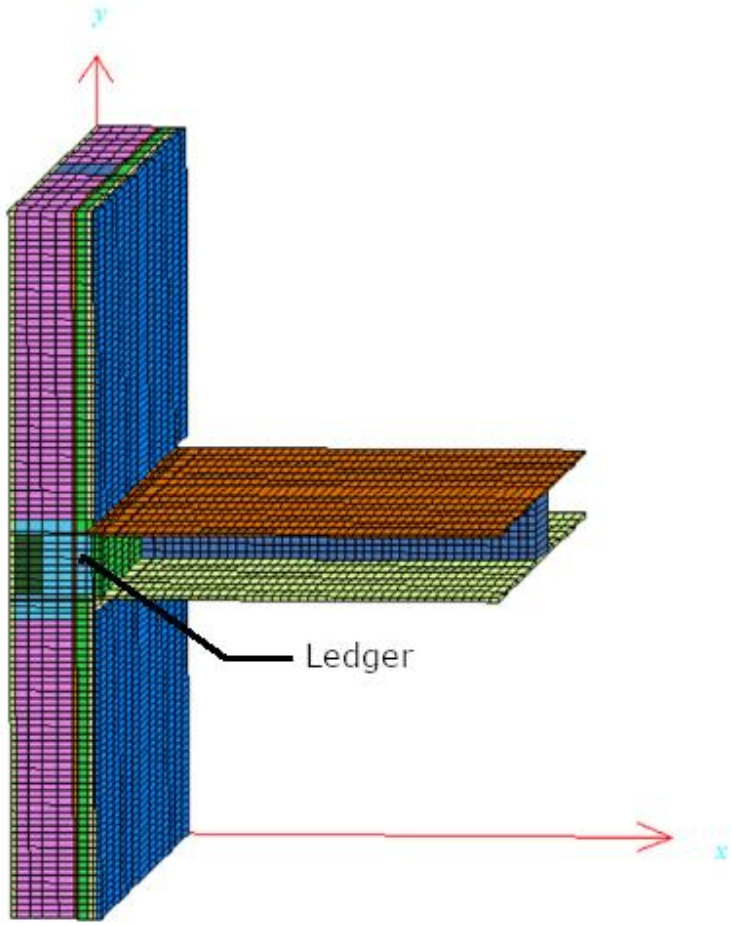

Figure 50. Ledger balcony connection without interior floor/ceiling modeled in HEAT3.

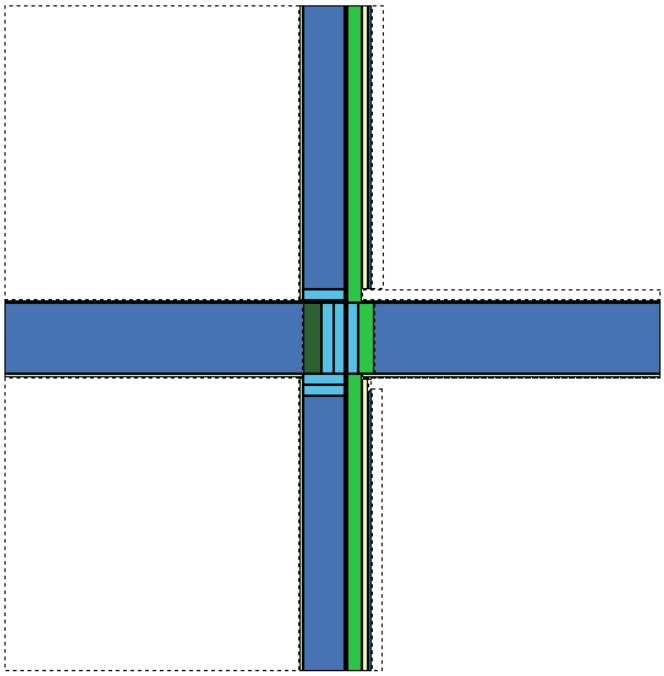

Figure 51. Crossed section of a ledger balcony connection (2x6 wall, 2x8 dimensional lumber beam at 400 mm o.c. with 2-inch exterior insulation) with the interior floor/ceiling.

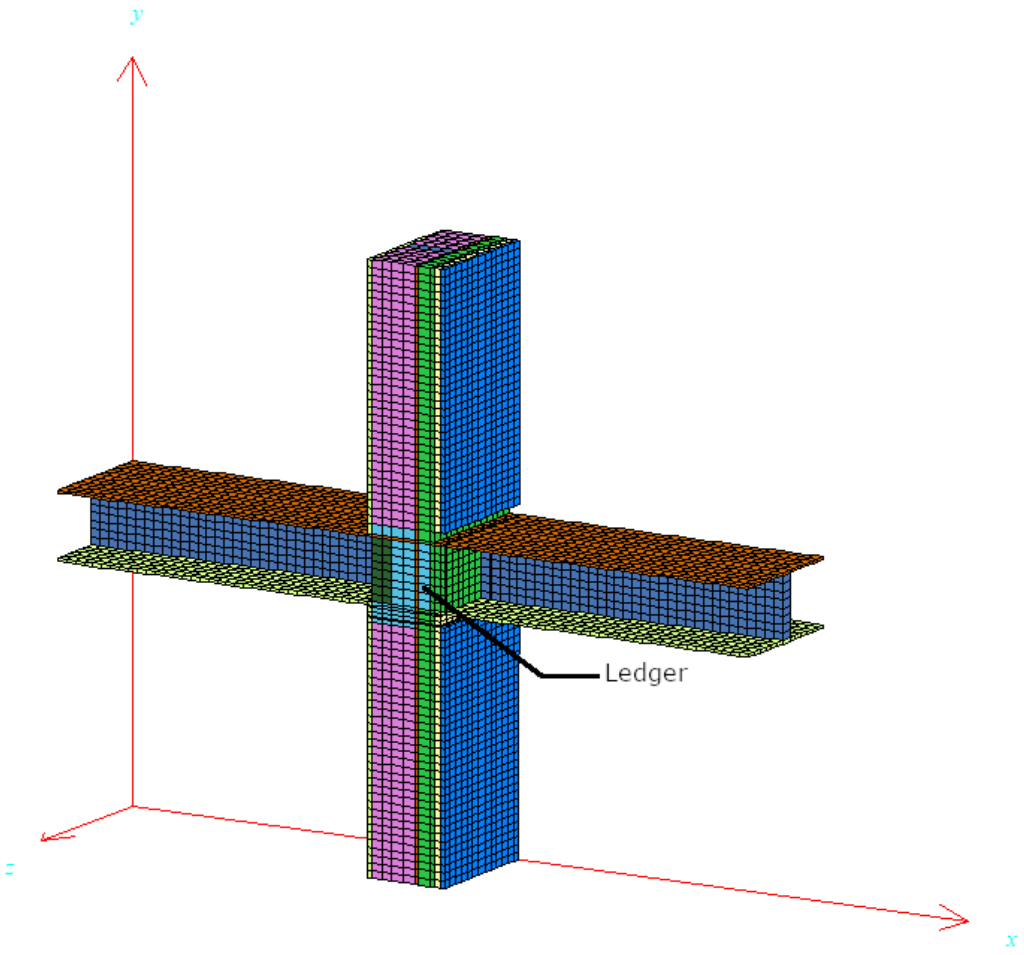

Figure 52. 2x6 wall 2x10 dimensional lumber beam at 400 mm o.c. spacing, with 2-inch exterior insulation ledger balcony connection with interior floor/ceiling modeled in HEAT3.

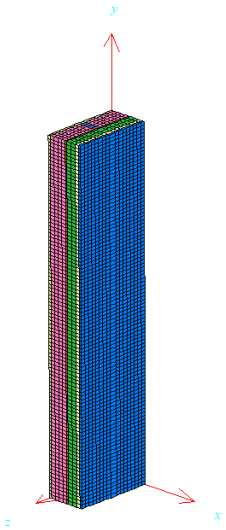

Figure 53. 400 mm, 2x6 wall with 2-inch exterior insulation clear field modeled in HEAT3.

4.4.4 Rim Joist

Rim joists (Figures 54-57) provide lateral stability to the floor joists which land on the bearing wall. These rim joists are typically constructed of one ply of continuous dimensional lumber matching the floor joists depth with blocking being provided between each joist for stability. The rim joists limit the builder's ability to insulate the floor space effectively as the rim joist and blocking take up considerable space along the top of the wall plate. Additionally, the wood joists can run perpendicular to the rim joists, creating a thermal bridge through what little insulation can be provided.

Linear transmittance along a rim joist/balcony connection (Figures 54 and 55) were studied. Variables studied include wall sizes, exterior insulation levels, spacing, and wood types and joist sizes, and they are listed in Table 7 below.

Table 7. Scenarios studied in determining linear transmittance along a rim joist balcony connection.

Wall Size (inch)	**Exterior Insulation Level (inch)**	**Spacing (mm)**	**Wood Type and Joist Size (mm/inch)**
2x4	0, 1, 2	300, 400, 600	Dimensional Lumber 38x184 (2x8), Dimensional Lumber 38x235 (2x10), Dimensional Lumber 38x286 (2x12), Engineered Wood Product 44x184 (2x8), Engineered Wood Product 44x235 (2x10), Engineered Wood Product 44x286 (2x12)
2x6	0, 1, 2, 3, 4		

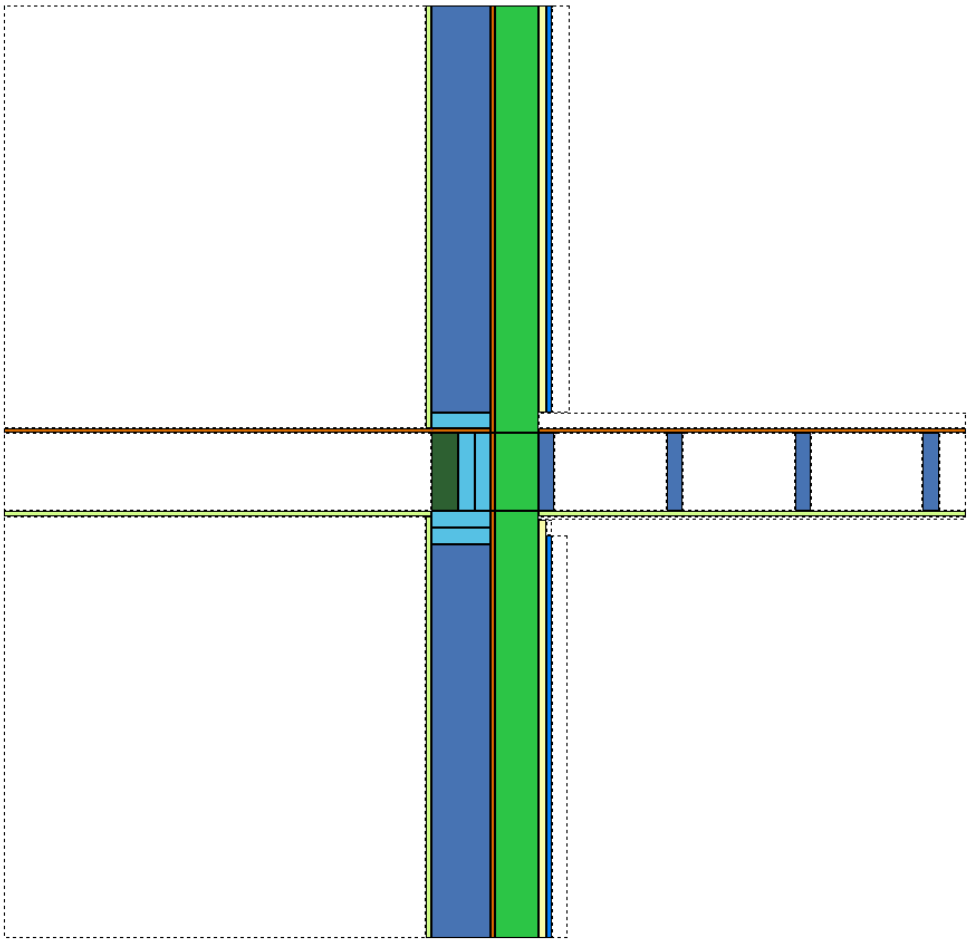

Figure 54. Cross section of a rim joist connection (2x4 wall, 2x8 beam dimensional lumber, 400 mm o.c. spacing, and 4-inch exterior insulation).

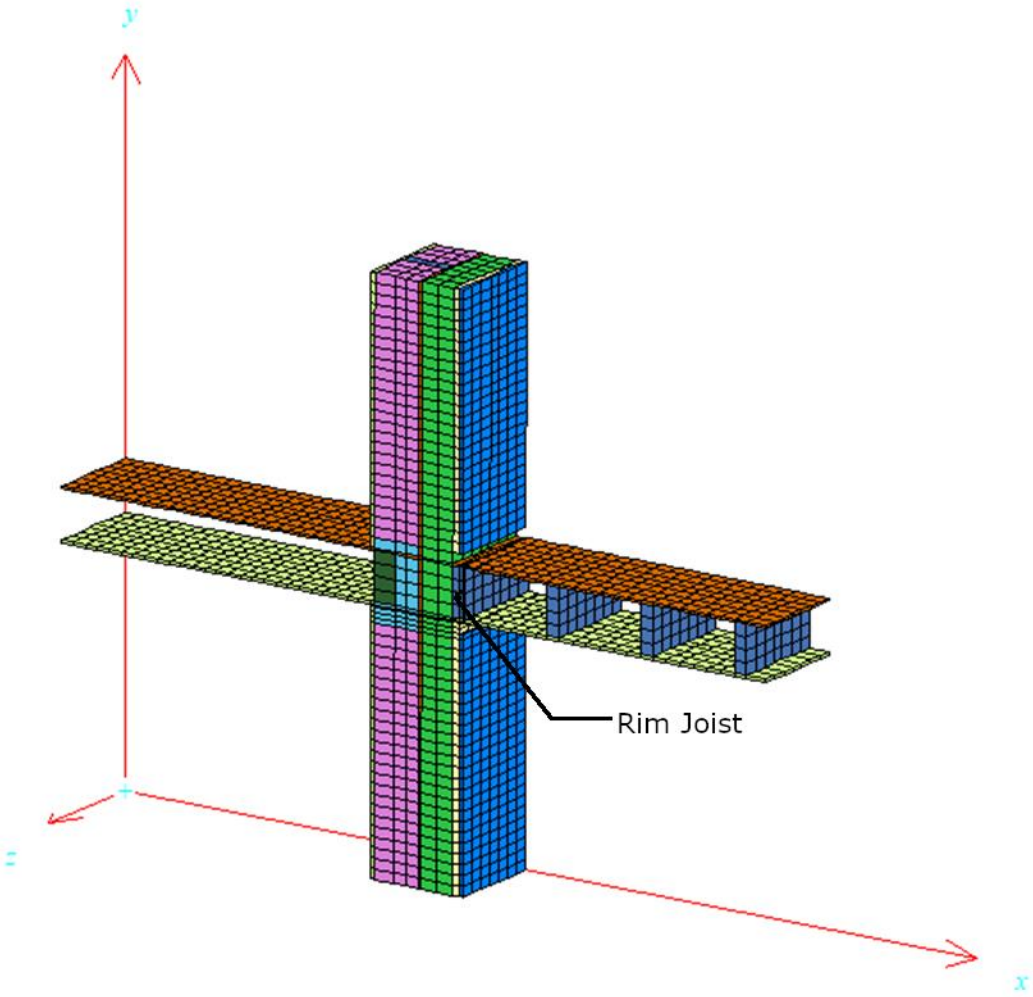

Figure 55. 2x4 wall, 2x10 dimensional lumber beam at 400 mm o.c. spacing with 4-inch exterior insulation rim joist connection modeled in HEAT3.

Point Transmittance at frames where floor joist attaching to the interior rim joist, at 300 mm o.c. (Figures 56 and 57) were also studied. The joists are assumed to be dimensional lumber. Variables studied are wall size, exterior insulation lev el, and joist size, they are listed in Table 8 below. This assembly is treated as point transmittance for convenience in calculation, although technically it is not a “point” penetration, however, we set every 300 mm depth of this frame as 1 unit and treated it as a “point”.

Table 8. Scenarios studied in determine the point transmittance at frames where floor joist attaching to the interior rim joist, at 300 mm o.c.

Wall Size (inch)	Exterior Insulation Level (inch)	Wood Type and Joist Size (mm/inch)
2x4	0, 1, 2	Dimensional Lumber 38x184 (2x8), Dimensional Lumber 38x235 (2x10), Dimensional Lumber 38x286 (2x12)
2x6	0, 1, 2, 3, 4	

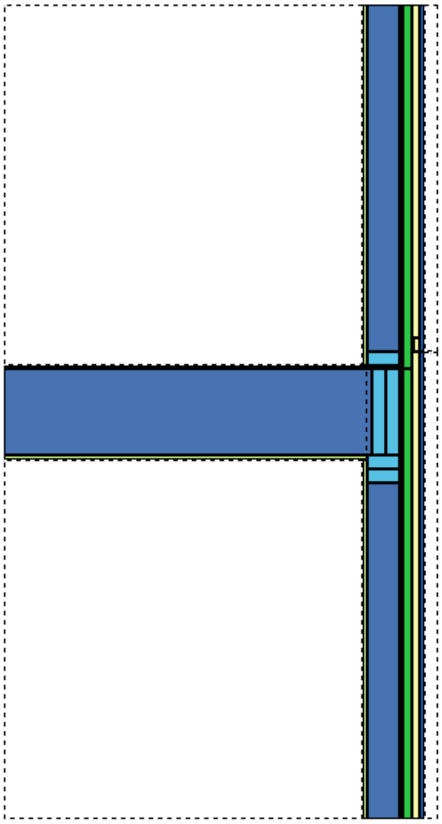

Figure 56. Cross section of a frame with floor joist attaching the interior rim joist.

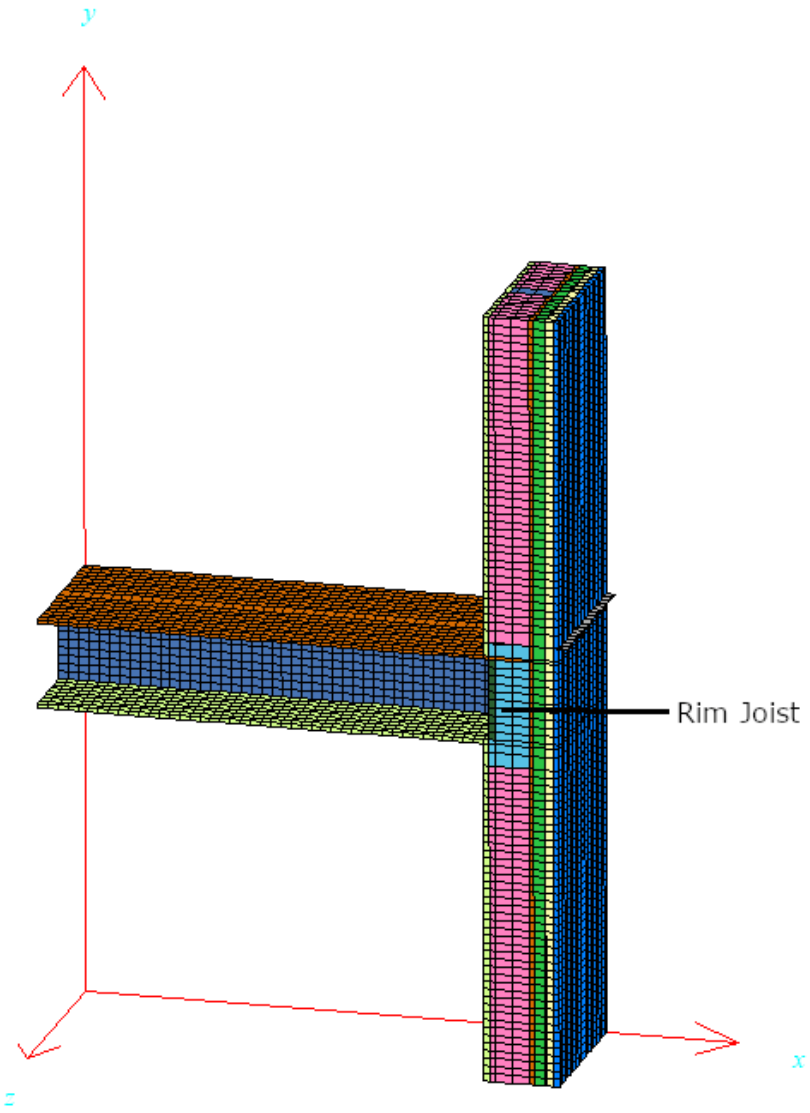

Figure 57. Frame of floor joist attaching to the interior rim joist (2x6 wall, 2x8 beam and 1-inch exterior insulation) modeled in HEAT3.

4.5 Material Properties

Thermal conductivities of materials used in the modeling are tabulated in Table 9. They are based off the thermal values provided by the National Building Code and British Columbia Building Code where available.

Table 9. Thermal conductivities of materials used in the modeling.

Materials	Thermal Conductivities (W/m·K)
Rock Wool	0.04385
Closed Cell Urethane Foam	0.02500
Dimensional Lumber - SPF	0.13000
Engineered Wood Products - LVL	0.12000
Sheathing - Plywood	0.12500
Gypsum Board	0.10000
Aluminum	225.940
Cementitious Cladding	0.24500
Air	0.02510
Vacuum Insulation Panel	0.0035

4.6 Assumptions

4.6.1 Framing Assumptions

Dimensional lumber is assumed to be Spruce-Pine-Fir (SPF), which is readily available and a typical choice of material in B.C. For joists, we limited out modeling to 2x8, 2x10 and 2x12. The joists were modeled at conventional spacing to suit plywood sheathing at 12'' (300 mm), 16'' (400 mm) and 24'' (600 mm) on-center.

For engineered wood products, it was assumed that Laminated Veneer Lumber (LVL) would be the primary type of product used as it handles weather exposure better than other engineered wood products. The thermal conductivity of LVL, while very close to that of dimensional lumber, was used in models incorporating engineered wood products. The size of the LVLs used in our models were selected to match the overall depth of dimensional lumber.

Two wall types were considered: 2x4 and 2x6, respectively. The spacing of the wall studs was assumed to match that of floor joists above. This assumption was chosen as it would provide the worst-case scenario of having the wall stud line up with the joist above. This configuration would increase the potential thermal bridging effects as multiple wood elements are in intimate contact. It is assumed that the walls would have a double plate on the top and a single plate on the bottom of the wall. The double bottom-plate, although not required, is assumed to be present due to the prevalence of concrete-topped floor systems in the industry.

4.6.2 Stud and Joist Placement

When completing models for built-up beams, an equivalent number of studs were place under the beam. This assumption was made as built-up beams carry significantly more load than single-ply beams, typically resulting in a need for additional studs below to transfer the load down to the foundation. Additional studs may not be necessary, depending on the structural requirements. This would reduce some of the thermal bridging through the wall system. The

assumption that the number of piles matches the number of studs will provide a conservative result for thermal bridging through the assembly.

4.6.3 Thermal Insulation Consistency

Many material's conductivity changes with temperature, with some varying. For instance, polyisocyanurate insulation varies considerably with temperature, with an average R value of 4.7 at -4°C and 5.7 at 24°C [43]. The software does not complete accommodate a variable conductivity value. As such, the analysis completed relies on fixed thermal values for materials, ignoring the temperature dependencies of various products.

4.6.4 Steady State Thermal Transmission

The analysis assumes a steady-state condition and does not incorporate potential variability caused by transient heat transfer, even though the thermal bridges will be experiencing a transient state through its service life.

4.6.5 Dimensional Consistency

The conductivity of wood varies when measured parallel-to-grain and perpendicular-to-grain. Moreover, there are variabilities with respect to the moisture content of the wood itself. As wood is a natural product, there is considerable variability in its overall properties, even between different species. The analysis completed assumes Spruce-Pine-Fir (SPF) lumber acting homogeneously between parallel and perpendicular grain directions with a consistent moisture content.

4.6.6 Rim Joist Spacing Simplification

When comparing modeling results, it was noted that the spacing of the joists landing adjacent to the rim joist provided negligible thermal difference between 300, 400 and 600 mm, respectively. To reduce the number of models required, the joist spacing rim joists was set at 300 mm at center to provide the potential worst case as it would create increased thermal bridging on a per-meter basis.

4.6.7 Floor Space Air Void Simplification

The air space in the interior floor joist cavity was not considered during modeling, with the faces of the joists being identified as a boundary condition. Although this air space would generally be included in the model, it was omitted for several reasons. Firstly, as the size of the cavity increases, the amount of convective currents through the space increases which reduces the thermal resistance of the air space. As the cavities are at least 189 mm in depth, the amount of thermal resistance provided by this air space would be limited. Further, to adequately determine the thermal resistance of this air space, we would require the total volume of air in the cavity, as this would vary depending on the construction. Moreover, there are situations where some areas are left unfinished such as a partially below-grade unfinished basement where no drywall ceiling is provided in which case the boundary layer would be the face of the joist. Finally, it is common engineering practice to provide additional flexibility in design to account for construction deficiencies. By omitting the air space thermal resistance, the thermal bridging would be more

pronounced than it may be in reality, providing a buffer for thermal performance. For these reasons, it was decided to model the cavity as a boundary condition in place of being modelled as a large air cavity.

4.6.8 Metal Flashing Simplification

Typical detailing requires the use of flashings throughout assemblies to allow water to shed from the surface of the enclosure. These metal flashings can create a thermal bridge through insulation layers. However, these metal flashings pose difficulties with respect to modeling as the thin elements upturn behind the insulation. Models were completed with the flashings included and it was determined that the metal through-wall flashings contributed the following additional thermal transmittance through the assembly.

Table 10. Additional thermal loss due to metal flashing.

Exterior Insulation (Metric / Imperial)	**2x4 Wall (W/m·K)**	**2x6 Wall (W/m·K)**
0 mm / 0"	0.016	0.008
25 mm / 1"	0.009	0.005
50 mm / 2"	0.006	0.004
75 mm / 3"	N/A	0.003
100 mm / 4"	N/A	0.002

These values were subsequently added to various models where the flashing was removed to simplify their preparation.

4.6.9 Single Ply Spacing

For dimensional lumber penetrations, single piles are assumed to act as a unit distance and thus vary between the standard spacing (300, 400 and 600 mm). This assumption is due to the fact a single ply joist will not be able to carry loads with a spacing greater than standard spacing. For multi-ply penetrations, the beams will be able to carry more than standard spacing and are thus considered to be a point bridge.

4.6.10 TJI Simplification

TJI stand for Truss Joist I-joist, it is commonly used in residential construction, particularly in situations where the spans dictate that dimensional lumber is no longer variable, either due to strength or span. Occasionally, TJIs are used when dimensional lumber should be an option as well. To assess whether the shape of the TJI had an influence on the overall performance, models of dimensional lumber vs. TJI were compared. It was determined that the influence was negligible (less than 1%). As such, it is assumed that the influence of the TJI compared to the dimensional lumber can be ignored.

Figure 58. Cross section of TJI beam.

4.7 Results and discussion

4.7.1 Linear Transmittance at Cantilever

Linear transmittance due to thermal bridge at cantilever connections are summarized in Appendix B, Table B1. No significant difference was found between 1 ply of penetrating beams, 2 plies, and 3 plies after the results were rounded up to 3 decimal digits, when the type of beam, the size of beam, and the level of insulation stayed the same. No significant difference was found between dimensional lumber and engineered wood product which were used as the penetrating beam at the thermal bridges. For both 2x4 and 2x6 walls, when the size of the beam stayed the same, the linear transmittance at the thermal bridge decreases linear as the level of insulation increases. For both 2x4 and 2x6 walls, when the plies of beam stayed the same, the linear transmittance due to thermal bridge increased linearly as the size of the penetrating beam increases. For a 2x6 wall, with 2x8 beam and 4-inch exterior insulation had the least linear thermal transmittance, which is 0.021 W/m·K. This is because this configuration had the highest level of insulation at both exterior wall and the wall cavity, at the same time the penetrating cross section at where the thermal bridging occurred was the smallest. When VIP was used as the insulation material at the junction cavity for a 2x6wall, 2x8 beam, 4-inch exterior insulation configuration, the linear transmittance was found to be 0.016 W/m·K, reduced by 26%.

4.7.2 Point Transmittance at Cantilever Corners

Point transmittance due to thermal bridge at cantilever corners are summarized in Appendix B, Table B2. For both 2x4 and 2x6 walls, while the size of beam stayed the same, the point thermal transmittance at where the slab penetrated a corner wall increases as the number of plies of beam increases, this is because as the number of plies of beams increases, the amount of thermal insulation in the wall cavity decreases, and the cross section area of the thermal bridging increases. As the level of exterior insulation increases, the point transmittance decreases, this result is as expected. The best thermal performance framing is the one with 2x6 wall, 2x8 beam, 1 ply beam, and 4-inch exterior insulation, the point transmittance at this configuration is 0.0033

W/K. When VIP was used as the insulation material at the wall cavities for the best performance configuration, the point transmittance was found to be 0.00325 W/K, reduced by 1.51%.

4.7.3 Linear Transmittance at Ledger and Rim Joist

Linear transmittance due to thermal bridges at ledger connections are summarized in Appendix B, Tables B3-B5, and at rim joist connections are summarized in Appendix B, Tables B6-B8. For linear transmittance determinations on the two Ledger frames (with and without interior floor/ceiling), and linear transmittance at rim joist connection, no significant differences were found between dimensional lumber and engineered wood product made beams. As the spacing between the floor joists increases, the linear thermal transmittance increases slightly. For the frames with same wall size and the same level of insulations, as the size of beam increases, the linear transmittance increases slightly as well. As level of exterior insulation increases, the linear transmittance decreases, as expected. As level of exterior insulation increases to 3-inch and 4-inch, the effect caused by the spacing of beam become negligible. Under the same conditions, 2x6 wall performed better than 2x4 wall because there is more space in the 2x6 wall cavity for insulation. Assemblies with 2x6 wall, 2x8 beam at 300 mm spacing and 4-inch exterior insulation had the best thermal performance, the linear transmittance due to thermal bridging was 0.023 W/m·K for ledger with interior floor/ceiling, 0.019 W/m·K for ledger without interior floor/ceiling, and 0.015 W/m·K for rim joist. After changing the junction insulation to VIP, the linear transmittance decreased to 0.017 W/m·K for ledger with interior floor/ceiling, 0.010 W/m·K for ledger without interior floor/ceiling, and the point transmittance decreased to 0.011 W/m·K for rim joist, in other words, the thermal performance improved by 25.8%, 45.5%, and 26% respectively.

4.7.4 Point Transmittance at Rim Joist

Point transmittance due to thermal bridges at rim joist are summarized in Appendix B, Table B9. As the beam size increases, the point transmittance increases slightly; as the exterior insulation level increases, the effect of beam size on thermal performance decreases to negligible. The best thermal performance case was found to be of a 2x6 wall, with 2x8 joist and 4-inch external insulation, the value for the point transmittance due to thermal bridging was 0.004 W/K. By applying VIP as the cavity insulation at the wall/floor junction, the point transmittance decreased to 0.002 W/K, by about 50%.

4.8 Conclusion

For all frame configurations studied, there were no significant differences found on the thermal performance between dimensional lumber and engineered wood product beams. Implementing exterior insulation reduces the thermal transmittance caused by thermal bridging, the higher level of exterior insulation, the better thermal performance. Overall, a combination of 2x6 wall, 2x8 beam and 4-inch exterior insulation make the best combination that yields the best thermal performance. Substituting the closed cell spray foam at the wall/floor junction with vacuum insulation panels showed increased effectiveness in thermal performance for all connection types.

The modeling methods and actual HEAT3 model creation and simulation in this study were checked and validated by the certified Canadian technical support team of this software.

4.9 Future Directions

Future studies in which new combinations of state-of-the-art building materials and framing methods are modelled and studied may improve our ability to further reduce heat loss at thermal bridges.

4.10 Funding

This study is sponsored by the Homeowners Protection Office (now New Home Warranty).

4.11 Acknowledgements

We gratefully acknowledge the team of Read Jones Christoffersen Engineers (RJC) for their work preparing and coordinating this study in collaboration with the University of Victoria.

CHAPTER 5 CONCLUSION AND FUTURE WORK

In Chapter 2, we summarized the thermal performance of the glass fiber core VIPs over the period of 2011–2018 in the Canadian subarctic climate in Whitehorse, Yukon. Findings from this study provided data to validate glass fiber core VIP accelerated aging test results and the aging rate of VIPs in a cold and dry climate was determined. The results from the energy retrofit project demonstrated promising and satisfactory performance of glass fiber core VIPs over a period of eight years. Analysis of the temperature showed a less than 0.9% per year change in the field thermal performance of the VIPs, indicating that aging of glass fiber core VIPs in cold climate proceeds at a very slow rate. We also noted many perceived challenges relating to the application of VIPs in the construction industry and how these could be addressed. This project provided valuable field data that can be used for validating theoretical VIP aging predictions and laboratory accelerated aging results.

In Chapter 3, we investigated the impact of high temperature and high humidity on the thermal conductivity of glass fiber core VIPs. Two sets of tests were conducted in laboratory, one under 70°C, and the other under 70°C and 95% RH. We observed significant changes in the rate of thermal conductivity change in VIPs aging under high temperature and high humidity and we discussed the combined effect of dry air and water vapour diffusion, specifically, increased heat transfer inside the panel through gas conduction, water vapour conduction and air-water convection. Equations of thermal conductivity change due to dry air and equations of thermal conductivity degradation due to water vapour of glass fiber VIPs with respect to aging time, and with respect to the increase of internal pressure were produced.

In Chapter 4, we investigate the significance of thermal bridges in wood-frame building and evaluate the potential improvement on reducing thermal bridges. Computer modeling software Heat3 was used to create and simulate simplified models of cantilever, ledger, and rim joist balcony/wall junctions. By creating scenarios with different combinations of wood types, joist/slab spacing, wall sizes, and adopting the state-of-art innovative insulating materials – Vacuum Insulation Panels for the junction cavity, the thermal loss due to thermal bridging were calculated and compared. We found no significant differences on the thermal performance between dimensional lumber and engineered wood product beams. Implementing exterior insulation reduces the thermal transmittance caused by thermal bridging, the higher level of exterior insulation, the better thermal performance. Overall, a combination of 2x6 wall, 2x8 beam and 4-inch exterior insulation make the best combination that yields the best thermal performance. Substituting the closed cell spray foam at the wall/floor junction with vacuum insulation panels showed increased effectiveness in thermal performance for all connection types.

In each chapter, we discuss potential areas for further research. Additional data collected from the retrofitting project in the Yukon via ongoing in situ temperature monitoring could be used to validate theoretical VIP aging predictions and laboratory accelerated aging results. Results from laboratory accelerated aging tests using different temperature and relative humidity combinations could aid in the development of a simplified long-term thermal performance

prediction model for glass fiber core VIPs. For the last section, modeling of new combinations of state-of-the-art building materials and framing methods could improve our ability to further reduce heat loss at thermal bridges.

REFERENCES

[1] B. C. Hydro, "Building Envelope Thermal Bridging Guide," 2016. Accessed: Jan 2019. [Online]. Available: https://www.bchydro.com/content/dam/BCHydro/customer-portal/documents/power-smart/builders-developers/building-envelope-thermal-bridging-guide-1.1.pdf

[2] H. Ritchie and M. Roser. Fossil Fuels [Online] Available: https://ourworldindata.org/fossil-fuels

[3] H. Ritchie and M. Roser. CO_2 and Greenhouse Gas Emissions [Online] Available: https://ourworldindata.org/co2-and-other-greenhouse-gas-emissions

[4] D. Ürge-Vorsatz, L. F. Cabeza, S. Serrano, C. Barreneche, and K. Petrichenko, "Heating and cooling energy trends and drivers in buildings," *Renewable and Sustainable Energy Reviews,* vol. 41, pp. 85-98, 2015, doi: 10.1016/j.rser.2014.08.039.

[5] Natural Resources Canada. "Energy Efficiency Trends in Canada 1990 to 2013." Natural Resources Canada. https://www.nrcan.gc.ca/energy/publications/19030#a3 (accessed January 14, 2019).

[6] *National Building Code of Canada 2015*, National Research Council Canada, 2015.

[7] L. Aditya *et al.*, "A review on insulation materials for energy conservation in buildings," *Renewable and Sustainable Energy Reviews,* vol. 73, pp. 1352-1365, 2017, doi: 10.1016/j.rser.2017.02.034.

[8] H. Simmler *et al.*, "Study on VIP-components and Panels for Service Life Prediction of VIP in Building Applications (Subtask A)," in "High Performance Thermal Insulation IEA/ECBCS Annex 39," September 2005.

[9] B. P. Jelle, "Traditional, state-of-the-art and future thermal building insulation materials and solutions – Properties, requirements and possibilities," *Energy and Buildings,* vol. 43, no. 10, pp. 2549-2563, 2011, doi: 10.1016/j.enbuild.2011.05.015.

[10] J. Fricke, H. Schwab, and U. Heinemann, "Vacuum insulation panels - exciting thermal properties and most challenging applications," *International Journal of Thermophysics,* vol. 27, pp. 1123-1139, 2006, doi: 10.1007/s10765-006-0106-6.

[11] D. MacLean, J. Korn, and P. Mukhopadhyaya, "Vacuum Insulation Panels (VIPs) Arrive in Northern Canada: Institutional Building Pilot Retrofit in Yukon," in *Proceedings of 10th International Vacuum Insulation Symposium (IVIS-X)*, Ottawa, ON, 2011, vol. 10.

[12] S. E. Kalnæs and B. P. Jelle, "Vacuum insulation panel products: A state-of-the-art review and future research pathways," *Applied Energy,* vol. 116, pp. 355-375, 2014, doi: 10.1016/j.apenergy.2013.11.032.

[13] National Research Council Canada. "Canadian Construction Materials Centre—About the CCMC." https://www.nrc-cnrc.gc.ca/eng/solutions/advisory/ccmc/about_ccmc.html (accessed January, 2019).

[14] U. Heinemann, "Long-Term Performance of Super-Insulating Materials in Building Components and Systems," International Energy Agency Energy in Buildings and Communities Programme, 2017.

[15] P. Mukhopadhyaya. (2006) High Performance Vacuum Insulation Panel - Research Update from Canada. *Global Insulation Magazine*. 9-15.

[16] P. Mukhopadhyaya, K. Kumaran, G. Sherrer, and D. van Reenen, "An investigation on long-term thermal performance of Vacuum Insulation Panels (VIPs)," in *10th International Vacuum Insulation Symposium (IVIS-X)*, Ottawa, ON, 2011, vol. 10.

[17] P. Mukhopadhyaya, D. MacLean, J. Korn, D. Van Reenen, and S. Molleti, "Field application and long-term thermal performance of Vacuum Insulation Panels (VIPs) in Canadian Arctic Climate," in *11th International Vacuum Insulation Symposium (IVIS-XI)*, 2013, pp. 97–98.

[18] P. Mukhopadhyaya, D. MacLean, J. Korn, D. van Reenen, and S. Molleti, "Building application and thermal performance of vacuum insulation panels (VIPs) in Canadian subarctic climate," *Energy Build,* vol. 85, pp. 672-680, 2014, doi: 10.1016/j.enbuild.2014.08.038.

[19] *Application of VIPs in Canada's North - Monitoring Results' ASTM International, STP1599*, P. Mukhopadhyaya, D. MacLean, J. Korn, and S. Mooney, West Conshohocken, PA, 2017.

[20] D. MacLean, P. Mukhopadhyaya, J. Korn, and S. Mooney, "Design details and long-term performance of VIPs in Canada's North," *Energy Procedia,* vol. 111, pp. 481-489, 2017, doi: 10.1016/j.egypro.2017.03.210.

[21] M. Morlidge, "Determining the Aging Performance of Vacuum Insulation Panels: Development of a Prediction Model," Master of Building Science, Building Science, Ryerson University, Toronto, 2012.

[22] "Climate and Weather Averages in Whitehorse, Yukon, Canada. Time and Date, 1995-2017." https://www.timeanddate.com/weather/canada/whitehorse/climate (accessed June 11, 2017).

[23] U. Heinemann, "Influence of water on the total heat transfer in 'evacuated' insulation. ," *Int J Thermophysics,* vol. 2008, no. 29, pp. 735-749, 2008.

[24] R. Baetens, B. Jelle, and J. Thue, "Vacuum insulation panels for building applications: a review and beyond," *Energy and Buildings,* vol. 42, pp. 147-172, 2010.

[25] E. Wegger, B. Jelle, E. Sveipe, S. Grynning, A. Gustavsen, and J. V. Thue, "Accelerated Ageing of Vacuum Insulation Panels (VIPs). ," in *Renewable Energy Conference*, Trondheim, Norway, 2010: Zero Mission Buildings.

[26] X. Di, Y. Gao, C. Bao, and S. Ma, "Thermal insulation property and service life of vacuum insulation panels with glass fiber chopped strand as core materials," *Energy and Buildings,* vol. 73, pp. 176-182, 2014.

[27] X. Di, Y. Gao, C. Bao, Y. Hu, and Z. Xie, "Optimization of glass fiber based core materials for vacuum insulation panels with laminated aluminum foils as envelopes," *Vacuum,* vol. 97, pp. 55-59, 2013.

[28] R. Kunič, "Vacuum Insulation Panels - An Assessment of the Impact of Accelerated Ageing on Service Life," *Journal of Mechanical Engineering,* vol. 58, no. 10, pp. 598-606, 2012.

[29] H. Simmler and S. Brunner, "Vacuum insulation panels for building application Basic properties, aging mechanisms and service life," *Energy and Buildings,* vol. 37, pp. 1122-1131, 2005.

[30] J.-H. Kim, F. E. Boafo, S.-M. Kim, and J.-T. Kim, "Aging Performance Evaluation of Vacuum Insulation Panel (VIP)," *Case Studies in Construction Materials,* vol. 7, no. 2017, pp. 329-335, 2017.
[31] P. Mukhopadhyaya, C. St-Onge, B. Di Lenardo, L. Carbary, W. Gregg, and A. Parekh, "Long Term Thermal Resistance of Vacuum Insulation Panel (VIP) - Experimental Observations & Predictions," in *12th International Vacuum Insulation Symposium*, China, September 19-21 2015.
[32] U. Heinemann, R. Caps, and J. Fricke, "Characterization and optimization of filler materials for vacuum super insulations," *Vuoto scienza e tecnologiz,* vol. 28, no. 1-2, pp. 43-46, 1999.
[33] *ASHRAE Standard 90.1 - Energy Standard for Buildings Except Low-Rise Residential Buildings*, American Society of Heating Refrigerating and Air-Conditioning Engineers, Atlanta, GA, USA, 2019.
[34] *National Energy Code of Canada for Buildings 2017*, National Research Council Canada, Canada, 2017.
[35] Natural Resources Canada. "Green Constuction through Wood (GCWood) Program." https://www.nrcan.gc.ca/science-data/funding-partnerships/funding-opportunities/forest-sector-funding-programs/green-construction-through-wood-gcwood-program/20046 (accessed 2018).
[36] *ASHRAE Handbook Foundamentals*, ASHRAE, Atlanta GA, 2017.
[37] N. Norris, M. Lawton, and P. Roppel, "The Concept of Linear and Point Transmittance and its Value in Dealing with Thermal Bridges in Building Enclosures," in *3rd Building Enclosure Science & Technology Conference*, Atlanta, 2012.
[38] H. Ge, V. R. McClung, and S. Zhang, "Impact of balcony thermal bridges on the overall thermal performance of multi-unit residential buildings: A case study," *Energy and Buildings,* vol. 60, pp. 163-173, 2013, doi: 10.1016/j.enbuild.2013.01.004.
[39] F. Baba and H. Ge, "Dynamic effect of balcony thermal bridges on the energy performance of a high-rise residential building in Canada," *Energy and Buildings,* vol. 116, pp. 78-88, 2016, doi: 10.1016/j.enbuild.2015.12.044.
[40] H. Ge and F. Baba, "Dynamic effect of thermal bridges on the energy performance of a low-rise residential building," *Energy and Buildings,* vol. 105, pp. 106-118, 2015, doi: 10.1016/j.enbuild.2015.07.023.
[41] *HEAT3 - Heat transfer in three dimensions*. (2017). Accessed: 2018. [Online]. Available: https://buildingphysics.com/heat3-3/
[42] *ISO 10211:2017 Thermal bridges in building construction - Heat flows and surface temperatures - Detailed calculations*, International Organization for Standardization, Switzerland, 2017.
[43] Building Science Corporation. "Info-502: Temperature Dependence of R-values in Polyisocynurate Roof Insulation." Building Science Corporation. https://www.buildingscience.com/documents/information-sheets/info-502-temperature-dependent-r-value (accessed June 2018, 2018).

APPENDIX A

SAMPLE CALCULATION

The following section demonstrates a sample calculation for determining percentage of total temperature difference across each insulation layer across the wall (Figure 6) in winter 2017. The maximum thermal gradient across the entire wall occurred between 0:00 – 06:00 AM on December 20, 2011 and the same time frame was used for analysis for the subsequent years. The calculation was performed on the data from 0:00 - 06:00 AM. on November 20, 2016, December 04, 2016, and January 09, 2017. Table A1 below shows the average measured temperatures on the selected time and dates.

Table A1: Maximum, minimum and average temperatures measured across the wall from 0:00 - 6:00 AM on November 20, 2016, December 04, 2016 and January 09, 2017.

Date	Average Measured Temperatures (°C)											
	T32 - Exterior of Brick			T34 – Exterior of 1st XPS			T35 – VIP Exterior			T36 – Exterior of 2nd XPS		
	Max	Min	Mean	Max	Min	Mean	Max	Min	Mean	Max	Min	Mean
Nov.20,2016	6.0	5.6	5.8	3.7	3.3	3.4	-6.0	-6.6	-6.4	-8.9	-9.7	-9.3
Dec.04, 2016	7.5	7.2	7.3	4.3	4.0	4.1	-8.8	-9.1	-9.0	-12.7	-13.1	-12.8
Jan. 09, 2017	-3.0	-3.5	-3.3	-6.0	-6.6	-6.3	-18.2	-19.2	-18.7	-21.8	-23.3	-22.6

Temperature drop calculation for January 09, 2017 are shown below, the mean temperatures were used in the calculation:

ΔT_{XPS1} = T32 – T34 = 3.0°C

ΔT_{VIP} = T34 – T35 = 12.4°C

ΔT_{XPS2} = T35 – T36 = 3.9°C

ΔT_{TOTAL} = T32 – T36 = 19.3°C

$\%\Delta T_{XPS1} = \Delta T_{XPS1}/\Delta T_{TOTAL}$ x 100% = 15.9%

$\%\Delta T_{VIP} = \Delta T_{VIP}/\Delta T_{TOTAL} \times 100\% = 64.2\%$

$\%\Delta T_{XPS2} = \Delta T_{XPS2}/\Delta T_{TOTAL} \times 100\% = 19.9\%$

Table A2 below shows the calculated temperature drop for selected time and dates, as well as the average of the three.

Table A2. Percentage of temperature drop across each insulation layer and the winter 2017 average.

Date	% of Temperature Drop Across Each Insulation Layer		
	First XPS	VIP	Second XPS
November 20, 2016	15.7%	65.0%	19.3%
December 04, 2016	15.8%	65.0%	19.2%
January 09, 2017	15.9%	64.2%	19.9%
Average	15.8%	64.7%	19.5%

It is to be noted that the exterior insulation layer includes 25 mm XPS and 6 mm flexible open-cell polyurethane foam. The thermal resistance offered by the 6 mm flexible open-cell polyurethane foam is negligible and was ignored in the calculations shown above. However, assuming the 6 mm flexible open-cell polyurethane foam contributed some thermal resistance, either 0.09 or 0.18 $m^2 \cdot K/W$, the corresponding actual temperature drop across the exterior XPS (thermal resistance 0.97 or 1.06 $m^2 \cdot K/W$) for Winter 2017 is calculated using the following equations respectively:

$\%\Delta T_{XPS2'}$ = $\%\Delta T_{XPS2}$ x (thermal resistance of XPS/ (total thermal resistance of XPS and foam)) = 19.5% x (0.88/0.97) =17.7 %

$\%\Delta T_{XPS2''}$ = $\%\Delta T_{XPS2}$ x (thermal resistance of XPS/ (total thermal resistance of XPS and foam)) = 19.5% x (0.88/1.06) = 16.2%

Where $\%\Delta T_{XPS2'}$ is the percentage of the temperature drop across the exterior XPS assuming the thermal resistance of the 6 mm foam is 0.09 $m^2 \cdot K/W$.

$\%\Delta T_{XPS2''}$ is the percentage of the temperature drop across the exterior XPS assuming the thermal resistance of the 6 mm foam is 0.18 $m^2 \cdot K/W$.

The temperature drop across wall components taking account of the thermal resistance contribution of the 6 mm foam (0.09 $m^2 \cdot K/W$ or 0.18 $m^2 \cdot K/W$) are graphed in Figure A1 and A2 respectively. It is clear that the temperature drops across the exterior XPS are higher than the interior XPS in both scenarios, therefore, the exterior layer of XPS is a more effective thermal insulator than the identical interior XPS layer due to the cooler exterior temperature.

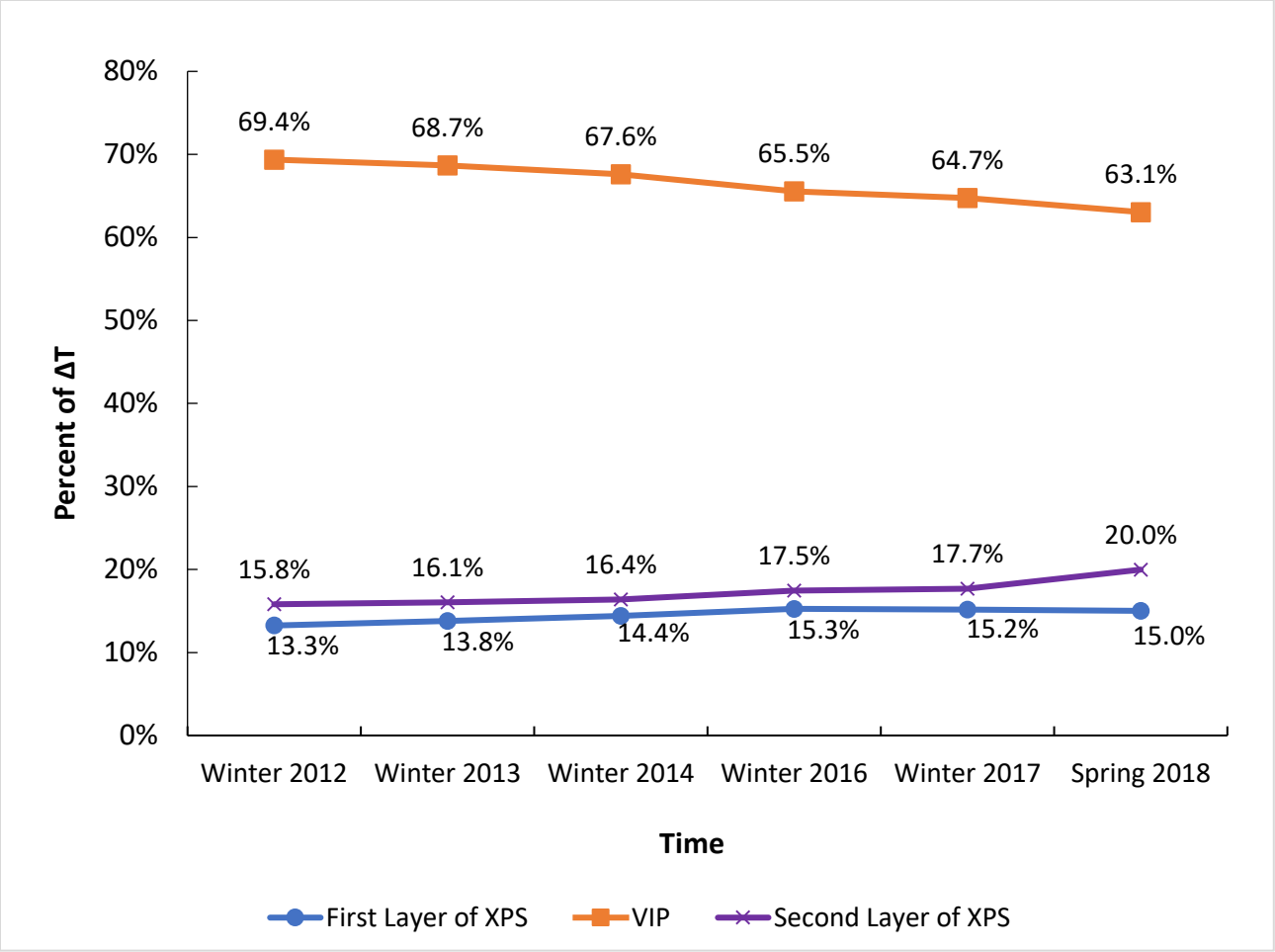

Figure A1 - Percentage of temperature drop across wall components (assume the thermal resistance of the 6 mm foam is 0.09 $m^2 \cdot K/W$), relative to the drop across the entire wall. Data averaged for the winter months of 2012 - 2017 and spring months of 2018.

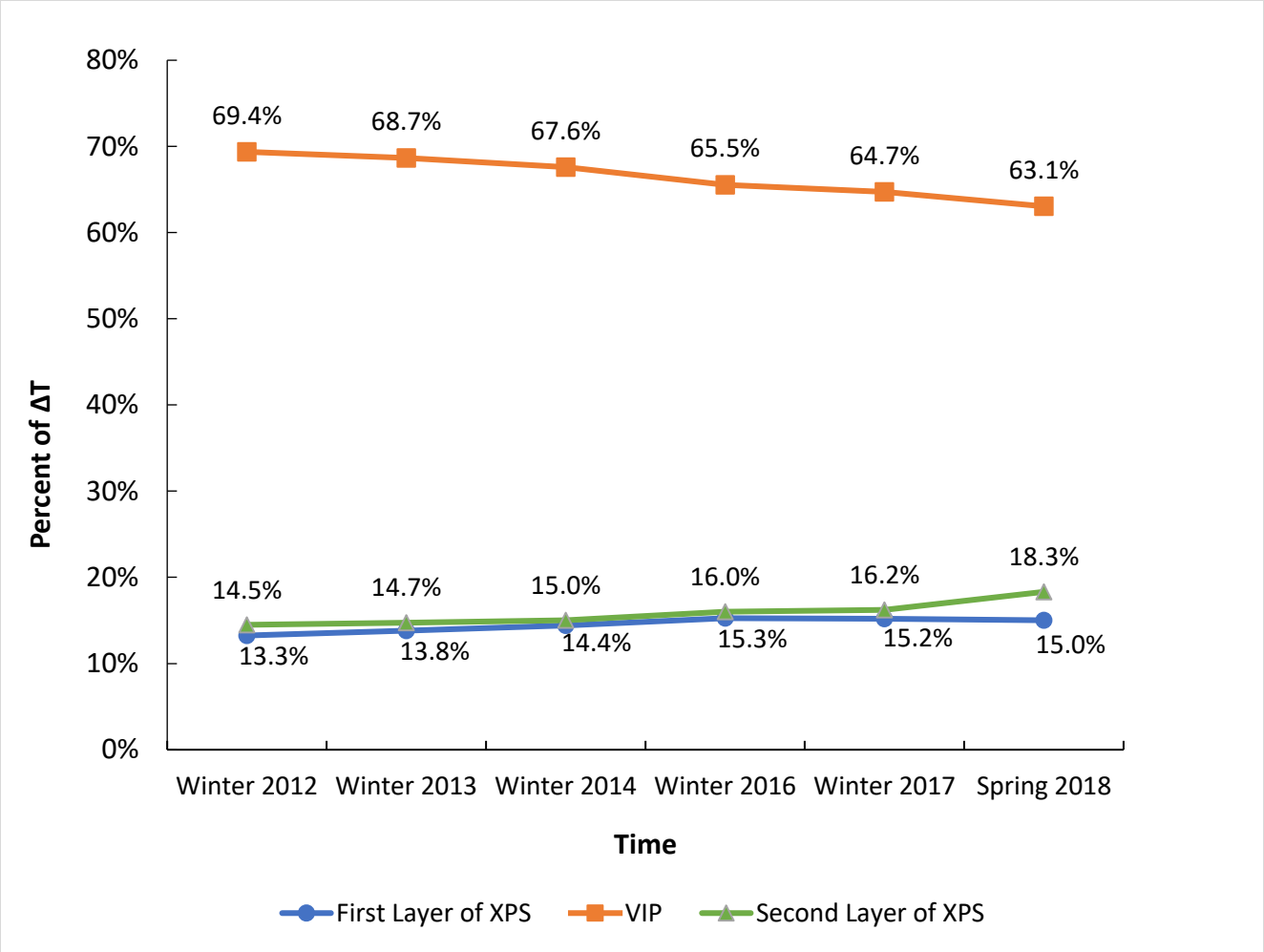

Figure A2 - Percentage of temperature drop across wall components (assume the thermal resistance of the 6 mm foam is 0.18 $m^2 \cdot K/W$), relative to the drop across the entire wall. Data averaged for the winter months of 2011-2017 and spring months of 2018.

APPENDIX B

Table B1. Linear thermal transmittance (W/m·K) along cantilevers caused by thermal bridging, modeled at 300 mm o.c. spacing between beams.

Dimensional Lumber										
Wall Size (inch)	**Ext. Insulation Level**	**38 x 184 (2x8)**			**38 x 235 (2x10)**			**38 x 286 (2x12)**		
		1-ply	**2-ply**	**3-ply**	**1-ply**	**2-ply**	**3-ply**	**1-ply**	**2-ply**	**3-ply**
2x4	0"	0.111	0.119	0.115	0.121	0.130	0.125	0.135	0.144	0.138
	1"	0.062	0.066	0.063	0.069	0.072	0.071	0.078	0.081	0.079
	2"	0.043	0.043	0.043	0.048	0.048	0.048	0.054	0.054	0.053

Engineered Wood Products										
Wall Size (inch)	**Ext. Insulation Level**	**44 x 184 (2x8)**			**44 x 235 (2x10)**			**44 x 286 (2x12)**		
		1-ply	**2-ply**	**3-ply**	**1-ply**	**2-ply**	**3-ply**	**1-ply**	**2-ply**	**3-ply**
2x4	0"	0.122	0.118	0.113	0.134	0.128	0.123	0.148	0.142	0.135
	1"	0.067	0.065	0.063	0.074	0.071	0.069	0.082	0.079	0.077
	2"	0.043	0.043	0.042	0.048	0.047	0.048	0.054	0.053	0.052

Dimensional Lumber										
Wall Size (inch)	**Ext. Insulation Level**	**38 x 184 (2x8)**			**38 x 235 (2x10)**			**38 x 286 (2x12)**		
		1-ply	**2-ply**	**3-ply**	**1-ply**	**2-ply**	**3-ply**	**1-ply**	**2-ply**	**3-ply**
2x6	0"	0.061	0.064	0.062	0.063	0.066	0.063	0.066	0.069	0.066
	1"	0.041	0.043	0.042	0.043	0.044	0.043	0.046	0.048	0.045
	2"	0.031	0.032	0.032	0.033	0.033	0.033	0.036	0.035	0.035
	3"	0.025	0.025	0.025	0.027	0.027	0.027	0.029	0.028	0.028
	4"	0.021	0.021	0.021	0.023	0.022	0.022	0.025	0.023	0.024

Engineered Wood Products										
Wall Size (inch)	**Ext. Insulation Level**	**44 x 184 (2x8)**			**44 x 235 (2x10)**			**44 x 286 (2x12)**		
		1-ply	**2-ply**	**3-ply**	**1-ply**	**2-ply**	**3-ply**	**1-ply**	**2-ply**	**3-ply**
2x6	0"	0.066	0.063	0.061	0.068	0.065	0.062	0.071	0.068	0.065
	1"	0.043	0.042	0.041	0.045	0.044	0.043	0.047	0.046	0.044
	2"	0.032	0.032	0.031	0.034	0.033	0.032	0.035	0.035	0.034
	3"	0.024	0.025	0.025	0.026	0.026	0.026	0.028	0.028	0.028
	4"	0.020	0.020	0.020	0.021	0.022	0.021	0.023	0.023	0.023

Table B2. Point thermal transmittance at corners, W/K.

Engineered Wood Products										
Wall Size (inch)	**Ext. Insulation Level**	**44 x 184 (2x8)**			**44 x 235 (2x10)**			**44 x 286 (2x12)**		
		1-ply	**2-ply**	**3-ply**	**1-ply**	**2-ply**	**3-ply**	**1-ply**	**2-ply**	**3-ply**
2x4	0"	0.021	0.042	N/A	0.026	0.052	N/A	0.036	0.068	N/A
	1"	0.010	0.021	N/A	0.013	0.026	N/A	0.017	0.033	N/A
	2"	0.006	0.013	N/A	0.007	0.017	N/A	0.011	0.013	N/A

Engineered Wood Products										
Wall Size (inch)	**Ext. Insulation Level**	**44 x 184 (2x8)**			**44 x 235 (2x10)**			**44 x 286 (2x12)**		
		1-ply	**2-ply**	**3-ply**	**1-ply**	**2-ply**	**3-ply**	**1-ply**	**2-ply**	**3-ply**
2x6	0"	0.007	0.010	0.051	0.008	0.012	0.066	0.009	0.014	0.081
	1"	0.004	0.006	0.032	0.005	0.007	0.041	0.005	0.009	0.051
	2"	0.004	0.005	0.023	0.004	0.006	0.030	0.005	0.007	0.037
	3"	0.003	0.005	0.019	0.004	0.006	0.024	0.004	0.006	0.029
	4"	0.003	0.005	0.016	0.004	0.005	0.020	0.004	0.006	0.024

Table B3. Linear transmittance due to thermal bridging at a ledger connection, no exterior insulation (W/m·K).

	Product Type	**Dimensional Lumber**			**Engineered Wood Products**		
	Ledger Size (mm)	**38 x 184 (2x8)**	**38 x 235 (2x10)**	**38 x 286 (2x12)**	**44 x 184 (2x8)**	**44 x 235 (2x10)**	**44 x 286 (2x12)**
300 mm o.c. 2x4 No exterior insulation	Without floor/ceiling	0.090	0.099	0.106	0.090	0.098	0.106
	With floor/ceiling	0.110	0.122	0.134	0.109	0.121	0.132
400 mm o.c. 2x4 No exterior insulation	Without floor/ceiling	0.095	0.105	0.113	0.095	0.104	0.113
	With floor/ceiling	0.114	0.127	0.138	0.114	0.126	0.138
600 mm o.c. 2x4 No exterior insulation	Without floor/ceiling	0.101	0.111	0.120	0.100	0.110	0.120
	With floor/ceiling	0.118	0.131	0.143	0.118	0.131	0.143
300 mm o.c. 2x6 No exterior insulation	Without floor/ceiling	0.045	0.044	0.430	0.044	0.044	0.043
	With floor/ceiling	0.060	0.063	0.066	0.060	0.063	0.065
400 mm o.c. 2x6 No exterior insulation	Without floor/ceiling	0.049	0.049	0.048	0.048	0.048	0.048
	With floor/ceiling	0.062	0.065	0.067	0.062	0.069	0.067
600 mm o.c. 2x6 No exterior insulation	Without floor/ceiling	0.053	0.053	0.054	0.052	0.053	0.054
	With floor/ceiling	0.064	0.067	0.069	0.064	0.067	0.069

Table B4. Linear transmittance due to thermal bridging at a ledger connection for 2x4 wall with exterior insulation (W/m·K).

		Product Type	**Dimensional Lumber**			**Engineered Wood Products**		
		Ledger Size (mm)	**38 x 184 (2x8)**	**38 x 235 (2x10)**	**38 x 286 (2x12)**	**44 x 184 (2x8)**	**44 x 235 (2x10)**	**44 x 286 (2x12)**
300 mm o.c.	1"	Without floor/ceiling	0.059	0.064	0.070	0.058	0.064	0.069
		With floor/ceiling	0.070	0.077	0.084	0.069	0.076	0.084
	2"	Without floor/ceiling	0.042	0.046	0.050	0.041	0.046	0.050
		With floor/ceiling	0.048	0.054	0.060	0.048	0.054	0.059
400 mm o.c.	1"	Without floor/ceiling	0.061	0.067	0.073	0.061	0.067	0.073
		With floor/ceiling	0.072	0.079	0.087	0.071	0.079	0.086
	2"	Without floor/ceiling	0.043	0.047	0.051	0.043	0.047	0.051
		With floor/ceiling	0.049	0.055	0.060	0.049	0.054	0.060
600 mm o.c.	1"	Without floor/ceiling	0.064	0.070	0.076	0.064	0.070	0.076
		With floor/ceiling	0.074	0.081	0.089	0.073	0.081	0.088
	2"	Without floor/ceiling	0.044	0.049	0.053	0.044	0.048	0.053
		With floor/ceiling	0.050	0.055	0.061	0.050	0.055	0.061

Table B5. Linear transmittance due to thermal bridging at a ledger connection for 2x6 wall with exterior insulation (W/m·K).

		Product Type	**Dimensional Lumber**			**Engineered Wood Products**		
		Ledger Size (mm)	**38 x 184 (2x8)**	**38 x 235 (2x10)**	**38 x 286 (2x12)**	**44 x 184 (2x8)**	**44 x 235 (2x10)**	**44 x 286 (2x12)**
300 mm o.c.	1"	Without floor/ceiling	0.036	0.034	0.033	0.033	0.033	0.033
		With floor/ceiling	0.044	0.046	0.049	0.044	0.046	0.048
	2"	Without floor/ceiling	0.027	0.027	0.027	0.027	0.027	0.027
		With floor/ceiling	0.034	0.036	0.038	0.034	0.036	0.038
	3"	Without floor/ceiling	0.022	0.023	0.023	0.022	0.023	0.023
		With floor/ceiling	0.028	0.030	0.032	0.028	0.030	0.031
	4"	Without floor/ceiling	0.019	0.019	0.020	0.019	0.019	0.020
		With floor/ceiling	0.023	0.025	0.027	0.023	0.025	0.027
400 mm o.c.	1"	Without floor/ceiling	0.036	0.037	0.037	0.036	0.036	0.036
		With floor/ceiling	0.045	0.048	0.049	0.045	0.047	0.049
	2"	Without floor/ceiling	0.028	0.029	0.029	0.028	0.029	0.029
		With floor/ceiling	0.035	0.037	0.039	0.035	0.037	0.038
	3"	Without floor/ceiling	0.023	0.024	0.024	0.023	0.024	0.024
		With floor/ceiling	0.028	0.030	0.031	0.028	0.030	0.031
	4"	Without floor/ceiling	0.019	0.020	0.021	0.019	0.020	0.021
		With floor/ceiling	0.023	0.025	0.027	0.023	0.024	0.021
600 mm o.c.	1"	Without floor/ceiling	0.039	0.040	0.040	0.039	0.040	0.040
		With floor/ceiling	0.046	0.049	0.050	0.046	0.048	0.050

	2"	Without floor/ceiling	0.030	0.031	0.031	0.030	0.032	0.031
		With floor/ceiling	0.035	0.037	0.039	0.035	0.037	0.037
	3"	Without floor/ceiling	0.024	0.025	0.025	0.024	0.025	0.025
		With floor/ceiling	0.028	0.030	0.031	0.028	0.029	0.031
	4"	Without floor/ceiling	0.020	0.021	0.021	0.020	0.021	0.021
		With floor/ceiling	0.023	0.024	0.026	0.023	0.024	0.026

Table B6. Linear transmittance due to thermal bridging at rim joist connection without exterior insulation (W/m·K).

Wall Size (inch)	Spacing (mm)	Dimensional Lumber			Engineered Wood Products		
		38 x 184 (2x8)	38 x 235 (2x10)	38 x 286 (2x12)	44 x 184 (2x8)	44 x 235 (2x10)	44 x 286 (2x12)
2x4	300	0.101	0.114	0.127	0.101	0.114	0.126
	400	0.105	0.119	0.132	0.105	0.118	0.131
	600	0.109	0.123	0.137	0.109	0.122	0.136
2x6	300	0.056	0.059	0.063	0.056	0.059	0.062
	400	0.059	0.061	0.064	0.058	0.061	0.064
	600	0.060	0.063	0.066	0.060	0.063	0.066

Table B7. Linear transmittance due to thermal bridging at rim joist connection for 2x4 wall with exterior insulation (W/m·K).

	Exterior Insulation Level	Dimensional Lumber			Engineered Wood Products		
		38 x 184 (2x8)	38 x 235 (2x10)	38 x 286 (2x12)	44 x 184 (2x8)	44 x 235 (2x10)	44 x 286 (2x12)
300 mm o.c.	1"	0.055	0.062	0.069	0.055	0.062	0.069
	2"	0.035	0.039	0.044	0.035	0.039	0.043
400 mm o.c.	1"	0.058	0.065	0.072	0.057	0.065	0.072
	2"	0.037	0.041	0.046	0.037	0.041	0.046
600 mm o.c.	1"	0.060	0.068	0.076	0.060	0.068	0.076
	2"	0.039	0.044	0.049	0.039	0.044	0.049

Table B8. Linear transmittance due to thermal bridging at rim joist connection for 2x6 wall with exterior insulation (W/m·K).

	Exterior Insulation Level	Dimensional Lumber			Engineered Wood Products		
		38 x 184 (2x8)	38 x 235 (2x10)	38 x 286 (2x12)	44 x 184 (2x8)	44 x 235 (2x10)	44 x 286 (2x12)
300 mm o.c.	1"	0.037	0.039	0.041	0.037	0.039	0.041
	2"	0.026	0.028	0.029	0.026	0.028	0.029
	3"	0.019	0.021	0.022	0.019	0.021	0.022
	4"	0.015	0.016	0.017	0.015	0.016	0.017
400 mm o.c.	1"	0.038	0.041	0.043	0.038	0.040	0.043
	2"	0.027	0.029	0.031	0.027	0.029	0.031
	3"	0.021	0.022	0.023	0.021	0.022	0.023
	4"	0.016	0.017	0.018	0.016	0.017	0.018
600 mm o.c.	1"	0.040	0.042	0.044	0.040	0.042	0.044
	2"	0.029	0.031	0.032	0.029	0.030	0.032
	3"	0.022	0.023	0.025	0.021	0.023	0.024
	4"	0.017	0.018	0.020	0.017	0.018	0.019

Table B9. Point transmittance (300 mm depth) due to thermal bridging at rim joist connection with exterior insulation, (W/K).

Wall Size (inch)	Exterior Insulation Level	Dimensional Lumber		
		38 x 184 (2x8)	38 x 235 (2x10)	38 x 286 (2x12)
2x4	0"	0.032	0.035	0.038
	1"	0.017	0.018	0.020
	2"	0.010	0.012	0.013
2x6	0"	0.015	0.015	0.015
	1"	0.010	0.010	0.013
	2"	0.007	0.007	0.007
	3"	0.005	0.005	0.005
	4"	0.004	0.004	0.004